GEOLOGICAL, STRUCTURAL AND GEOCHRONOLOGICAL FRAMEWORK OF THE VELADERO NORTH AREA, CORDILLERA FRONTAL, ARGENTINA

By

DIEGO CHARCHAFLIÉ

Licenciado en Ciencias Geológicas, Universidad de Buenos Aires, 1994

A THESIS SUBMITTED IN PARTIAL FULFILMENT OF
THE REQUIREMENTS FOR THE DEGREE OF

MASTER OF SCIENCE

In

THE FACULTY OF GRADUATE STUDIES
(Department of Earth and Ocean Sciences)

We accept this thesis as conforming
to the required standard

THE UNIVERSITY OF BRITISH COLUMBIA
January 2003

In presenting this thesis in partial fulfilment of the requirements for an advanced degree at the University of British Columbia, I agree that the Library shall make it freely available for reference and study. I further agree that permission for extensive copying of this thesis for scholarly purposes may be granted by the head of my department or by his or her representatives. It is understood that copying or publication of this thesis for financial gain shall not be allowed without my written permission.

Department of Earth & Ocean Sc.

The University of British Columbia
Vancouver, Canada

Date February 05, 2003

DE-6 (2/88)

Abstract

The Veladero North area, located in the northern part of the El Indio-Pascua Belt within the Cordillera Frontal of Argentina and Chile, contains gold reserves and resources that combined exceed 370 tons (12 Moz). Throughout the Belt, mineralization is related to Miocene magmatic activity and both high- and low-sulfidation systems have been mined. The Miocene volcanic rocks form several formations separated by unconformities from underlying Carboniferous to Triassic volcanic and plutonic rocks. Whereas age and structural relationship of these rocks are well known in Chile, the geology of the Argentinan flank is poorly documented. This study defines the stratigraphy, geology and tectonic evolution of the Veladero North area and clarifies the regional framework of the Cordillera Frontal in Argentina.

Thrust faults that dip steeply (70° to 90°) to the west and back-thrusts that dip steeply (70° to 90°) to the east define the overall geometry of the Miocene fold and thrust belt around the Veladero North area. The thrust panels comprise Permian (259 ± 0.7 Ma to 254 ± 4.2 Ma, U-Pb) rhyolitic volcanic and volcaniclastic rocks assigned to the Guanaco Sonso Formation and late Oligocene to early Miocene (24.5 ± 0.2 Ma to 22.8 ± 1.7 Ma, U-Pb) andesitic to dacitic pyroclastic and sedimentary rocks equivalent to the Tilito Formation. Middle Miocene (15.8 ± 1 Ma, U-Pb and 12.7 ± 0.9 Ma to 11.0 ± 0.2 Ma, ^{40}Ar-^{39}Ar) pyroclastic rocks and shallow intrusives of the Cerro de las Tórtolas Formation and Infiernillo Unit, and Vacas Heladas Formation in the study area unconformably overlie the fold and thrust belt. These strata are sub-horizontal or dip shallowly (<20°) to the east, and are separated from the thrusted rocks by two regional, low-relief unconformities. A Pliocene (2.1 ± 0.5 Ma, ^{40}Ar-^{39}Ar) rhyolitic dome in the eastern part of the district forms the Cerro de Vidrio Formation, the youngest recognized unit of the region.

Previously published and new geochronological data suggest that late Paleozoic to

Triassic magmatism in the Cordillera Frontal occurred as a series of plutonic and volcanic episodes isolated by periods of magmatic quiescence. The Choiyoi Group apparently comprises two independent volcanic units emplaced before and after a 25 m.y. volcanic lull, of which, the older and widespread Permian Guanaco Sonso Formation is exposed in the Veladero North area.

Structural relations and geochronology indicate that the largest part of Tertiary deformation in the study area occurred throughout the Miocene, and is best explained by multiple phases of shortening.

The youngest host rock of the Veladero North epithermal deposit is a volcanic succession dominated by heterolitic bedded breccias, volcaniclastic sandstones and dome-related rocks equivalent to the (16 Ma to 14.9 Ma) Cerro de las Tórtolas Formation and its intrusive counterpart, the Infiernillo Unit. If the mineralization in Veladero North is the same age as that in the rest of El Indio-Pascua Belt (9.5 Ma to 6 Ma), the volcaniclastic package is then several million years older than the mineralization. Thus, the genesis of the package bears little relationship to gold mineralization except for forming a porous host rock for it.

Table of contents

Chapter 1

General Introduction

Chapter 2

Late Paleozoic to early Mesozoic rocks of the Cordillera Frontal of Argentina and Chile with emphasis on the Veladero North Area, San Juan Province, Argentina

Chapter 3

Geological framework of the Veladero North area, Cordillera Frontal, Argentina

Chapter 4

Conclusions and recommendations for future research

Appendices

List of Tables

Chapter 2

Chapter 3

List of Figures

Chapter 1

Chapter 2

Chapter 3

Acknowledgements

I arrived to Vancouver in September 2000 with several vague ideas. At that time, the more clearly delineated ones were to complete a research program related to the geology of Veladero North deposit and to spend more than two weeks in a row with my girlfriend. Time went by very fast, many and diverse things happened and, a little more than two years later, I defended my M.Sc. thesis. There are many people that I would like to thank for their contributions to this thesis. First, I would like to thank Dick Tosdal for the countless revisions and suggestions to the manuscript. I am indebted to Dick for his support in academical as well as non-academical issues during all this time.

I also wish to thank the members of the committee, Dick Chase, Jim Mortensen, James Scoates and Kelly Russell for their additional suggestions to the thesis. Particularly, I would like to thank Kelly who survived a visit the study area and fuelled interesting geologic discussions.

This project was funded by MDRU and Homestake, with additional support from the Thomas and Marguerite MacKay Memorial Scholarship. This research would not have been possible without the collaboration and incentive of Homestake geologists: Don Lewis, Bill Wright and Ricardo Martínez. David Heberlain and Jay Hodgson from Barrick provided assistance when visiting Lama as well as a thoughtful discussion on the geochronologic results. I would like to thank Thomas Bissig for providing some of his figures, maps and data before its publication and Alfredo Vitaller for interesting discussion during the first part of this research.

I am indebted to Veladero project geologists and staff for the logistical support in the field, largely provided by Ismael Chavez, Mary Carrizo, Jose Luis Gomez and Chris Jones. I will always remember Gabriel Campillay for managing to cook out-of-the-menu-then-tasty dishes that made life in the Cordillera more enjoyable.

I would also like to thank my friends and fellows graduate students from UBC:

Lawrence Winter, Geoffrey Bradshaw, Simon Haynes, Scott Heffernan and Pat Hayman who contributed to this thesis and to the insertion into a different culture in Canada. Although over the past years they were unsuccessful in attempting to introduce me to hockey, I am grateful for revealing to me other Canadian fundamentals.

There are many people that I would like to thank for their support. My parents Chacha and Marie; my family Ivan, Machy, Marina, Ricardo, Alicia and Angel. Also my spanish-speaking friends of Vancouver: Sergio and Paola Jaramillo, Carlos and Mar Ramírez Medina, Sergi Molins and Ursula Cass; my friends from Argentina: Benoit and Vanesa Remy, Juan Manuel and Alexandra Molinari, Fernando Ruarte, Laura Net and many others that I am probably forgetting.

Finally, I would like to thank my wife Diana for her patience, companionship and encouragement during the past two years. Of all the individuals that supported this research, it is with her that I am most indebted.

Chapter 1

General Introduction

The Veladero North deposit is located in the northern part of the 150-km long El Indio-Pascua Belt that straddles the international border between Argentina and Chile (Figure 1-1). The belt is named after the El Indio mine, a multi-million ounce gold deposit discovered *ca.* 1978, and Pascua, one of the major ongoing exploration projects of the region. Veladero North, together with the nearby Pascua and Lama prospects represent one of the largest undeveloped gold and silver mining properties in the world with gold reserves of over 30 million ounces and 71.3 million ounces of silver reserves (Barrick data, 2002). To date (December 2002), reserves and resource estimation for the Pascua-Lama-Veladero are in aggregate nearly 2.5 times the total metal production from the El Indio-Pascua Belt. Mineralization and alteration throughout the El Indio-Pascua Belt was related to epithermal processes intimately associated to Tertiary magmatism, largely Miocene, and are hosted by late Paleozoic as well as Cenozoic rocks (Deyell, 2001; Bissig et al, 2001). Most deposits and exploration targets in the Belt are classified as high-sulfidation, and include venous (El Indio) and breccia-hosted (Tambo) mineralization. The Río del Medio deposit is the only known occurrence of low-sulfidation veins of economic mineralization in the region.

The El Indio-Pascua Belt occupies the centre of the present-day amagmatic segment of the Central Andes between the volcanically active Central and Southern Volcanic Zones (e.g. Jordan et al., 1983). The amagmatic nature of the segment has been related to the current shallow subduction angle (<10°) of the Nazca oceanic plate beneath the South American plate (Barazangi and Isacks, 1976). However, subduction-related magmatism and deformation in the general area of the El Indio-Pascua Belt were active throughout the Tertiary, as well as during the late Paleozoic to early

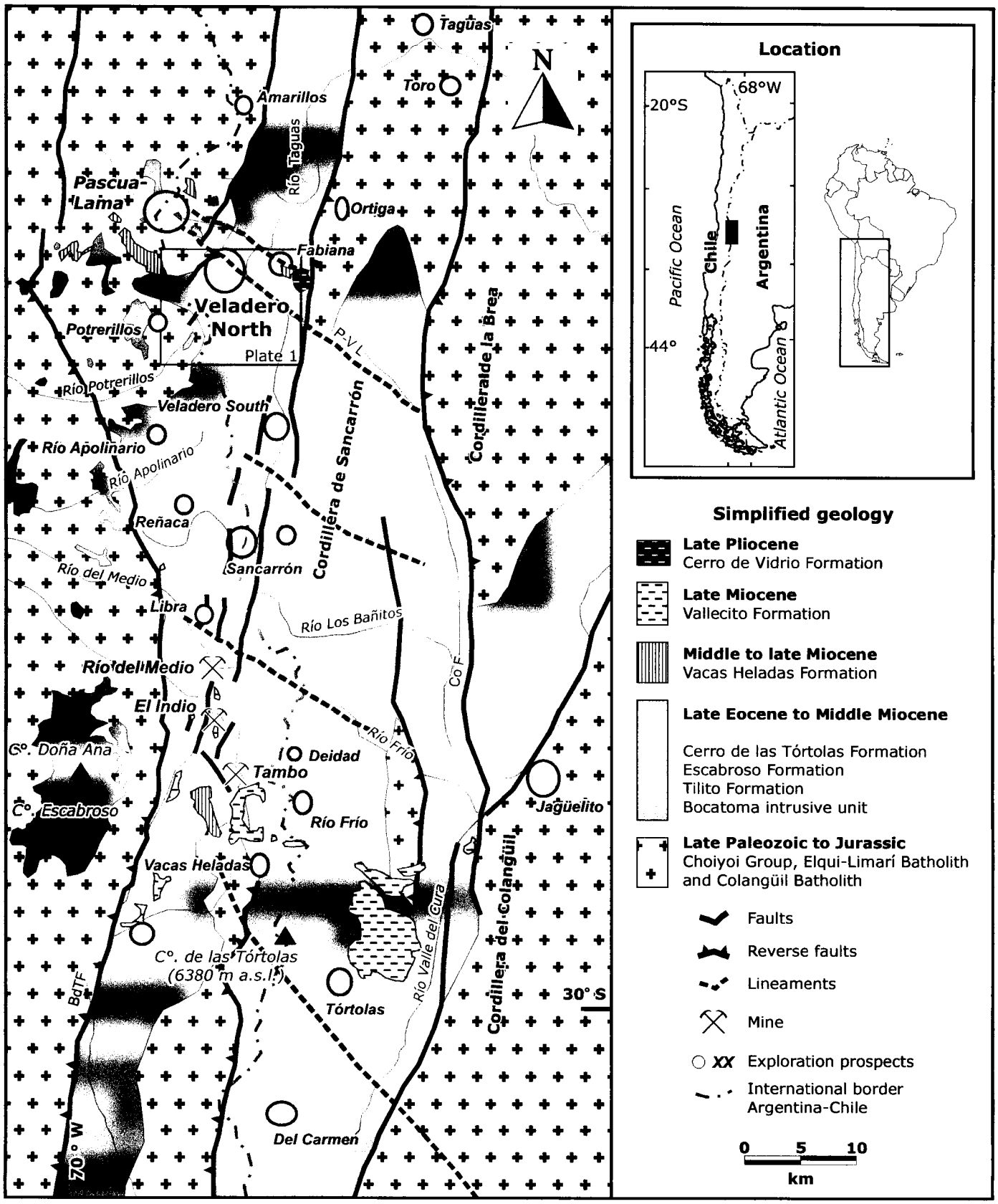

Figure 1-1: Regional Geology of the El Indio-Pascua Belt and location of major alteration zones and mines. Modified from Bissig et al. (2001). Box represents the study area and the location of the 1:20,000 scale map in Plate 1. Abbreviations: BdTF=Baños del Toro Fault, P-V L= Pascua-Veladero Lineament, Co F=Colangüil Fault.

Mesozoic (e.g. Martin et al., 1995). Porphyry and epithermal systems as well as Cenozoic and Paleozoic igneous units record the evolution of the convergent margin and define the tectonic setting in which they were emplaced. The absence of thick Mesozoic sedimentary units characterizes the Cordillera Frontal, and differentiates the morphostructural province where the El Indio-Pascua Belt is entirely comprised from the Cordillera Principal to the south (e.g. Hervé et al., 1987).

The purpose of this study is to clarify the geology of the Veladero North epithermal deposit at the northern end of the El Indio-Pascua Belt. The deposit is the southernmost of three epithermal deposits, Pascua, Lama and Veladero that are aligned along a WNW trending zone. Specifically, the aim is to map the distribution and structure of lithostratigraphic units and to determine their age. This work provides the foundation upon which to build a mineralization model of the Veladero North deposit, and is a prelude to further regional investigation in the Argentinan side of the El Indio-Pascua Belt.

Methodology

Geological mapping of the over 120 km^2 study area was done at 1:10,000 scale using aerial photos and GPS to locate the scattered outcrops among the colluvial covered slopes. In total, approximately four months were spent in the field. The collected field data included lithology, alteration and structural fabrics as well as rock samples (see appendix II for data collection stations). Field mapping also recorded the location of planar landforms recently interpreted as Miocene erosion surfaces (Bissig et al., 2001).

Eight volcanic units and four intrusive phases were defined based on stratigraphy and lithology. Ninety-two samples were prepared for petrographic analysis to describe unit lithologies and mineralogical assemblages. An initial suite of 68 samples representing the least altered rocks was submitted to Bondar-Clegg in Vancouver for major and minor element analysis via X-Ray Fluorescence (XRF). Based on the petrology

and the initial geochemistry, 34 samples were selected and sent to Memorial University of Newfoundland for Inductively Coupled Plasma Mass Spectrometry (ICP-MS) analysis (See appendix III for detection limits). The high-quality of the ICP-MS data provided a basis to compare the igneous chemistry from the Veladero North area with previous studies in the El Indio-Pascua Belt (Bissig, 2001; Kay et al., 1987; Malizia et al, 1997; Mpodozis and Kay, 1992; Llambías and Sato, 1990).

Twelve rock samples from intrusive and volcanic units were dated using conventional U-Pb techniques in the Geochronology Laboratory of the University of British Columbia. Three additional Sensitive High-Resolution Ion Microprobe (SHRIMP) U-Pb age determinations were completed in the facilities of Stanford University, California by Richard Tosdal (written communication, 2002). The U-Pb method was required in this study because the pervasive and locally intense hydrothermal alteration of the rocks around the Veladero North epithermal deposit preclude the use of other techniques (e.g. K-Ar system).

Presentation

This research is presented as two separate scientific communications that will be submitted to peer-reviewed journals for publication.

The first communication, entitled "Late Paleozoic to early Mesozoic rocks of the Cordillera Frontal of Argentina and Chile with emphasis on the Veladero North Area, San Juan Province, Argentina" (Chapter 2), describes the Permian volcanic, volcaniclastic and intrusive rocks that account for as much as half of the outcrops of the study area, and although previously unrecognized, may be a significant host to gold, as they are at Pascua. The late Paleozoic rocks are unmetamorphosed and have the same overall petrologic character when altered as do the Cenozoic rocks, which are largely late Oligocene to Miocene in age (Martin et al., 1995). In many cases, major and trace-element geochemistry or geochronological studies can distinguish the rocks of such

disparate age. The chapter also reviews available geochronologic and geochemical information of the Cordillera Frontal of Argentina and Chile, and proposes a revision of the magmatic stratigraphy with special attention to the volcanic rocks that form the Choiyoi Group. The latter volcanic rocks are a major rock unit in the study area.

The second communication (Chapter 3) focuses on the Miocene volcanic sequences that hosts the Veladero North epithermal deposit. The primary objective is to document the character and age of the volcanic rocks, structural geometry and timing of deformation in the Veladero North area. The local information is then combined with regional data to place the study area in a geologic context. This chapter also evaluates whether specific volcanic rocks might be related to the mineralization in the area.

Complementary information is presented in the appendixes of the thesis. The Appendix I is a detailed description of the methodology and results obtained by U-Pb geochronology and referred to in the text. The Appendixes II to IV group additional data regarding sample location, geochemistry and alteration.

Alteration

Hydrothermal alteration is superimposed on practically all rocks around the Veladero North epithermal deposit. Determination of the precise nature and timing of the hydrothermal alteration, and hence of the mineralization in the study area, are beyond the scope of this research. Although such investigations are currently in progress (e.g. La Motte, in prep.), the present contribution does not benefit from preliminary or unpublished results. Discussion of mineralization and alteration of the Veladero North deposit (Chapter 3) is based on data collected immediately north of the study area as part of a region-scale investigation (Bissig et al., 2001).

Four major hydrothermal alteration events have been documented in the Cenozoic rocks of El Indio-Pascua Belt. Geochronologic studies suggest that, although discrete hydrothermal activity has been associated with every magmatic episode

between ~36 Ma and ~11 Ma, auriferous epithermal mineralization is limited to the 9.5 Ma to 6 Ma interval (Bissig et al., 2001). In addition, late Paleozoic to Jurassic subvolcanic porphyries also have associated alteration halos, although these appear to be barren and of more limited extent.

In the Veladero North area, recognized alteration assemblages are propyllitic, advanced argillic and silicic (Deyell, 2001; Bissig, 2001; Jones et al., 1999). Typical assemblages in propylitic alteration zones consist of chlorite, clays (kaolinite-illite) with rare epidote. Fine-grained masses of clays partly replace feldspars and ferromagnesian minerals. Pyrite is an accessory component but, if present, is finely disseminated. The rock texture is normally preserved in this type of alteration. Advanced argillic alteration is characterized by alunite, quartz and clays (kaolinite, illite, dickite or pyrophyllite). The altered rock is pervasively replaced and the original texture is commonly obliterated. Silicified rocks are widespread in the study area. Commonly, if the clays have been leached out, the resulting alteration assemblage is formed exclusively by quartz, and the texture and the original mineralogy of the rock are completely obliterated. The spatial association of silicification and gold mineralization is of particular interest on the Veladero North area. Mineralogical and geochemical characteristics of the alteration assemblages were extensively described by Deyell (2001) and are listed in the Appendix IV.

References

Barazangi, M., and Isacks, B.L., 1976, Spatial distribution of earthquakes and subduction of the Nazca Plate beneath South America: Geology (Boulder), v. 4, p. 686-692.

Barrick 2002, (http://www.barrick.com/6_About_Barrick/6_02_History.asp).

Bissig, T., 2001, Metallogenesis of the Miocene El Indio-Pascua gold-silver-copper Belt, Chile/Argentina: geodynamic, geomorphological and petrochemical controls on epithermal mineralization [Ph.D. thesis]: Kingston, Queen's University.

Bissig, T., Lee, J., W, Clark, A., H, and Heather, K., B, 2001, The Cenozoic history of volcanism and hydrothermal alteration in the Central Andean Flat-Slab Region: New ^{40}Ar-^{39}Ar constraints from the El Indio-Pascua Au (-Ag, Cu) Belt, 29°20'-30°30' S: International Geology Review, v. 43, p. 312-340.

Bissig, T., Clark, A., H, Lee, J., W, and Hodgson Jay, C., 2002, Miocene Landscape Evolution and Geomorphologic Controls on Epithermal Processes in the El Indio-Pascua Au-Ag-Cu Belt, Chile and Argentina: Economic Geology, v. 97, p. 971-996.

Deyell, C.L., 2001, Alunite and high sulfidation gold-silver-copper mineralization in the El Indio-Pascua belt, Chile-Argentina [Ph. D. thesis]: Vancouver, Mineral Deposit Research Unit. University of British Columbia. Canada.

Hervé, F., Godoy, E., Parada, M.A., Ramos, V., Rapela, C.W., Mpodozis, C., and Davidson, J., 1987, A general view on the Chilean-Argentine Andes, with emphasis on their early history, in Monger, J.W.H., and Francheteau, J., eds., Circum-Pacific orogenic belts and evolution of the Pacific Ocean basin., Volume 18: Geodynamics Series: Washington, DC, United States, American Geophysical Union, p. 97-113.

Jones, P.J., Martínez, R.D., Vitaller, A.O., Chavez, I., Carrizo, M.M., La Motte, M.G., and Riveros, S.E., 1999, El Depósito Epitermal Aurífero Veladero, San Juan, in Zappettini, E.O., ed., Recusos Minerales de la República Argentina, Volume Anales 35: Buenos Aires, Instituto de Geología y Recursos Minerales SEGEMAR, p. 1673-1648.

Jordan, T.E., Isacks, B.L., Allmendinger, R.W., Brewer, J.A., Ramos, V.A., and Ando, C.J., 1983, Andean tectonics related to geometry of subducted Nazca Plate: Geological Society of America Bulletin, v. 94, p. 341-361.

Kay, S.M., Maksaev, V., Moscoso, R., Mpodozis, C., and Nasi, C., 1987, Probing the evolving Andean lithosphere; mid-late Tertiary magmatism in Chile (29 degrees - 30 degrees 30') over the modern zone of subhorizontal subduction: Journal of Geophysical Research, B, Solid Earth and Planets, v. 92, p. 6173-6189.

Llambías, E.J., Sato, A.M., and Castro, C.E., 1990, Relaciones entre el grupo Choiyoi y el Batolito de Colangüil, Actas del Décimo primer Congreso Geológico Argentino, Volume 1: San Juan, Asociación Geológica Argentina, p. 79-82.

Malizia, D., Limarino, C.O., Sosa Gomez, J., Kokot, R., Nullo, F.E., and Gutierrez, P.R., 1997, Hoja geológica Cordillera del Zancarrón (Provincia de San Juan) N° 3169-26 y 25: Buenos Aires, Servicio de Geología y Minería de Argentina (SEGEMAR), 197 p.

Martin, M.W., Clavero, J., Mpodozis, C., and Cuitiño, L., 1995, Estudio geológico regional de la franja El Indio Cordillera de Coquimbo, Servicio Nacional de Geología y Minería, Compañía Minera San José, 238 p.

Mpodozis, C., and Kay, S.M., 1992, Late Paleozoic to Triassic evolution of the Gondwana margin; evidence from Chilean Frontal Cordilleran batholiths (28° S to 31° S); with Suppl. Data 92-22: Geological Society of America Bulletin, v. 104, p. 999-1014.

Chapter 2

Late Paleozoic to early Mesozoic rocks of the Cordillera Frontal of Argentina and Chile with emphasis on the Veladero North Area, San Juan Province, Argentina

Abstract

In the Veladero North area, located in the Cordillera Frontal of Argentina and Chile, late Paleozoic rocks form homoclinal or smoothly folded volcanic sequences that define three north-south trending structural packages; each comprising similar volcanic, volcaniclastic and intrusive rocks. The sequence is included within the Choiyoi Group and is separated from Tertiary units by an angular unconformity or by Tertiary thrust or normal faults. Rhyolitic to dacitic ignimbrite with varying degrees of welding is the dominant extrusive facies, followed by interbedded volcaniclastic sandstone and conglomerate beds. Relatively small (less than 1 km^2), intensely altered, plagioclase- and quartz-bearing dacitic to rhyolitic stocks intrude the volcanic rocks. Uranium-lead geochronology and distinct geochemical characteristics indicate that volcanic and intrusive rocks in the study area are equivalent, and were emplaced between 259 ± 0.7 Ma and 254 ± 4.2 Ma.

Revision to published and new geochronologic data hint that late Paleozoic to Mesozoic magmatic activity in the Cordillera Frontal occurred during distinct episodes. Plutonism is represented by the (320 Ma to 280 Ma) Guanta and Cochiguás units, the (270 Ma to 325 Ma) Chollay-El León Unit and the (220 Ma to 190 Ma) Los Colorados and Carricitos units. The (275 Ma to 250 Ma) Guanaco Sonso Formation and the (225 Ma to 210 Ma) Los Tilos Formation constitute two independent volcanic episodes that overlap partially with plutonic events, suggesting diachronism between plutonic and volcanic pulses.

Introduction

Paleozoic to early Mesozoic magmatism along the Pacific margin of southern South America (Gondwana) extended from northern Perú to southern Argentina over a distance of almost 5000 km (Mpodozis and Kay, 1990, 1992; Kay *et al.*, 1989; Ramos *et al.*, 1988; Bell, 1987; Mpodozis and Ramos, 1989; Petersen, 1999; MacFarlane *et al.*, 1999; Sato and Llambías, 1993). Magmatism was accompanied by complex transpressional and extensional tectonic regimes that are poorly constrained (Mpodozis and Ramos, 1989; Kay *et al.*, 1989; González Bonorino, 1991). In particular, the recent proposals linking Paleozoic margin activity to early Paleozoic interactions between Gondwana and Laurentia (North America) remain a topic of current debate (Dalziel, 1997; Ramos, 1988; Hervé, 1988). Establishing whether such a linkage existed is important because Paleozoic and early Mesozoic geology strongly influenced the younger and superposed middle Mesozoic to Recent Andean arc (e.g. Ramos *et al.*, 1996).

The 2500-km long segment of late Paleozoic to early Mesozoic rocks between northern Chile-western Bolivia and southern Argentina is the best known part of the Gondwanan arc (Figure 2-1). Through reconnaissance geological studies, plutonic complexes and volcanic successions with local formation names have been broadly grouped into Paleozoic arc rocks or into a Gondwana granite-rhyolite province, or simply referred to as pre-Andean magmatic rocks (Mpodozis and Kay, 1990, 1992; Ramos, 1988; Parada, 1990; Heredia *et al.*, 2002). These rocks in central Chile have been well documented by mapping at different scales (Mpodozis and Cornejo, 1988; Nasi *et al.*, 1990; Martin *et al.*, 1995; 1999). Reconnaissance geochemical and geochronological studies support the established stratigraphic relationships (Pankhurst *et al.*, 1996; Parada *et al.*, 1991; Parada, 1990; Mpodozis and Kay, 1990; Ribba *et al.*, 1988; Nasi *et al.*, 1985).

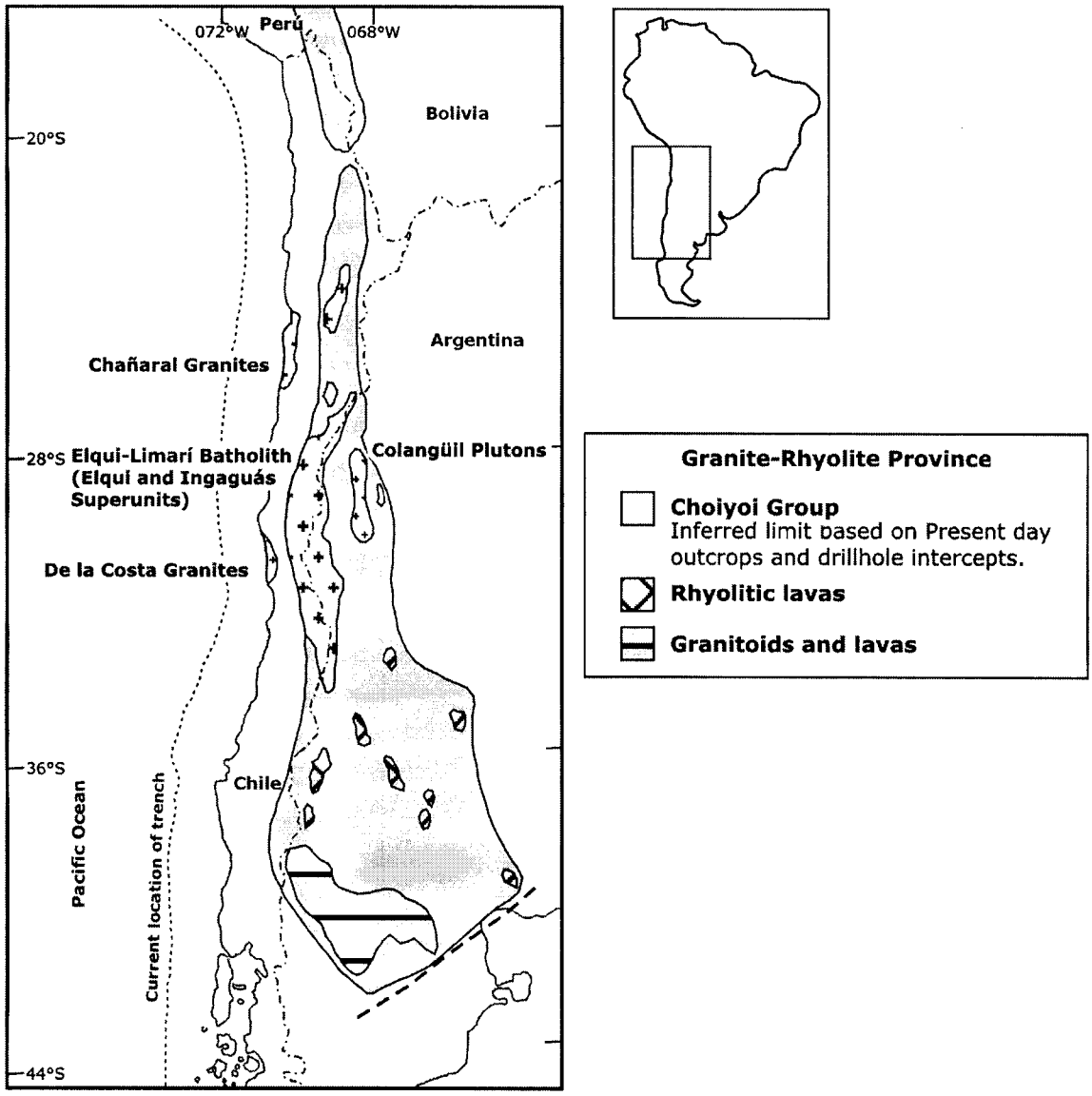

Figure 2-1: Distribution of late Paleozoic - early Mesozoic magmatism of western South America. Modified from Kay et al. (1989) and Petersen (1999). Southeastern boundary of the granite-rhyolite province (dashed line) is represented by the approximate contact with the Chon-Aike volcanic province (not shown).

In stark contrast to Chile, the late Paleozoic and early Mesozoic Gondwanan arc in Argentina is poorly understood (Heredia *et al.*, 2002; Malizia *et al.*, 1997; Llambías and Sato, 1995). Most studies in the Argentinan Andes have focused on Tertiary rocks (e.g. Bissig, 2001). The volumetrically more important Paleozoic to early Mesozoic rocks have been largely ignored except for several local investigations of Paleozoic volcanic sequences and plutonic complexes (Sato and Llambías, 1993; Rapalini and Vilas, 1991; Llambías *et al.*, 1990; Llambías and Sato, 1990, 1995; Llambías *et al.*, 1987). As a

general rule, all Paleozoic volcanic rocks in Argentina are assigned to the Choiyoi Group, which is part of the granite-rhyolite province. Locally, the rocks have been subdivided into formations (Mirré, 1966; Coira and Koukharsky, 1976; Rodríguez Fernández *et al.*, 1997; Heredia *et al.*, 2002), but the distribution of the formations throughout the granite-rhyolite province is not known, nor are their temporal relationships. Both features limit the regional utility of formation names and they are not used herein except for those in the region adjoining the study area.

Miocene shortening in the Veladero North (Argentina) and Pascua-Lama (Chile-Argentina) (Figure 2-5) area has superposed contrasting late Paleozoic volcanic and subvolcanic rocks as well as granitic rocks (Nasi *et al.*, 1985; Nasi *et al.*, 1990; Martin *et al.*, 1995, 1999; Bissig, 2001; Charchaflie *et al.*, 2002). This chapter examines the Paleozoic rocks found in several of the Miocene thrust sheets in the Veladero North area. The 1:10,000 scale mapping, together with U-Pb geochronologic and geochemical data provide the basis for establishing a late Paleozoic geologic framework for the Veladero North and Pascua-Lama areas (Martin *et al.* 1995, 1999; Bissig, 2001). Collectively, the late Paleozoic igneous framework established in this portion of the Andean Cordillera provides a starting point for addressing the definition of a late Paleozoic framework for the eastern flank of the Andes.

Regional late Paleozoic to early Mesozoic geologic framework

Morphostructural elements

The Chile-Argentina Andes between 28°S and 33°S (Figure 2-2) comprise four morphostructural elements including, from west to east, Cordillera de la Costa, Cordillera Principal, Cordillera Frontal and Precordillera.

Late Paleozoic sedimentary and volcanic rocks unconformably overlain by a thin

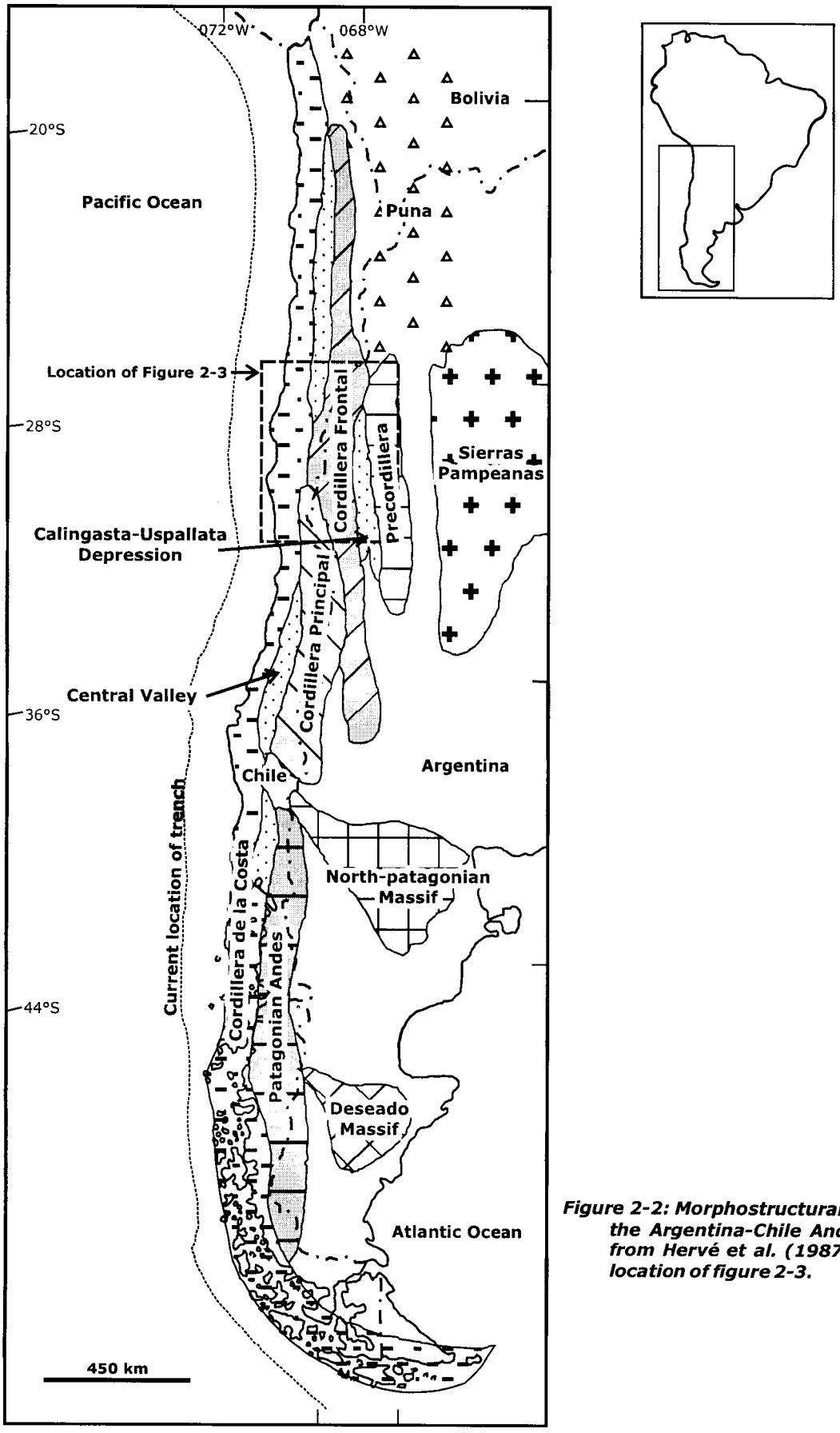

Figure 2-2: Morphostructural elements of the Argentina-Chile Andes modified from Hervé et al. (1987). Outline of location of figure 2-3.

veneer of Tertiary rocks underlie the Cordillera Frontal of Argentina and Chile. Towards the southwest, deformed Mesozoic rocks underlie the Cordillera Principal. A Tertiary (?) tectonic depression, the Central Valley, separates the Cordillera Frontal from the paired metamorphic belt that outcrops along the present coastline of Chile in the Cordillera de la Costa. To the east, the Calingasta-Uspallata depression defines the boundary between the Cordillera Frontal and the Precordillera. Allochthonous Ordovician to Devonian sedimentary rocks that form most of the Precordillera are not found in the adjacent Cordillera Frontal. Ramos and others (1984, 1986) proposed that Chilenia, the basement of the Cordillera Frontal, was accreted to South America during Devonian times. Since the Devonian, both morphostructural elements share a common geologic evolution. Carboniferous sedimentary rocks that cover the early to middle Paleozoic rocks in the Precordillera are also present in the Cordillera Frontal and constitute the youngest common lithological unit between these morphostructural elements.

Basement

Two early Paleozoic metamorphic complexes and sedimentary sequences form the basement of the Cordillera Frontal. The oldest known rocks are early Paleozoic (?) micaceous orthogneisses known as La Pampa gneisses, which were metamorphosed in the Silurian (415 ± 4 Ma, Ribba *et al.*, 1988). The gneisses have a restricted distribution and are the metamorphosed remanent of the Chilenia terrane sialic crust (Ribba *et al.*, 1988). Middle Paleozoic metabasites, quartz-muscovite schists, quartzites and marbles form the El Tránsito Metamorphic Complex in northern Chile (Ribba *et al.*, 1988; Hervé, 1982). Whereas the age of the protolith is not known, Ribba and others (1988) argue that they were metamorphosed around 335 ± 20 Ma or 304 ± 40 Ma, based on poorly defined Rb-Sr isochrons, referred to as "error-chrons". The El Tránsito Metamorphic Complex represents the Carboniferous forearc accretionary prism formed during eastward subduction beneath Chilenia terrane (Ribba *et al.*, 1988; Ramos *et al.*, 1984).

Late Carboniferous and Early Permian quartz-feldspar sandstone and siltstone, as thick as 7000 metres, form the eastern margin of the Cordillera Frontal and are known in the western flank of the Andes (Figure 2-3). In Chile, these rocks, known as Las Placetas Formation, contain marine fossils and flora of Late Carboniferous age. Las Placetas Formation represents shallow marine and lacustrine deposits formed in intra-arc basins (Bell, 1985, 1987). In Argentina at the latitude of the El Indio Belt, equivalent rocks of the Cerro Agua Negra Formation consist of sandstones, greywackes, siltstones and minor conglomerates locally metamorphosed by late Paleozoic and Tertiary intrusives. Malizia *et al.* (1997) proposed that the sedimentary rocks evolved from marine nearshore and deltas in the lower section to continental facies in the middle and upper sections. This sedimentary sequence was deposited in a back arc basin located east of the Gondwana plutons (Ramos, 1988).

Gondwana Magmatism

Late Paleozoic volcanic rocks in Argentina are included within the Choiyoi Group, one of the major rock packages of the granite-rhyolite province (Kay *et al.*, 1989). The Choiyoi volcanic province and four batholiths, Montosa-El Potro, Chollay and Elqui-Limarí in Chile and the Colangüil in Argentina constitute the Gondwana magmatic products in the northern part of the Cordillera Frontal. Batholiths in the western margin of South America have been divided into Units and Superunits following the petrologic division in the Coastal Batholith of Perú (Cobbing and Pitcher, 1972). Units that are common throughout the batholiths are defined on the basis of similarities in texture, colour, composition and contact relationships. An assemblage of units that occurs in close association and that has similar relative and absolute ages form superunits. In Chile, Nasi and others (1985) grouped the Montosa-El Potro, Chollay, and Elqui-Limarí batholiths into two Superunits: Elqui and Ingaguás. The Colangüil Batholith, although formed by independent intrusive units, is not referred to as a Superunit in the literature, but could be considered to constitute a similar set of related igneous rocks (Figure 2-4).

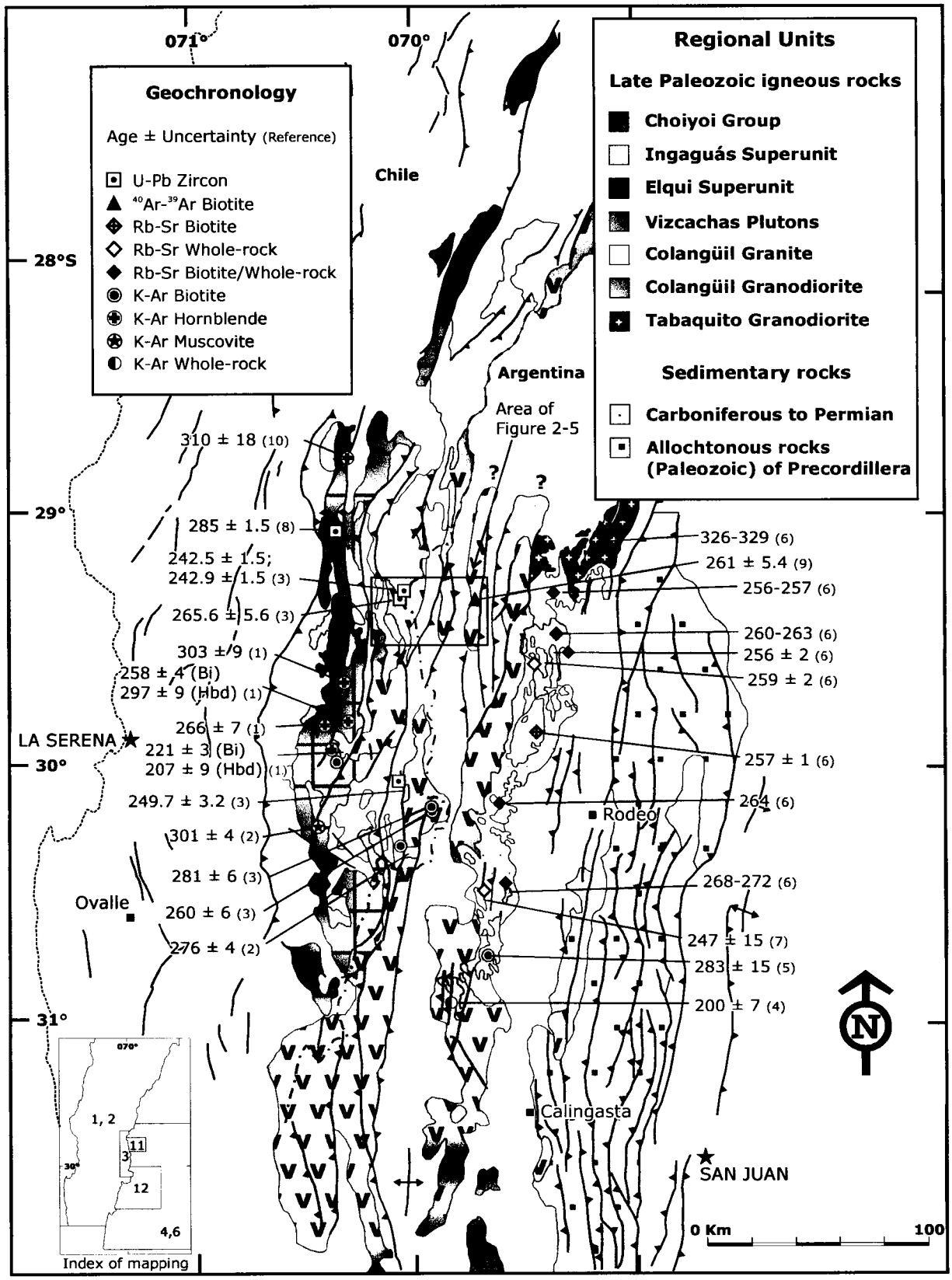

Figure 2-3: Geology of the Cordillera Frontal of Argentina and Chile and geochronological data summary. Compiled from: 1: Nasi et al., 1985; 2: Mpodozis and Cornejo, 1990; 3: Martin et al., 1995; 4: Rodríguez Fernández et al., 1997; 5: Linares and Llambías, 1974; 6: Llambías and Sato, 1995; 7: Sato and Kawashita, 1988; 8: Pankhurst et al., 1996; 9: Bissig, 2001; 10: Hervé in Ribba, 1985; 11: Malizia et al., 1997; 12: Cardó et al., 2000. Uncertainties reported as published.

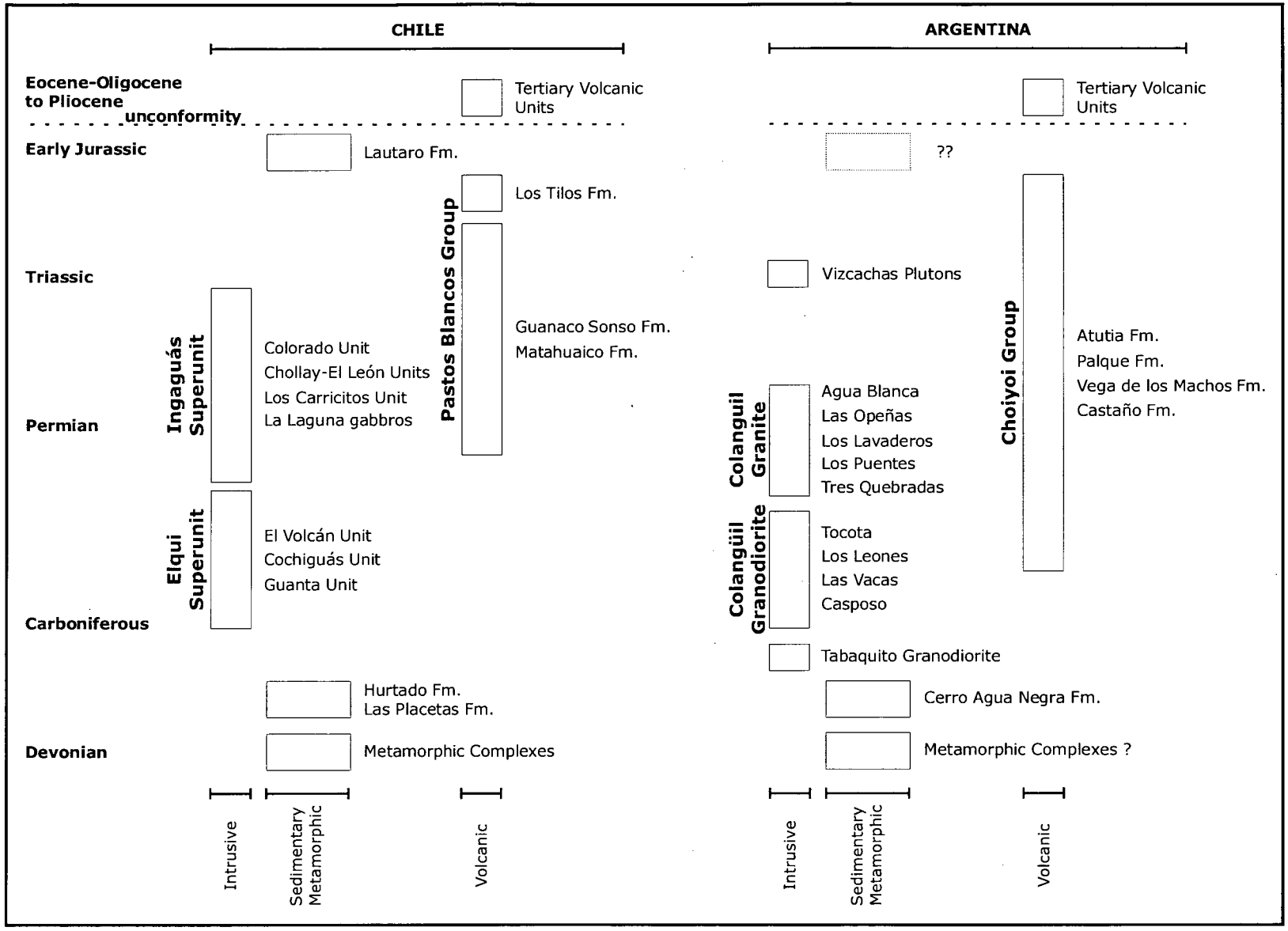

Figure 2-4: Relative magmatic stratigraphy in the Cordillera Frontal of Argentina and Chile. Field cross-cutting relationship define the position of the Units and Batholiths in the column. Compiled from Nasi et al. (1985), Sato and Llambías (1993) and Llambías and Sato (1995).

Volcanic rocks

Choiyoi Group

The Choiyoi Group in Argentina is the extensive volcanic sequence outcropping throughout the Cordillera Frontal and to the north and southeast in the Cordillera Principal and Precordillera (Figures 2-1 and 2-3). Initially referred as "Choiyoilitense" after an Araucano name (Groeber, 1946), it was first defined as a formation in west-central Argentina (Rolleri and Criado Roque, 1969) and elevated to group status once regional studies defined an internal stratigraphy and demonstrated the lateral equivalence of locally delimited formations (Stipanicic *et al.*, 1968). Equivalent rocks in Chile are known as far north as the Bolivian border over a distance close to 2500 km long (Figure 2-1). The Choiyoi Group is divided into a lower, andesitic section and an upper rhyolitic section. In the western flank of the Cordillera Frontal (Chile), most rocks are part of the upper section; the lower member is not well known.

In the eastern part of the Cordillera Frontal (Argentina), a relatively thin (~250 m) sequence of andesite, minor dacite, clastic rocks and basalt forms the lower andesitic section of the Choiyoi Group (Cortés, 1985; Llambías and Sato, 1993; Caminos, 1979). Volcanic rocks and lesser conglomerates from the lower section unconformably overlie Late Carboniferous rocks. K-Ar and Rb-Sr geochronology (297 Ma to 289 Ma) from volcanic and intrusive rocks indicate a Late Carboniferous age for the lower section (Vilas and Valencio, 1982; Mpodozis and Cornejo, 1988; Llambías and Sato, 1993). The basalts have arc affinities and reflect deposition in a normal-subduction setting (Poma and Ramos, 1994). Sato and Llambías (1993) postulated that the andesites are broadly equivalent to the calc-alkaline granodiorites of the Colangüil Batholith and to the early phases of the Elqui Superunit (see below and Figure 2-4).

Table 2-1: Lithology and geochemistry of Gondwana magmatic products in the Cordillera Frontal (Argentina-Chile)

	Unit	Lithology	Mineralogy	Geochemistry	initial $^{87}Sr/^{86}Sr$
(1, 2)	**Guanta**	Tonalite Granodiorite	Coarse Grained Hornblende and Biotite	55-69% SiO2 Metaluminous ASI= 0.88 to 0.94 medium- high K Ta-Ti depleted /La Th-U-alkalis enriched LREE depleted Low Sr Negative Eu Concave-up REE End -2.9-3.7	0.7058- 0.7063
(1, 2)	**Montosa**	Granodiorite	Biotite and Hornblende	65-73% SiO2 Peraluminous ASI= 1-1.08 flat HREE	
(1, 2)	**Cochiguás**	Granodiorites Monzodiorites	Muscovite or Biotite	73-74% SiO2 Peraluminous ASI = 1.14-1.18 Steep HREE Variable Eu anomaly	~ 0.707
(1, 2)	**El Volcán**	Granite Granodiorite	Coarse to very coarse Biotite	71-77% SiO2 Peraluminous ASI = 1.06-1.18 High K2O Low K2O/ Na2O Large Negative Eu anomaly LREE flattest in SiO2 rich rocks	0.708- 0.724
(1, 2)	**Los Carricitos**	Granodiorite	Medium grained Biotite and Hornblende	68-70% SiO2 Low K2O Alkalis enriched Ti-Ta depleted Meta to Peraluminous ASI = 0.95-1.14 High Sr Steep LREE Moderate to steep HREE Small Eu anomaly	0.7046- 0.7052
(1, 2)	**Chollay**	Monzogranite Syenogranite Granodiorite	Coarse Grained	69-78% SiO2 High Na2O (>3%) K2O variable Metaluminous to peraluminous ASI = 0.96-1.14	0.704
(1, 2)	**El León**	Monzogranite	Biotite		0.705 - 0.706
(1, 2)	**El Colorado**	Monzogranite Porphyritic rhyolites		Flat REE Moderate to large negative Eu anomaly	0.705 - 0.706
(3)	**Tabaquito Granodiorite**	Granodiorite	Biotite and amphibole	65-70% SiO2 Metaluminous high-K High Sr/Rb High LIL/ HSF	0.7052-0.7065
(3,5,6)	**Colangüil Granodiorites**	Granodiorites Quartz diorite Monzodiorite	Biotite or amphibole	55-67% SiO2 Metaluminous to peraluminous A/CNK 0.82-1.17 more sodic than potassic High LIL/ HSF	0.7041-0.7064
(3,5,6)	**Colangüil Granites**	Granites Leucogranites		72-77% SiO2 Peraluminous A/CKN 0.99-1.23 K2O/Na2O 1.24-1.99	0.7072-0.7045
		Las Opeñas	Cordierite	High HSF (Nb, Y, Zr, Th)	0.7099-0.7130
(5,6)	**Vizcachas Plutons**	Tonalite Granites (Subvolcanic Andesites)		High-K metaluminous 0.93-1	
(3,5,6)	**Choiyoi Group**	Andesites		54-67% SiO2 Metaluminous to peraluminous A/CNK 0.9-1.06	0.7057
		Rhyolites		70-76% SiO2 Peraluminous A/CNK 0.99-1.31 Depleted Sr and Ba	0.7081

(1):Mpodozis and Kay (1990, 1992); (2):Nasi et al. (1985); (3): Llambías and Sato (1995); (4): Sato and Llambías (1993); (5): Heredia et al. (2002); (6): Rodríguez Fernández et al. (1999).

Rhyolitic and dacitic flows with subordinate continental clastic rocks form the upper and better-known section of the Choiyoi Group. The thickness of the upper section is typically obscured by Tertiary faults, but may be as much 2000 m or more in thickness (Groeber, 1946; Caminos, 1976, Thiele, 1954; Mpodozis and Cornejo, 1988; Heredia *et al.*, 2002). Permian fossiliferous rocks, such as the Matahuaico Formation in Chile, are interfingered within the volcanic sequence. In contrast, Liassic marine sedimentary rocks or Late Triassic continental sequences cover the Choiyoi Group in the Cordillera Principal. In the El Indio Belt to the west of Veladero North, silicic rocks equivalent to the Choiyoi Group are currently known as the Pastos Blancos Group (Thiele, 1964; Nasi *et al.*, 1990; Mpodozis and Cornejo, 1988; Martin *et al.*, 1999).

The volcanic Guanaco Sonso Sequence forms the base, and the bimodal Los Tilos Sequence forms the top of the Pastos Blancos Group. Rhyolitic welded ashflow tuffs and minor volcaniclastic rocks form the Guanaco Sonso Sequence. K-Ar biotite ages of 281.0 ± 6 Ma, 262.0 ± 6 Ma and 260.0 ± 6 Ma as well as U-Pb zircon age of 265.8 ± 5.6 Ma (Martin *et al.*, 1999) indicate a Permian age for the rocks. Bimodal basaltic-andesitic to dacitic volcanic rocks and sedimentary rocks form the Los Tilos Sequence. A dacitic tuff from this unit yielded a Middle Triassic K-Ar biotite age of 235.0 ± 5.0 Ma (Martin *et al.*, 1999). Geochronological studies are not conclusive on the minimum age of Los Tilos Sequence. In Argentina, Rodríguez Fernández *et al.* (1997) and Malizia *et al.* (1997) report Late Triassic K-Ar whole-rock ages (Table 2-2). Based on the gradational nature of the upper contact of Los Tilos Sequence with Early Jurassic Lautaro Formation, Martin *et al.* (1999) proposed that the transition is Early Jurassic in age, the estimated maximum age of the overlying formation. As defined, the Pastos Blancos Group lacks an andesitic basal section and tentatively extends into the Jurassic, but otherwise is comparable to the Choiyoi Group.

The geochemistry of the upper, rhyolitic section of the Choiyoi Group has not been studied in detail. Sato and Llambías (1993) point out that the rhyolites and the

granites of the Colangüil Batholith have similar major and trace element geochemistry and ^{87}Sr-^{86}Sr initial ratios. They propose a common magmatic origin because the granites and rhyolites are spatially related. Likewise, Martin and others (1999) correlate the Los Tilos Sequence to El Colorado Unit (see Ingaguás Superunit below) in the El Indio Belt. Late Permian and Early Triassic units form post-orogenic volcanic successions produced by crustal melting inferred to correspond to an extensional tectonic environment (Llambías and Sato, 1995; Sato and Llambías, 1993; Mpodozis and Kay, 1992; Heredia *et al.*, 2002).

Plutonic rocks

Elqui Superunit

In west-central Chile, the Elqui Superunit as defined by Nasi and others (1985) comprises a series of tabular plutons that range from coarse grained and foliated gabbros to granite. These rocks constitute a belt in the western side of the Elqui-Limarí Batholith (Figure 2-3). The Guanta, Cochiguás and El Volcán Units form the Elqui Superunit.

Tonalite, hornblende-biotite granodiorite and minor diorite and gabbro of the Guanta Unit are the oldest known intrusive phase of the Gondwana magmatism. The intrusive rocks are Carboniferous based on K-Ar ages from amphiboles of 303 ± 9 Ma and 297 ± 9 Ma (Nasi *et al.*, 1985) and conventional U-Pb ages of 298 ± 2 Ma (Tosdal, unpublished data) and 285.7 ± 1.5 Ma (Pankhurst *et al.*, 1996). Granitoids of the Guanta Unit are metaluminous, calc-alkaline and have I-type affinities. Mpodozis and Kay (1992) associated the Guanta granitoids with a Late Carboniferous subduction zone.

Granodiorite and monzogranite with biotite and muscovite are the main lithologies of the Cochiguás Unit. Granitoids from the El Volcán Unit in Chile also range in composition from monzogranites to granodiorites, but muscovite is not a primary igneous mineral. They form two different units, although transitional contacts are very

common (Nasi *et al.*, 1985). El Volcán granitoids also crosscut Cochiguás plutons. Geochronologic data (K-Ar in muscovite of 301 ± 4 Ma from Mpodozis and Cornejo (1988) and a preliminary conventional U-Pb determination of 296 ± 3 Ma from Tosdal, unpublished data) indicate that the Cochiguás Unit is of similar age as the Guanta Unit. Geochronological study of the El Volcán Unit, however, is restricted to one K-Ar biotite age of 247 ± 4 Ma (Mpodozis and Cornejo, 1988). Although that age is consistent with the intrusive relationship between El Volcán and Cochiguás Units, analysis of the age patterns of the volcanic and plutonic rocks (see below) argues that the Permian age is a minimum. Based on transitional intrusive relationships only, the El Volcán plutons are inferred to be broadly time-equivalent to the Guanta and Cochiguás Units rocks. Cochiguás and El Volcán are peraluminous granitoids with low Na_2O-K_2O ratios and high FeO / MgO. High K_2O content of El Volcán Unit is a typical S-type granitoid feature that is not present in the Cochiguás plutons. Mpodozis and Kay (1992) inferred that the source of the bulk of both units was relatively shallow and that the older Cochiguás granitoids were formed in a feldspar-poor garnet-bearing thickened continental crust. Mpodozis and Kay (1992) (see also Rapalini, 1989; Rapalini and Vilas, 1991) suggest an oblique subduction setting at the time of formation of El Volcán and Cochiguás Units, an environment that should also apply to the broadly contemporaneous Guanta Unit.

Ingaguás Superunit

The Ingaguás Superunit forms the easternmost part of the Elqui-Limarí Batholith (Figure 2-3). The Superunit is predominately granitic and granodioritic in composition but includes subordinate gabbro. The main differences with the Elqui Superunit and the most common characteristics of Ingaguás rocks are the fine grain size, absence of deformation fabrics, common presence of miarolic cavities and very restricted occurrence of xenoliths and mafic dikes (Nasi *et al.*, 1985). Ingaguás plutons intrude the Elqui Superunit and rhyolitic units of the Pastos Blancos Group, which are equivalent to

the upper section of the Choiyoi Group. Nasi and others (1985), based on mineralogical and textural similarities, distinguished five plutonic units: La Laguna, Los Carricitos, El León, Chollay and El Colorado. Previous geochronological studies (Mpodozis and Cornejo, 1988; Nasi *et al.*, 1985) are not conclusive on the absolute age of the units and indicate a range of ages between 250 Ma and 207 Ma (Table 2-2).

The oldest plutons of the Ingaguás Superunit are 250 Ma to 240 Ma granitoids. Pink monzogranite, granodiorite and syenogranite with biotite and rare amphibole form the Chollay and El León Units (Nasi *et al.*, 1985). Martin and others (1999) prefer the composite name Chollay-El León to refer to those plutons and they include dacitic and quartz porphyries into this Unit. Limited major element geochemistry of the granitoids shows that the Chollay Unit is less siliceous than the El León Unit and that both units range from metaluminous to peraluminous compositions. The granitoids are inferred to have been emplaced in a relatively thin crust, under an extensional regime that followed the collision of an unrecognized terrane (Mpodozis and Kay, 1992).

The youngest plutons of the Ingaguás Superunit form a group that ranges in age from 212 Ma to 200 Ma, or as young as 190 Ma if ^{40}Ar-^{39}Ar dating (Bissig, 2001) is taken into account. Based on geochemical and petrological characteristics, the younger group should be further subdivided into Los Carricitos and El Colorado Units.

Biotite and hornblende granodiorite exclusively form the Los Carricitos Unit. The plutons of this unit represent a small volume of the Ingaguás Superunit, and they are intruded by the El Colorado Unit. Conventional U-Pb geochronology studies yields an age of 212 ± 2 Ma (Tosdal, unpublished data) in agreement with a hornblende K-Ar age of 207 ± 9 Ma (Nasi *et al.*, 1985). Los Carricitos Unit displays a distinctive geochemistry (high Sr, steep REE pattern and very small Eu anomaly) typically associated with a relatively high-pressure, plagioclase-poor, garnet-bearing source. Los Carricitos plutons have been interpreted as post-collisional granitoids that were formed at the base of a thick crust and emplaced during the initial stages of extension and relaxation (Mpodozis

and Kay, 1990, 1992).

Distinctive red granites intrude Elqui Superunit granitoids, the older parts of the Ingaguás Superunit and the Pastos Blancos Group and constitute the El Colorado Unit (Nasi *et al.*, 1985). Martin and others (1999), in their revision of the geology of the region, included within this unit quartz-feldspar rhyolitic porphyries and dikes, mafic intrusives that form dikes or hypabyssal bodies and medium to coarse-grained gabbro and diorite assigned to El León Unit and La Laguna Unit in previous 1:250000 scale maps (for example Nasi *et al.*, 1990). The bimodal nature of the El Colorado Unit has been correlated to the succession of andesite and dacite flows of the Los Tilos sequence (Martin *et al.*, 1999). From granitic rocks previously included in older plutonic suites, U-Pb geochronology yields an age of 201 ± 5 Ma (Tosdal, unpublished data) for the granitoids whereas an ^{40}Ar-^{39}Ar method on biotite from granite produced an age of 190.1 ± 3.2 Ma (Bissig, 2001). No intermediate rocks from the El Colorado Unit have been analyzed, but in general, the granites range from metaluminous to peraluminous compositions and none is peralkaline. REE patterns are consistent with a low-pressure, plagioclase-rich, garnet-free source (Mpodozis and Kay, 1992). El Colorado Unit, similar to Chollay-El León plutons, was emplaced in an extensional, post-collisional regime (Mpodozis and Kay, 1990, 1992). Proposed models for both Chollay-El León and El Colorado Units assume melting of large volumes of crust driven by the underplating of hot mantle material.

Colangüil Batholith

The Colangüil Batholith is located in west-central Argentina and represents the eastern extension of the Gondwana plutons. The north-striking belt formed by the Colangüil plutons was initially considered to represent an inner arc parallel to the outer Elqui-Limarí Batholith (Llambías *et al.*, 1987). Recent mapping in the Argentinan side of the Andes, supported by geochronological studies, extends the occurrence of late

Paleozoic to early Mesozoic plutons as far west as the international border between Argentina and Chile (Heredia *et al.*, 2002; Rodríguez Fernández *et al.*, 1997). Thus, the two batholiths may have formed a single entity that was further dismembered by Mesozoic and Cenozoic tectonics.

In west-central Argentina, the Colangüil Batholith contains a series of plutons that intrude Late Carboniferous sedimentary rocks and late Paleozoic volcanic rocks (Figure 2-3). The major units of the Colangüil Batholith are the Tabaquito Granodiorite, Las Piedritas Granodiorite, Colangüil Granite and the Vizcachas Plutons. They are monolithological and have similar known ages. Minor units include rhyolitic porphyries and dikes associated with the granitoids. The Colangüil plutons, unlike the Elqui Superunit, lack deformation fabrics and rocks with SiO_2 comprised between 68 and 72 wt%. The silica gap and difference in some major and trace element geochemistry underline the genetic independence between granodiorites and granites (Llambías and Sato, 1995, 1990; Sato and Llambías, 1993; Rodríguez Fernández *et al.*, 1997).

Biotite and hornblende granodiorite forms the Tabaquito Granodiorite that is the oldest unit with a calculated Rb-Sr isochron age of 329 Ma to 326 Ma (Llambías and Sato, 1995). Geochemical analyses indicate that the Tabaquito Granodiorite is a calc-alkaline, high Sr intrusion formed in a volcanic arc related to a destructive margin (Llambías and Sato, 1995).

The Las Piedritas Granodiorite includes five plutons (Las Piedritas, Romo, Tocota, Agua Negra and Los Leones) formed by amphibole and biotite granodiorite with reabsorbed xenoliths and fresh metamorphic inclusions. Isochron ages of the Las Piedritas plutons, calculated by the Rb-Sr method, span from 272 Ma to 260 Ma (Llambías and Sato, 1995, 1990). The calc-alkaline rocks formed by mixing of lower and upper crustal melts, emplaced during the waning stages of a subduction-related magmatic arc (Heredia *et al.*, 2002; Llambías and Sato, 1995, 1990). The granodiorites and probably some granites (e.g. the Los Patos Granite of Rodríguez Fernández *et al.*

(1997) located along the Argentina-Chile border in the central part of Figure 2-3) of the Colangüil Batholith are equivalent to the Guanta Unit in Chile.

Five biotite granite plutons form the Colangüil Granites Unit (Figure 2-4). The plutons composition is homogeneous throughout the batholith. The Las Opeñas granitic pluton is the only exception, and it is a cordierite-bearing intrusion (Llambías and Sato 1995, 1990). A Rb-Sr whole-rock isochron shows that the Colangüil Granites were emplaced in a very short period between 259 Ma and 257 Ma (Llambías and Sato, 1995; Sato and Llambías, 1993). Except for the Las Opeñas pluton, the slightly potassic and peraluminous Colangüil Granites share lithological and geochemical characteristics with the Ingaguás Complex in Chile (Llambías and Sato 1995, 1990). A post-collisional, extensional tectonic setting has been proposed at the time of emplacement of the granitic Colangüil plutons (Llambías and Sato 1995, 1990; Sato and Llambías, 1993).

Heredia *et al.* (2002) and Rodríguez Fernández *et al.* (1997) exclude from the Colangüil Batholith a series of small plutons located in the southern part of pre-Tertiary intrusive belt (Figure 2-3). The Vizcachas granodiorite is the larger intrusive but granite and tonalite also form the Vizcachas Pluton. A single K-Ar whole-rock analysis of the granodiorite yields an Early Jurassic age of 200 ± 7 Ma (Rodríguez Fernández *et al.*, 1997), similar to the age of the youngest plutons of the Ingaguás Superunit. Preliminary geochemistry (Rodríguez Fernández *et al.*, 1997) reveals that the Vizcachas pluton is formed by high-K calc-alkaline rocks with A/CNK less than one. Rodríguez Fernández and others (1997) justify the exclusion from the Gondwana magmatic cycle because the Vizcachas pluton has geochemical characteristics that conflict with the anorogenic nature predicted by Llambías and Sato (1995).

Veladero North area geologic setting

The El Indio Belt, where Pascua-Lama-Veladero North area is located, is entirely situated within the Cordillera Frontal morphostructural province (Figure 2-2). In the study area, late Paleozoic rocks form homoclinal or gently folded sequences that define three north-south structural packages and constitute the basement to the Tertiary volcanic sequence (Figure 2-5 and Plate 1). No contact with younger Mesozoic rocks is defined in the Veladero North area; this is in contrast to the gradational contact reported in Chile for the Lautaro Formation (Martin *et al.*, 1995, 1999). The top of the sequence and the base of the Tertiary strata is an angular unconformity, but more commonly, Paleozoic and Cenozoic rocks are found in separate thrust sheets. In the eastern part of the study area, late Paleozoic rocks are thrust over Oligocene volcanic rocks. Conversely, in the west of the mapped area, Tertiary volcaniclastic rocks unconformably cover Paleozoic rocks or they were brought into contact by normal faults. The age of normal faulting is not precisely constrained by geochronological data or field relations, however, normal faults are more likely to be Tertiary since they also offset Oligocene (?) volcaniclastic rocks. Thrusts faults are Tertiary as supported by field evidence and the age of a series of dacitic and andesitic intrusives emplaced along the faults (see Chapter 3 for discussion and timing of deformation).

From east to west, the structural packages are: Río Taguas, Guanaco Zonzo and Potrerillos-Canito. Each structural package contains stratigraphically equivalent volcanic, volcaniclastic and intrusive rocks. The following description focus on the lithological and geochronological aspects of the effusive and intrusive rocks and then summarizes their geochemical characteristics.

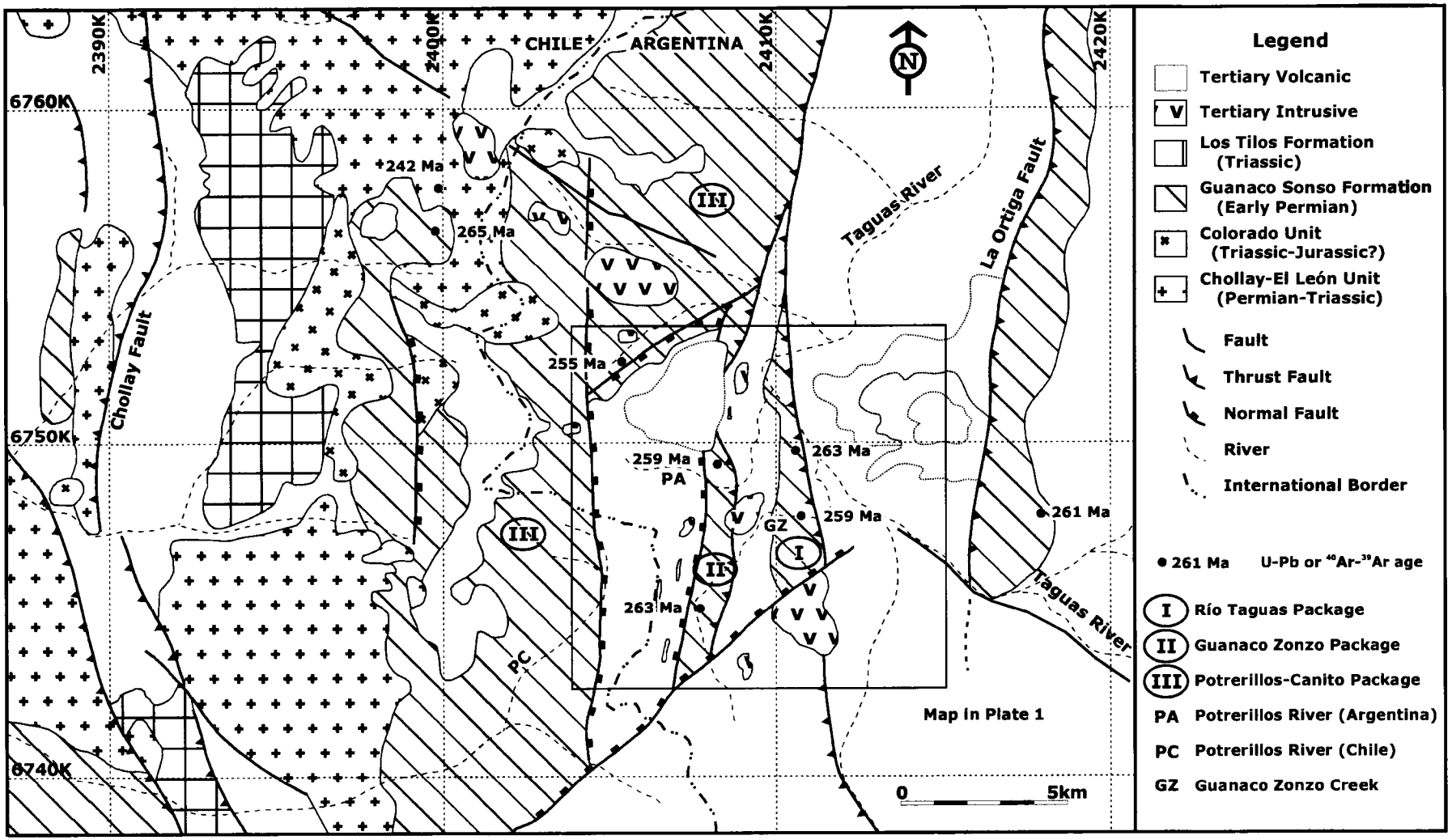

Figure 2-5: Geology of the Veladero North-Pascua-Lama area. Area mapped in detail enclosed in box and in Plate 1. Geology outside of detail map modified from Martin et al. (1999) and Deyell (2001).

Table 2-2: Compilation of previous geochronological studies in the Cordillera Frontal (Argentina and Chile)

Unit names, absolute ages and associated uncertainties are reported as published.

				Sub-Unit	Method	Material	Age	Uncertainty
Choiyoi-Pastos Blancos	Malizia et al., 1997 a-b			Choiyoi	K-Ar	WR	203	30
	Malizia et al., 1997 a-b			Choiyoi	K-Ar	WR	214	11
	Martin et al., 1995			Los Tilos	K-Ar	Bi	235	5
	Martin et al., 1995			Los Tilos	U-Pb	U-Pb	217	7.5
	Martin et al., 1995			Guanaco Sonso	K-Ar	Bi	260	6
	Martin et al., 1995			Guanaco Sonso	K-Ar	Bi	262	6
	Martin et al., 1995			Guanaco Sonso	K-Ar	Bi	281	6
	Rodriguez Fernandez et al., 1997			Choiyoi	K-Ar	WR?	214	5
	Rodriguez Fernandez et al., 1997			Choiyoi	K-Ar	WR?	288	5
	Malizia et al., 1997 a-b			Choiyoi	K-Ar	WR	287	15
	Malizia et al., 1997 a-b			Choiyoi	K-Ar	WR	315	15
	Malizia et al., 1997 a-b			Choiyoi	K-Ar	WR	333	70
	Sato and Llambias, 1993			Rhyolite Dyke	Rb-Sr	isochrone	247.6	3
	Sato and Llambias, 1993			Andesites	Rb-Sr	isochrone	289.2	19.3
	Bissig, 2001			Basement GS?	Ar-Ar	Bi	261	5.4
	Martin et al., 1985			Guanaco Sonso	U-Pb	U-Pb	265.8	5.6
	This study		DC-119	Guanaco Sonso	U-Pb	U-Pb	263.7	0.7
	This study		DC-239	Guanaco Sonso	U-Pb	U-Pb	262.6	0.7
	This study		DC-181	GS intrusives	U-Pb	U-Pb	254	4.2
	This study		DC-142	GS intrusives	U-Pb	U-Pb	259	0.7
	This study		DC-162	GS intrusives	U-Pb	U-Pb	258	1.25
Ingaguas	Martin et al., 1995			Colorado	K-Ar	Musc	221	5
	Bissig, 2001			Basement, Colorado?	Ar-Ar	Bi	190	3.2
	Nasi et al., 1985			Chollay	K-Ar	Bi	238	6
	Mpodozis and Cornejo, 1990			El Leon	K-Ar	Bi	238	4
	Mpodozis and Cornejo, 1990			El Leon	K-Ar	Bi	276	4
	Tosdal, unpublished			El Leon	U-Pb	U-Pb	201	5
	Martin et al., 1995			Chollay-El Leon	U-Pb	U-Pb	242	1.5
	Martin et al., 1995			Chollay-El Leon	U-Pb	U-Pb	242.5	1.5
	Martin et al., 1995			Chollay-El Leon	U-Pb	U-Pb	249.7	3.2
	Nasi et al., 1985			Los Carricitos	K-Ar	Bi	221	3
	Nasi et al., 1985			Los Carricitos	K-Ar	Bi	238	4
	Nasi et al., 1985			Los Carricitos	K-Ar	Hbd	207	9
	Tosdal, unpublished			Los Carricitos	U-Pb	U-Pb	212	2
	Parada et al., 1981			Ingaguas	Rb-Sr	Rb-Sr	197	5
Elqui	Mpodozis and Cornejo, 1990			El Volcan	K-Ar	Bi	247	4
	Mpodozis and Cornejo, 1990			Cochiguas	K-Ar	Musc	259	6
	Mpodozis and Cornejo, 1990			Cochiguas	K-Ar	Musc	301	4
	Martin et al., 1995			Cochiguas	K-Ar	Bi	219	5
	Mpodozis and Cornejo, 1990			Cochiguas	K-Ar	Bi	235	6
	Pankhurst et al., 1996			Cochiguas	Rb-Sr	Rb-Sr	256	10
	Martin et al., 1995			Cochiguas	U-Pb	U-Pb	311	19
	Tosdal, unpublished			Cochiguas	U-Pb	U-Pb	296	3
	Nasi et al., 1985			Guanta	K-Ar	Bi	245	4
	Mpodozis and Cornejo, 1990			Guanta	K-Ar	Bi	250	4
	Ribba, 1985			Guanta	K-Ar	Bi	252	6
	Nasi et al., 1985			Guanta	K-Ar	Bi	258	4
	Ribba, 1985			Guanta	K-Ar	Bi	260	6
	Nasi et al., 1985			Guanta	K-Ar	Hbd	256	7
	Nasi et al., 1985			Guanta	K-Ar	Hbd	266	7
	Nasi et al., 1985			Guanta	K-Ar	Hbd	297	9
	Nasi et al., 1985			Guanta	K-Ar	Hbd	303	9
	Hervé in Ribba, 1985			Guanta	K-Ar	Hbd	310	18
	Parada et al., 1981			Elqui	Rb-Sr	Rb-Sr	328	21
	Pankhurst et al., 1996			Guanta	U-Pb	U-Pb	285.7	1.5
	Tosdal, unpublished			Guanta	U-Pb	U-Pb	298	2
Colanguil	Rodriguez Fernandez et al., 199	Granodiorite		Las Vizcachas	K-Ar	WR?	200	7
	Sato and Kawashita, 1988	Granite		Chita	Rb-Sr	isochrone	247	15
	Sato and Llambias, 1995	Granite		Los Lavaderos	Rb-Sr	isochrone	259	2
	Sato and Llambias, 1995	Granite		Las Openas	Rb-Sr	Rb-Sr WR-Bi	256	2
	Sato and Llambias, 1995	Granite		El Fierro	Rb-Sr	Rb-Sr WR-Bi	256.5	0.5
	Sato and Llambias, 1995	Granite		Los Puentes	Rb-Sr	Rb-Sr Bi	257	0.5
	Sato and Llambias, 1995	Granodiorite		Tocota	Rb-Sr	Rb-Sr WR-Bi	268	1
	Linares and Llambias, 1974	Granodiorite		Tocota	K-Ar	Bi	283	15
	Espina et al., 1998	Granodiorite	Las Vacas and Casposo?		K-Ar	WR?	261	6
	Espina et al., 1998	Granodiorite	Las Vacas and Casposo?		K-Ar	WR?	250	8
	Sato and Llambias, 1995	Granodiorite		Las Piedritas	Rb-Sr	Rb-Sr WR-Bi	261.5	1.5
	Sato and Llambias, 1995	Granodiorite		Romo	Rb-Sr	Rb-Sr WR-Bi	264	1.1
	Sato and Llambias, 1995	Granodiorite		Tocota	Rb-Sr	Rb-Sr WR-Bi	268	1
	Sato and Llambias, 1995	Granodiorite		Los Leones	Rb-Sr	Rb-Sr WR-Bi	270	2
	Sato and Llambias, 1995	Granodiorite		Tabaquito	Rb-Sr	Rb-Sr WR-Bi	327.5	1.5
Hurtado								
	Martin et al., 1995			Hurtado	K-Ar	WR	254	8

List of abbreviations: GS= Guanaco Sonso Formation; WR= Whole-rock; Bi= Biotite; Musc= Muscovite; Hbd= Hornblende; Rb-Sr WR-Bi= Whole-rock and Biotite isochrone

Volcanic and volcaniclastic rocks

Río Taguas Package

Late Paleozoic rocks along the Taguas River in the eastern part of the study area define a 750 m wide by 6 km long north-northeast trending belt. The lower contact is a thrust fault, and the upper contact is a slight angular unconformity with Tertiary volcanic rocks. Light grey and yellow rhyolitic to dacitic ignimbrites with varying degrees of welding and interbedded green volcaniclastic sandstones that dip to the west form the structural package (Figure 2-6). Ignimbrites dominate the package, but volcaniclastic rocks account for as much as 20% of the outcrop. Embayed quartz phenocrysts are very common and differentiate the late Paleozoic volcanic rocks from Tertiary volcanic rocks (see chapter 3).

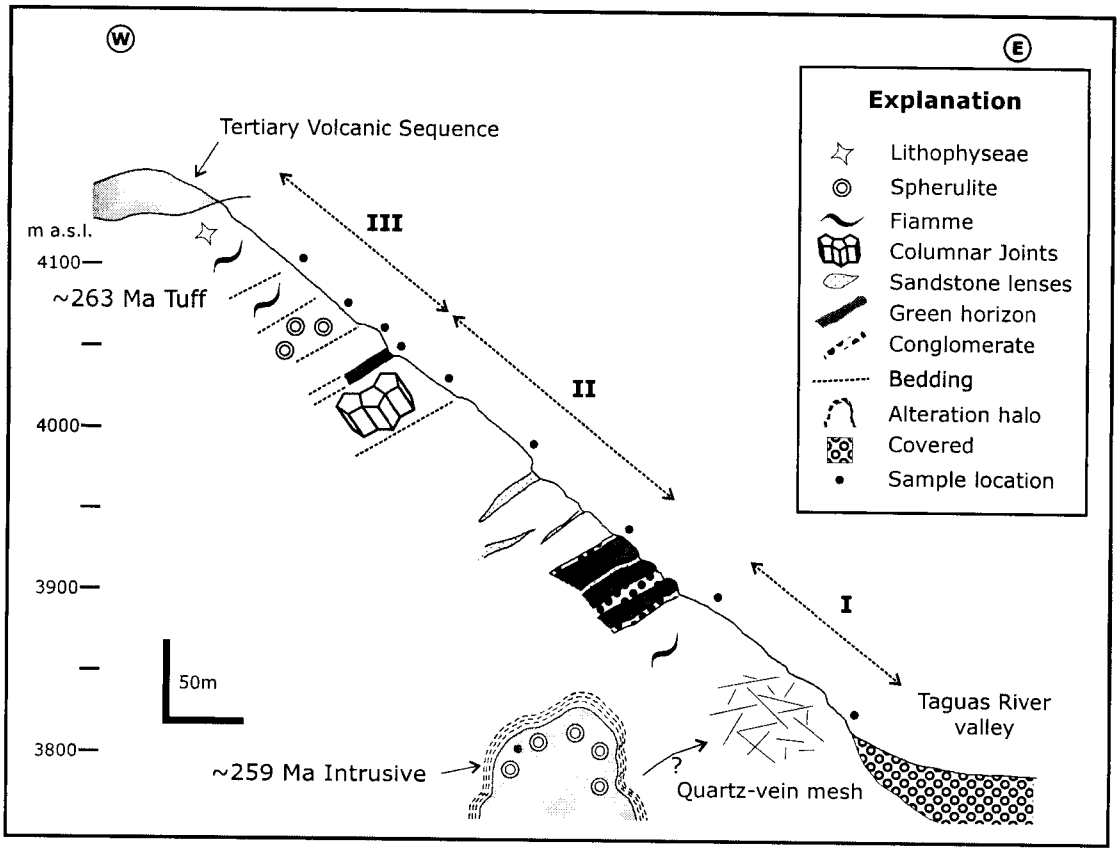

Figure 2-6: East-west cross-section of the late Paleozoic rocks exposed along the Río Taguas. I, II and III represent outflow, pyroclastic units separated by beds that are predominantly clastic. No vertical exaggeration.

Sample DC-119 is from an advanced argillic altered, matrix-supported, quartz-rich, lapilli-tuff with small fiammes located at the top of the Río Taguas late Paleozoic structural package (Figure 2-6). No accessory lithic fragments are present and all the material is representative of a primary pyroclastic deposit. The age of the package, determined by U-Pb geochronology, is 263.7 ± 0.7 Ma (Table 2-3, Figure 2-7, see Appendix for detailed discussion of U-Pb systematics).

Guanaco Zonzo Package

Isolated outcrops of late Paleozoic rocks define the 900 meters wide, north-northeast trending, Guanaco Zonzo structural package in the centre of the study area (Figure 2-5). To the east, a west-dipping thrust fault forms the contact with Tertiary rocks. Towards the west, a west-dipping normal fault brings the late Paleozoic rocks in contact with Tertiary sequences and, in the northern part of the map, with intensely silicified dacites assigned to the late Paleozoic. Light grey and purple dacitic to rhyolitic spherulitic welded lapilli-tuffs, intensely altered lithic-rich dacitic (?) tuff-breccias, fine conglomerates and sandstones are the predominant rock types in the Guanaco Zonzo area. Tertiary and late Paleozoic dacitic porphyries intrude the package.

A sample of advanced argillic altered, poorly sorted, matrix-supported, (volcanic) lithic-poor dacite with fiamme-like and feldspar vughs (sample DC-239) was dated using U-Pb method (Figure 2-5). Accessory volcanic lithic fragments form less than 5% of the rock volume and were removed during the sampling stage in order to collect volcanic material only. U-Pb geochronology yields an age of 262.6 ± 0.7 Ma (Table 2-3, Figure 2-7, see Appendix for discussion of U-Pb systematics).

Table 2-3: Summary of U-Pb geochronology in the Veladero North area

Sample Fraction[1]	Wt. (mg)	U[2] (ppm)	Pb*[3] (ppm)	$^{206}Pb/^{204}Pb$[4]	Pb[5] (pg)	^{208}Pb[3] %	Isotopic Ratios (1σ, %)[6] $^{206}Pb/^{238}U$	$^{207}Pb/^{235}U$	$^{207}Pb/^{206}Pb$	Apparent Age 2σ, Ma[6] $^{206}Pb/^{238}U$	$^{207}Pb/^{235}U$	$^{207}Pb/^{206}Pb$
DC-119 (‡)												
A c, n2, m, p	0.343	353	15	693	449	16.7	0.039519 (0.19)	0.27926 (0.45)	0.05125 (0.37)	249.9 (0.9)	250.1 (2.0)	252.1 (17.0)
B m, n2, m, p	0.213	386	18	1188	183	17.3	0.041725 (0.14)	0.29640 (0.51)	0.05152 (0.46)	263.5 (0.7)	263.6 (2.4)	264.2 (21.2)
C m, n2, m, p	0.367	408	18	1396	280	17.5	0.041084 (0.11)	0.29292 (0.33)	0.05171 (0.28)	259.6 (0.6)	260.9 (1.5)	272.6 (12.8)
D m, n2, n, n	0.181	291	13	499	281	17.8	0.040776 (0.14)	0.28955 (0.79)	0.05150 (0.73)	257.6 (0.7)	258.2 (3.6)	263.4 (33.9)
F f, n2, n, n	0.026	243	11	1210	13	18.9	0.040463 (0.09)	0.28672 (0.67)	0.05139 (0.63)	255.7 (0.5)	256.0 (3.0)	258.4 (29.3)
DC-239 (‡)												
A m, n2, n, n	0.065	152	7	543	48	19.9	0.040104 (0.14)	0.28190 (0.63)	0.05098 (0.57)	253.5 (0.7)	252.2 (2.8)	239.9 (26.5)
B m, n2, s, p	0.170	293	13	1719	76	18.2	0.041207 (0.09)	0.29354 (0.22)	0.05166 (0.15)	260.3 (0.5)	261.3 (1.0)	270.6 (7.0)
E m, n2, m, p	0.055	200	9	1913	15	19.5	0.041595 (0.11)	0.29531 (0.45)	0.05149 (0.41)	262.7 (0.6)	262.7 (2.1)	262.9 (19.1)
F m, n2, m, p	0.230	369	17	1380	165	16.7	0.041550 (0.10)	0.29792 (0.22)	0.05200 (0.14)	262.4 (0.5)	264.8 (1.0)	285.5 (6.5)
G m, n2, s, p	0.110	335	15	1032	94	18.2	0.040963 (0.11)	0.29242 (0.26)	0.05177 (0.19)	258.8 (0.5)	260.5 (1.2)	275.5 (8.8)
DC-142 (◇)												
A m, n2, m, p	0.076	658	29	1452	88	15.3	0.040812 (0.15)	0.28774 (0.66)	0.05113 (0.62)	257.9 (0.7)	256.8 (3.0)	246.9 (28.6)
C c, n2, s, p	0.191	568	26	1198	244	15.9	0.042104 (0.12)	0.30381 (0.35)	0.05233 (0.29)	265.9 (0.6)	269.4 (1.7)	300.0 (13.5)
D c, n2, s, p	0.129	560	25	1571	118	15.5	0.041013 (0.12)	0.29038 (0.47)	0.05135 (0.43)	259.1 (0.6)	258.9 (2.2)	256.6 (19.7)
E c, n2, s, p	0.158	614	27	820	314	16.0	0.040992 (0.13)	0.29227 (0.40)	0.05171 (0.34)	259.0 (0.6)	260.3 (1.9)	272.7 (15.8)
F f, n2, s, p	0.030	649	28	1517	33	15.1	0.040990 (0.12)	0.29188 (0.62)	0.05164 (0.58)	259.0 (0.6)	260.0 (2.8)	269.7 (26.7)
DC-181 (◇)												
A vc, n2, s, s (¤)	0.098	129	6	1247	26	20.8	0.039528 (0.10)	0.28030 (0.24)	0.05143 (0.17)	249.9 (0.5)	250.9 (1.1)	260.2 (7.7)
B vc, n2, s, s (¤)	0.067	114	5	3064	6	21.7	0.039147 (0.14)	0.27708 (0.23)	0.05133 (0.18)	247.5 (0.7)	248.3 (1.0)	255.9 (8.1)
C vc, n2, n, n (¤)	0.169	151	7	754	83	21.7	0.037265 (0.10)	0.26338 (0.27)	0.05126 (0.19)	235.9 (0.5)	237.4 (1.1)	252.6 (9.0)
D vc, n2, s, p	0.211	149	7	686	125	19.9	0.041833 (0.09)	0.33786 (0.26)	0.05858 (0.18)	264.2 (0.5)	295.5 (1.3)	551.3 (8.0)
E vc, n2, s, p	0.336	132	6	607	183	21.8	0.038240 (0.09)	0.27298 (0.28)	0.05177 (0.20)	241.9 (0.4)	245.1 (1.2)	275.5 (9.0)
G f, n2, m, p	0.014	85	4	991	3	23.8	0.037339 (0.17)	0.26825 (0.75)	0.05210 (0.71)	236.3 (0.8)	241.3 (3.2)	290.0 (32.9)
H f, n2, n, n (¤)	0.030	155	7	509	22	23.8	0.036498 (0.10)	0.25859 (0.55)	0.05139 (0.50)	231.1 (0.5)	234.3 (1.5)	258.2 (13.2)
I f, n2, n, n (¤)	0.026	165	7	1140	9	23.6	0.036290 (0.11)	0.25540 (0.30)	0.05104 (0.24)	229.8 (0.5)	231.0 (1.2)	242.8 (11.1)
DC-162 (◇)												
A m, n2, s, p	0.146	175	8	402	171	17.3	0.040924 (0.13)	0.28952 (1.20)	0.05131 (1.20)	258.6 (0.7)	258.2 (5.7)	254.7 (55.4)
C m, n2, n, n	0.035	132	6	313	39	16.7	0.039147 (0.11)	0.27911 (0.47)	0.05171 (0.40)	247.5 (0.6)	250.0 (2.1)	272.6 (18.2)
E c, n2, m, p	0.028	158	6	688	16	15.6	0.037046 (0.11)	0.26361 (0.35)	0.05161 (0.29)	234.5 (0.5)	237.6 (1.5)	268.1 (13.3)
G m, n2, s, p	0.030	130	6	62	235	15.7	0.040772 (0.16)	0.30673 (1.80)	0.05456 (1.70)	257.6 (0.8)	271.6 (8.7)	394.3 (77.2)

[1]Zircon fraction identifier. Zircons are non-magnetic on a Frantz magnetic separator at field strength of 1.8 A with: m5 and m2 magnetic at side slope of 5° and 2° n2=non-magnetic at side slope of 2°, n1=non-magnetic at side slope of 1°. Grain size: vc=>134 µm, c=<134 µm and >104 µm, m=<104 µm and >74 µm, f=<74 µm. Air abraided fractions are marked with s=strong, m=medium, n=non abraded. Grain shape: el=elongate, p=prismatic, s=stubby or n=needles

[2]U blank correction of 1 pg ± 20%; U fractionation corrections were measured for each run with a double ^{233}U-^{235}U spike (about 0.005/amu).

[3]Radiogenic Pb.

[4]Measured ratio corrected for spike and Pb fractionation of 0.0035/amu ± 20% (Daly collector) and 0.0012/amu ± 20% and laboratory blank Pb of 1-3 pg ± 20%. Laboratory blank Pb concentrations and isotopic compositions based on total procedural blanks analyzed.

[5]Total common Pb in analysis based on blank isotopic composition.

[6]Corrected for blank Pb, U and common Pb. Common Pb corrections based on Pb isotopic compositions of feldspars of equivalent, non-altered rocks from Martin et al. (1999). Isotopic compositions have uncertainties of less than 0.1% (2σ).

(◇) Sub-volcanic rocks were corrected with Pb isotopic composition of IM-113.1: $^{208}Pb/^{204}Pb$=38.51, $^{207}Pb/^{204}Pb$=15.57 and $^{206}Pb/^{204}Pb$=18.71.

(‡) Volcanic rocks were corrected with Pb isotopic composition of IM-108.2: $^{208}Pb/^{204}Pb$=38.43, $^{207}Pb/^{204}Pb$=15.60 and $^{206}Pb/^{204}Pb$=18.61.

(¤) Fractions used to fit regression line

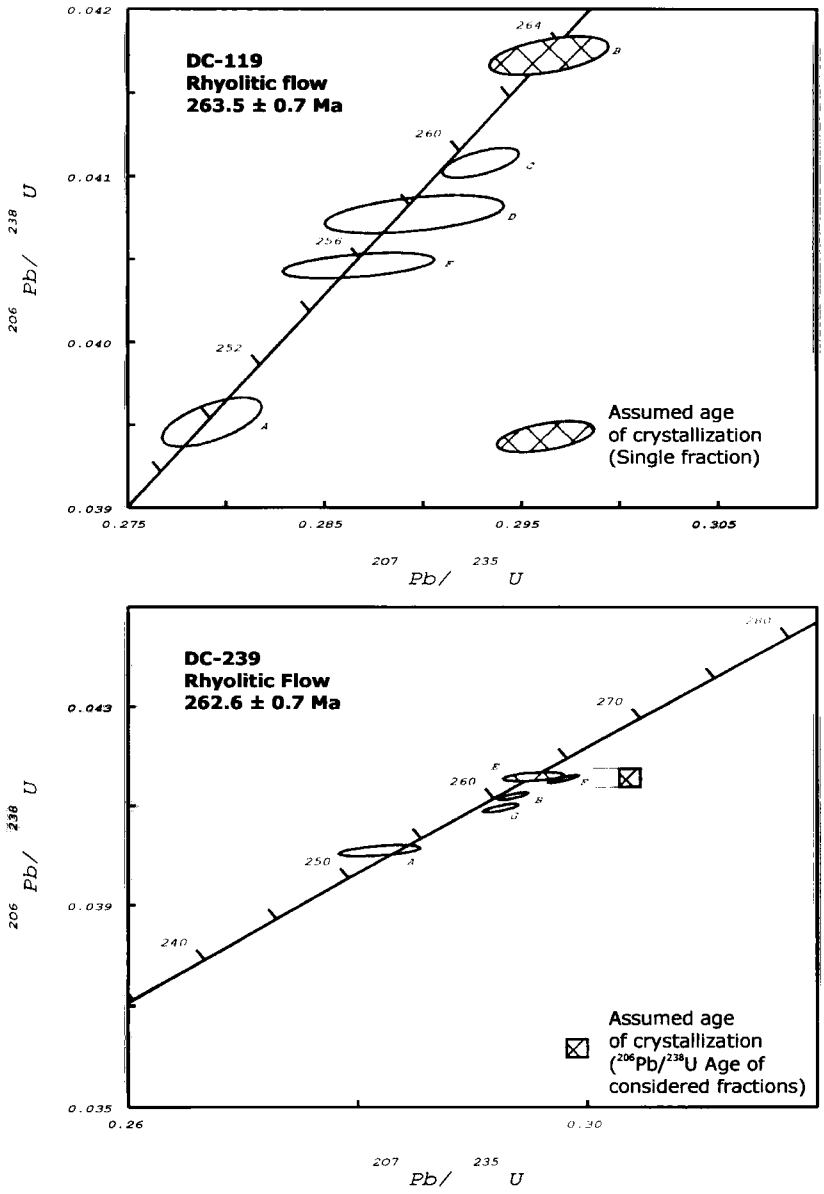

Figure 2-7: Concordia diagrams from volcanic rocks in the Veladero North area. Reported age of crystallization is $^{206}Pb/^{238}U$ age of indicated fractions. Uncertainty in age is based upon range of uncertainty of considered fractions and reflects maximum and minimum probable ages at 2 sigma level. See appendix for age determination and Table 2-3 for analytical data and results. Uncertainty ellipses shown at 2 sigma level.

Potrerillos-Canito Package

Late Paleozoic rocks exposed in the western part of the study area underlie the international border and extend to the east down the Canito creek forming the largest structural package in the map (Figure 2-5). In this area, the rocks crop-out between 5000 m a.s.l. and 3900 m a.s.l. and extend into Chile where it links with mapping of Martin *et al.* (1995, 1999). North-striking normal faults drop the blocks to the east thereby repeating the sequence. The minimum stratigraphic thickness is 650 m. The strata dip between 30° and 40° to the southeast or east and are unconformably overlain by Tertiary volcanic and sedimentary rocks along a gently angular unconformable to disconformable contact. Brown and purple dacitic to rhyolitic welded tuff, quartz-phyric dacites and minor lenses of coarse sandstones are the common rock types. A diorite porphyry that yielded a biotite(?) K-Ar age of 31 Ma (Thompson, 2000; personal communication) and four mapped small dacitic domes with vertical flow banding (see below) intrude the package. Martin *et al.* (1995, 1999) proposed the name Guanaco Sonso Sequence to refer to the late Paleozoic volcaniclastic rocks that crop-out in Chile, immediately west to the rocks previously described. U-Pb geochronology studies determined that the age of the Guanaco Sonso Sequence is 265.8 ± 5.6 Ma (Martin *et al.*, 1999).

Intrusive rocks

Small (< 1 km diameter) intrusives cut the late Paleozoic volcanic and volcaniclastic rocks. The plagioclase and quartz-bearing dacite-rhyolite porphyry intrusions are commonly altered with advanced argillic mineral assemblages. Quartz phenocrysts are embayed and plagioclase is altered to clays. Where less altered, the phenocrysts average 0.5 cm but reach up 1 cm in length. The groundmass is fine grained and it is normally completely recrystallized to quartz and feldspars (?). Flow foliation and spherulitic devitrification are common, but not unique, textures in the late

Paleozoic intrusive rocks. Tertiary intrusives have the same overall aspect and, in the absence of cross-cutting relationships, are practically identical. Monomict, clast-supported dacitic to rhyolitic breccias with very angular fragments are often associated to the intrusives, indicating near-surface magmatic activity.

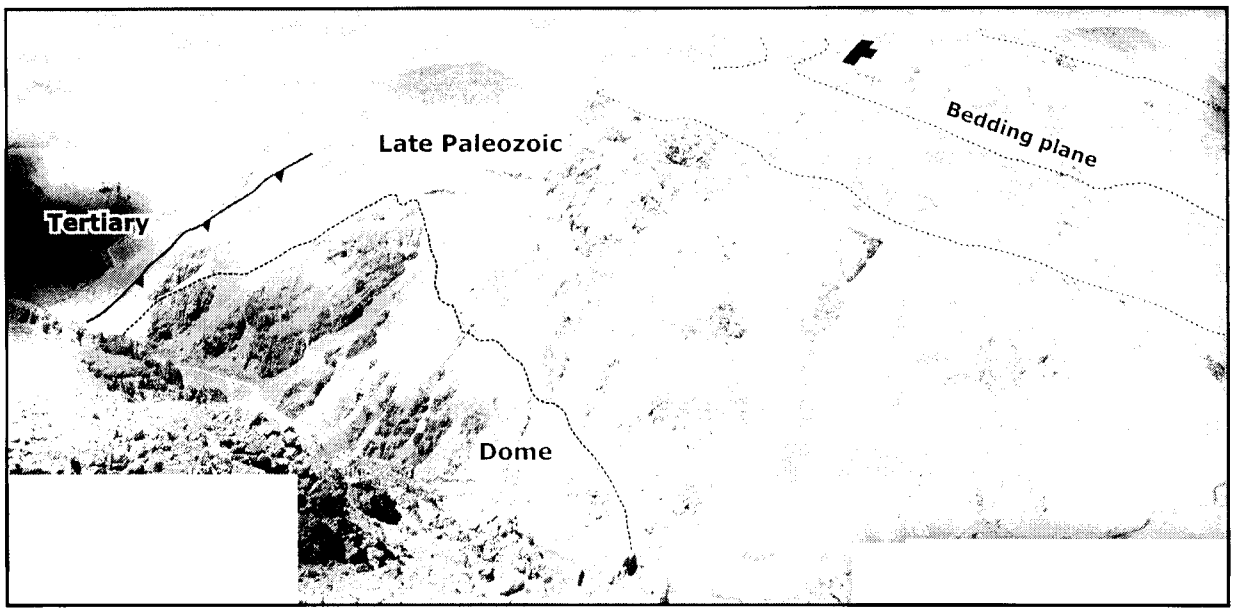

Figure 2-8: View of the Guanaco Zonzo creek exposures looking south. The shallow dacitic dome with spherulites forcefully intrudes the volcanic succession. Approximately 250 m (vertical) exposed from the creek to the summit.

The Guanaco Zonzo creek, in the south central part of the map area, cuts across a spherulitic dacitic dome that forcefully intruded late Paleozoic rocks of the Río Taguas package. In the 250 m of vertical exposure along the creek (Figure 2-8), no evidence that the dome vented to the surface has been observed. The sampled dome rock, DC-142, is a clay and silica (?) altered, porphyritic, intensely recrystallized dacite with spherulites. U-Pb geochronology studies determined that the age of the dome is 259 ± 0.7 Ma (Table 2-3, Figure 2-9). Although the common occurrence of spherulites in the lithology of the dome is similar to one ash-flow tuff located in the upper section of the late Paleozoic package (sample DC-043 in Figure 2-6), field relationship and geochronological data argue that the dome is younger and not part of the same volcanic event that formed the spherulitic tuff.

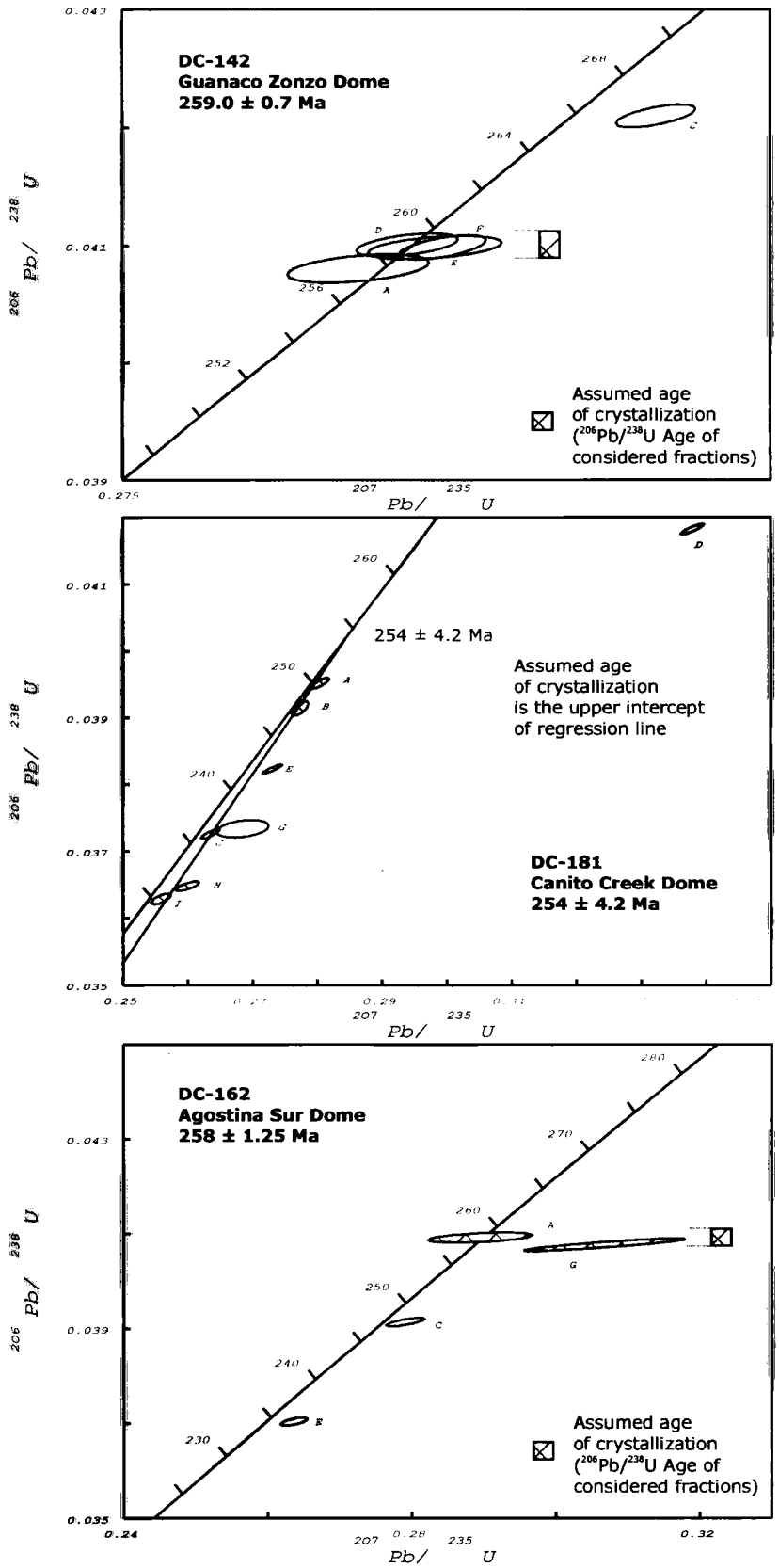

Figure 2-9: Concordia diagrams from intrusive rocks in the Veladero North area. See appendix for age determination and Table 2-3 for analytical data and results. Uncertainty in age is based upon range of uncertainty of considered fractions and reflects maximum and minimum probable ages at 2 sigma level. Uncertainty ellipses shown at 2 sigma level.

Other rhyolite-dacite intrusives, such as the domes in the northern part of the study area, have less clear crosscutting relationships with their host rocks. Two porphyries were sampled for geochronological study. Coarse grained, matrix-supported, porphyritic rhyolite-dacite with clay altered feldspars and rounded quartz crystals larger than 5 mm form the intrusive dome located in the northern part of the map where sample DC-181 has been collected (Figure 2-5). The U-Pb age of the intrusive is 254 ± 4.2 Ma (Figure 2-9, Table 2-3). In the central part of the Veladero North area, also known as Agostina Sur, advanced argillic altered, quartz-phyric porphyritic dacite with relict flow-banding texture characterize the late Paleozoic intrusive facies sampled as DC-162. Preliminary U-Pb data indicate that the maximum age of this dome is 258 ± 1.25 Ma (Figure 2-9, Table 2-3, see Appendix for detailed discussion of U-Pb systematics). Both domes have been previously mapped as Miocene intrusions and related to the Miocene high-sulfidation alteration system at Veladero North.

Geochemistry of late Paleozoic rocks of the Veladero North area

Geochemistry is used to classify volcanic and plutonic rocks and to compare magmatic units at a regional scale. Rock geochemistry, by analogy to modern examples, is also an effective approach to constrain the tectonic setting where the magmatism occurred. In this study, new geochemical data of pre-Tertiary rocks are presented and compared to available regional information (Tables 2-1 and 2-4).

Hydrothermal alteration affects nearly all rocks in the study area and the data reported in Table 2-4 are from fresh and altered rocks. The alteration effects are quantified comparing data from the literature (Bissig, 2001; Malizia *et al.*, 1997; Sato and Llambías, 1993) to the data presented in this study (see Appendix IV). The REEs from all volcanic samples are considered but only some samples are taken into account for the major and trace element characterization. Table 2-4 outlines which elements from the dataset are used to describe the lithogeochemistry of the Veladero North area.

Table 2-4: Geochemistry of late Paleozoic rocks of the Veladero North area.

		Río Taguas package								Potrerillos-Canito package				Guanaco Zonzo p		Intrusives		
Sample		DC-044	DC-119	DC-042	DC-043	DC-049	DC-050	DC-060	DC-155	DC-183	DC-184	DC-168	DC-099	DC-239	DC-283	DC-181	DC-141	DC-167
SiO_2	wt%	79.69	81.45	81.99	78.23	79.17	81.46	71.22	81.25	83.31	72.92	79.99	80.42	79.87	79.79	80.14	80.23	84.56
TiO_2	wt%	0.09	0.12	0.11	0.13	0.07	0.07	1.04	0.09	0.06	0.39	0.12	0.28	0.06	0.11	0.36	0.06	0.13
Al_2O_3	wt%	12.12	10.65	10.41	12.75	12.41	11.75	16.05	11.68	10.72	14.04	12.13	14.50	11.98	11.81	14.32	11.62	9.95
Fe_2O_3	wt%	0.83	0.48	0.47	0.95	0.87	0.90	1.95	0.60	1.13	2.59	0.58	1.33	0.86	0.81	1.78	0.6	0.78
MnO	wt%	0.001	0.01	0.01	0.01	0.02	0.06	0.01	0.06	0.02	0.08	0.02	0.01	-0.01	0.01	0.02	0.01	0.07
MgO	wt%	0.13	0.13	0.11	0.13	0.16	0.20	0.44	0.31	0.28	0.47	0.15	0.31	0.09	0.35	0.53	0.07	0.27
CaO	wt%	0.05	0.21	0.26	0.12	0.01	0.02	0.20	0.10	0.13	1.42	0.1	0.31	0.06	0.15	0.04	-0.01	1.61
Na_2O	wt%	0.08	0.12	0.10	0.12	0.05	0.04	0.51	0.06	2.04	3.66	2.11	0.08	2.15	2.78	-0.01	0.05	0.07
K_2O	wt%	6.97	6.76	6.49	7.52	7.20	5.45	8.49	5.80	2.26	4.32	4.75	2.67	4.88	4.12	2.7	7.31	2.51
P_2O_5	wt%	0.04	0.05	0.05	0.05	0.04	0.04	0.08	0.04	0.05	0.11	0.04	0.08	0.04	0.06	0.11	0.04	0.04
LOI	wt%	1.84	1.62	1.57	2.15	1.88	1.58	4.22	2.08	2.54	2.11	1.52	6.56	2.26	2.32	6.57	1.49	3.23
Total	wt%	*100*	*100*	*100*	*100*	*100*	*100*	*100*	*100*	*100*	*100*	*100*	*100*	*100*	*100*	*100*	*100*	*100*
Sr	ppm	7	28	19	11	5	9	63	10	58	144	39	35	20	49	92	7	59
Zr	ppm	222	259	255	292	200	164	180	220	122	245	240	229	160	135	137	150	128
Rb	ppm	309	264	263	323	339	288	411	282	104	183	169	114	210	189	131	324	89
Y	ppm	46	48	49	50	58	46	25	55	41	40	52	37	53	49	103	50	33
Nb	ppm	14	13	13	14	16	11	13	16	13	14	13	12	15	19	13	16	12
Ba	ppm	989	2208	1986	1810	482	1056	761	459	1737	1589	645	621	198	1107	692	511	912
La	ppm	42.5	53.8							30.7	35.1	45.3		33.0		35.2	13.9	19.8
Ce	ppm	74.0	106.8							67.0	76.2	102.1		67.0		86.7	25.4	49.6
Pr	ppm	10.6	11.9							7.9	9.6	11.4		8.7		12.7	3.5	6.1
Nd	ppm	42.4	44.5							30.9	37.7	45.2		34.7		56.1	13.3	24.3
Sm	ppm	8.0	7.9							6.3	6.9	9.4		8.0		12.0	2.9	6.0
Eu	ppm	1.0	1.7							0.3	1.6	1.1		0.3		2.8	0.2	1.2
Gd	ppm	5.9	7.2							6.0	6.6	7.9		7.8		15.3	3.9	5.4
Tb	ppm	0.9	1.0							1.0	1.0	1.2		1.3		2.9	0.7	0.9
Dy	ppm	5.6	6.6							6.7	6.3	7.6		8.2		19.4	5.6	5.7
Ho	ppm	1.5	1.3							1.4	1.3	1.5		1.6		3.6	1.2	1.1
Er	ppm	4.4	3.7							4.3	3.8	4.3		4.6		10.5	3.7	3.3
Tm	ppm	0.7	0.5							0.7	0.6	0.6		0.7		1.6	0.6	0.5
Yb	ppm	4.5	3.6							4.7	3.9	4.1		4.5		10.2	3.6	3.6
Lu	ppm	0.6	0.5							0.7	0.6	0.6		0.7		1.4	0.5	0.6
Hf	ppm	8.7	5.9							5.8	6.6	6.8		6.7		6.0	4.0	4.2
Ta	ppm	1.1	1.1							0.6	0.8	0.3		0.5		0.9	1.0	0.8
Th	ppm	16.9	15.1							15.0	10.7	14.1		17.7		10.5	12.5	9.0
La/Sm		5.3	6.8							4.9	5.1	4.8		4.1		2.9	4.8	3.3
Sm/Yb		1.8	2.2							1.3	1.8	2.3		1.8		1.2	0.8	1.7
La/Yb		9.5	15.1							6.5	9.0	11.1		7.3		3.5	3.8	5.6
Ba/La		27.5	39.9							63.0	49.9	12.4		7.3		22.0	34.5	40.7
Sr/Y		0.3	0.8	0.4	0.2	0.1	0.2	2.5	0.2	1.6	4.4	0.9	0.9	0.5	1.0	1.1	0.2	2.0
Eu*/Eu		7.8	13.1							2.0	11.9	8.2		2.4		21.4	1.8	8.9
Rb/Sr		44.1	9.4	13.8	29.4	67.8	32.0	6.5	28.2	1.8	1.3	4.3	3.3	10.5	3.9	1.4	46.3	1.5
A/CNK											1.057							
		m, REE	REE							REE	m, REE	REE		REE			REE	

Major oxides concentration is recalculated to 100 wt% without accounting for Loss on Ignition (LOI)
Major oxides and Sr, Zr, Rb, Y, Nb and Ba from Bondar Clegg XRF
Other data from Memorial University of Newfoundland ICP-MS

m: major oxide concentration considered in description
REE: Rare earth elements concentration considered in description

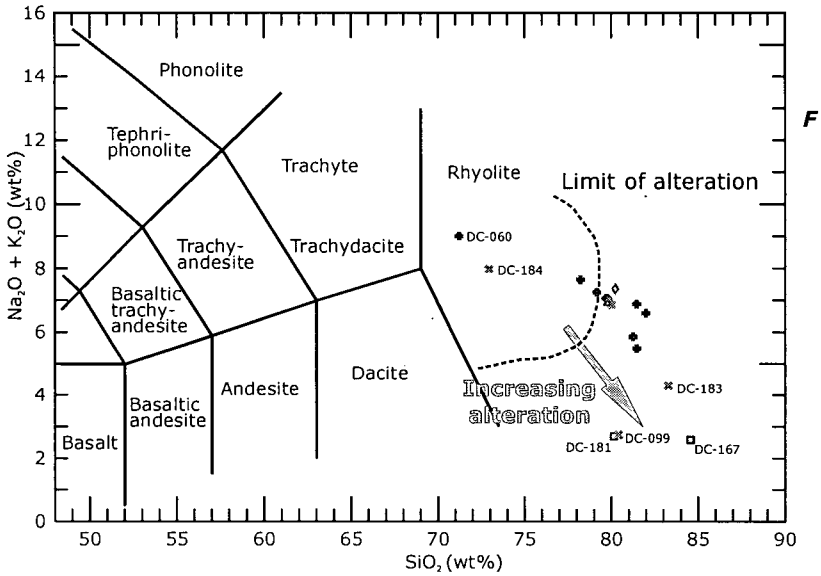

Figure 2-10a: TAS rock classification for late Paleozoic rocks from the Veladero North area. Limit of alteration defined by unaltered rocks from the literature (Bissig, 2001; Malizia et al., 1997 and Sato and Llambías, 1993). Samples DC-060 and DC-184 are from the least altered rocks in the study area used to characterize major oxide concentrations.

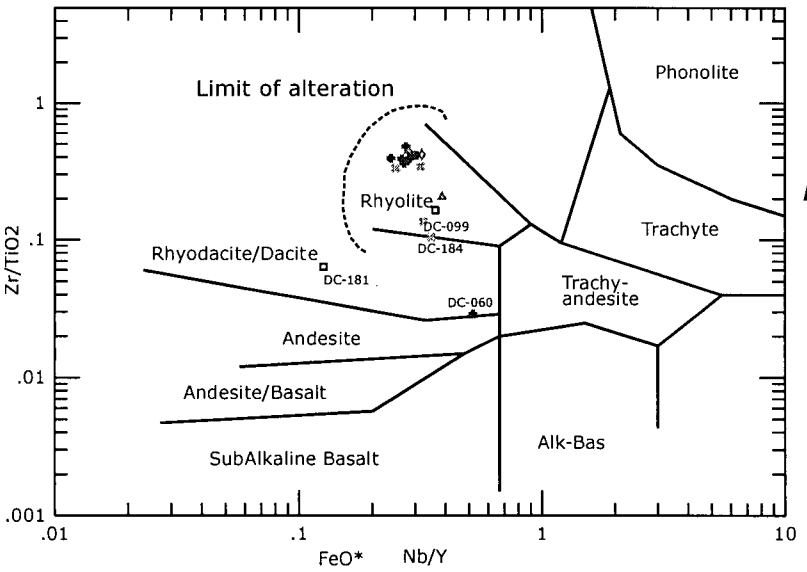

Figure 2-10b: Geochemical classification of Veladero North late Paleozoic rocks based on partially immobile elements. from Winchester and Floyd (1977).

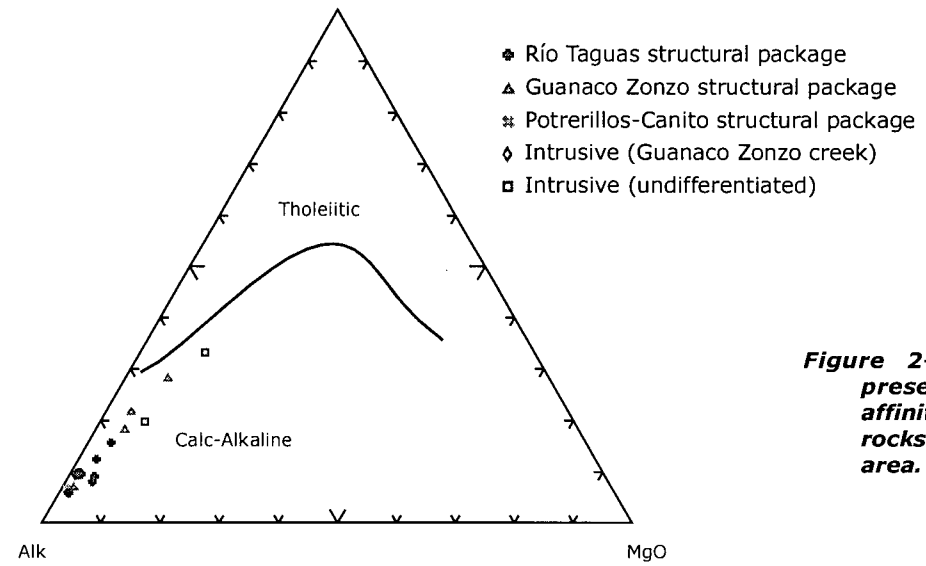

Figure 2-10c: AFM diagram presents the calk-alkaline affinity of the late Paleozoic rocks in the Veladero North area.

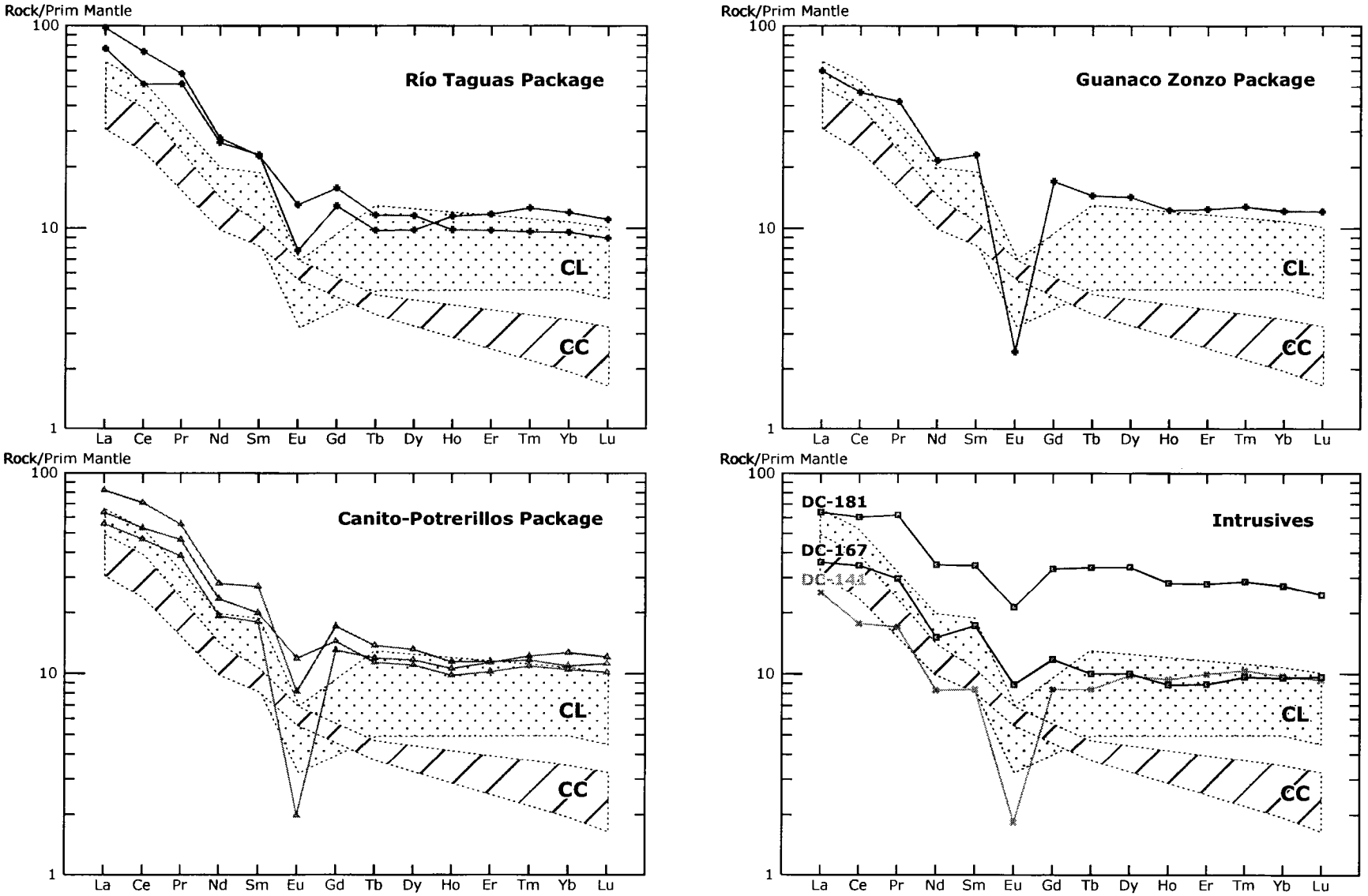

Figure 2-11: Veladero North samples REE patterns by structural package normalized to Primitive Mantle model of Taylor and McLennan (1985). CL (Chollay-El León Unit) and CC (Carricitos-Cochiguás Units) fields outline from Mpodozis and Kay (1992) data. Note that Veladero North volcanic rocks display a pattern similar to the CL but are slightly enriched. Samples DC-181 and DC-167 are from intensely altered rocks whereas DC-141 is from less altered intrusive.

Major and trace element geochemistry

Late Paleozoic volcanic rocks include mainly calc-alkaline rhyolites and dacites with K_2O contents over 4 wt% and subordinate andesites (Figure 2-10, Table 2-4). Late Paleozoic intrusives plot in the rhyolite field of Winchester and Floyd (1977) and their trace element concentrations suggest that their composition, compared to that of volcanic rocks, tends towards intermediate rocks (Samples DC-099 and 184 in Figure 2-10). Data from unaltered samples suggest that the volcanic rocks are slightly peraluminous (molar A/CNK > 1) which could be a primary compositional feature or perhaps due to alkali loss during devitrification or weathering. Strontium concentrations are low in the analysed rocks (7 to 144 ppm) and Rb has medium to high concentrations (104 to 411 ppm). The Rb/Sr ratio is variable but greater than one. Compared to Tertiary rocks, late Paleozoic rocks have high Rb/Sr ratios that may indicate upper crust affinity. Yttrium values are high and average 40 ppm reflecting that high-pressure minerals in the source have not retained this element during magma genesis (e.g. Mpodozis and Kay, 1992).

Rare earth element geochemistry

REE abundances of late Paleozoic rocks are overall one to two orders of magnitude greater than primitive mantle Taylor and McLennan (1985) and HREE display moderately flat patterns (Figure 2-11). The three volcanic packages are geochemically indistinguishable. In detail, LREE (La to Sm) are slightly enriched and have a moderately steep slope averaging 3.2 log units. HREE (Tb to Lu) show little fractionation (slope ~1). Negative europium anomalies are moderate to strong in the volcanic rocks. Late Paleozoic intrusives show similar HREE patterns and moderate to strong negative europium anomalies but exhibit flatter LREE patterns.

The geochemical characteristics have been interpreted as resulting from melting of a garnet-free, plagioclase-bearing source located in a relatively low-pressure

environment (e.g. Mpodozis and Kay, 1992). These magmas may be related to anatexis of felsic granitoids and/or pelitic material.

Discussion

Summary of Veladero North Sequence

Volcanic and volcaniclastic rocks of the Cordillera Frontal are assigned to the Permian-Triassic Choiyoi Group. In the Veladero North area, late Paleozoic rocks are exposed in three structural packages that represent time equivalent pyroclastic and volcaniclastic deposits and shallow intrusive facies emplaced under similar conditions. In terms of lithology and age, these volcanic rocks are comparable to the Guanaco Sonso Sequence in Chile (Martin *et al.*, 1995, 1999), herein referred as Guanaco Sonso Formation to fulfill stratigraphic nomenclature standards. Because of those similarities, the Guanaco Sonso Formation is extended into Argentina and intends to designate the volcanic and volcaniclastic rocks emplaced during the Permian in this portion of the Cordillera Frontal of Argentina and Chile. Uranium-lead and ^{40}Ar-^{39}Ar geochronological studies in the region (Figures 2-5 and 2-12) show that the volcanic rocks of the Guanaco Sonso Formation were emplaced in a relatively short period between 265 Ma and 260 Ma.

Geochronological data and field relationships indicate that the shallow volcanic porphyries in the Veladero North area intruded the Guanaco Sonso rocks immediately after their emplacement. Uranium-lead geochronology constrains their age to between 260 Ma and 255 Ma. The Guanaco Sonso intrusives, although relatively small and lithologically similar to Tertiary and other Paleozoic to Mesozoic porphyries, form an individual map unit previously unrecognized in regional surveys. Whereas the intrusives are slightly younger than the Guanaco Sonso Formation, their spatial relationship and similar lithology imply they are part of the same magmatic episode. How far the Guanaco Sonso Formation extends eastward is not precisely known yet, but it is very

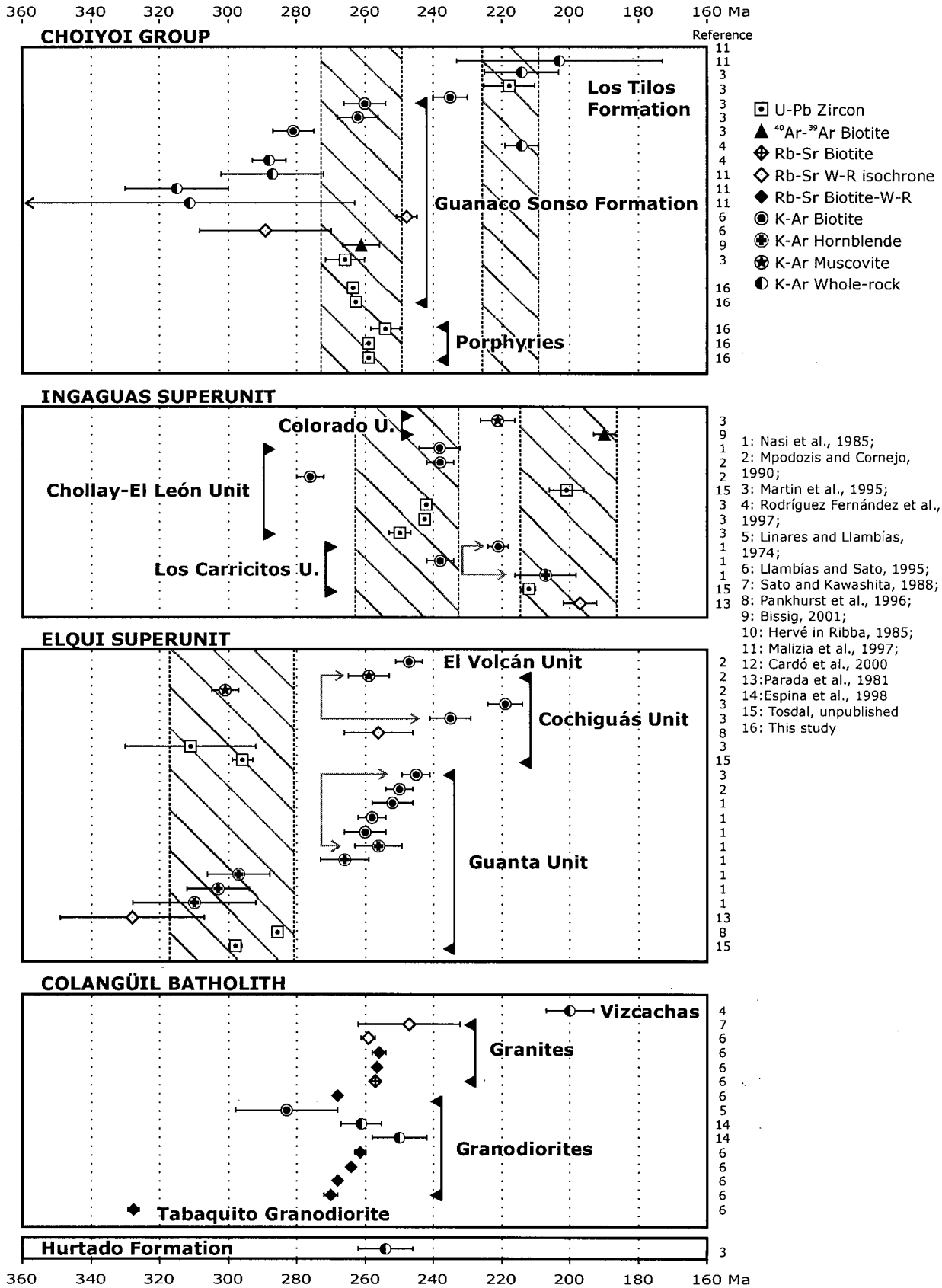

Figure 2-12: Compilation of late Paleozoic and Mesozoic ages from the Cordillera Frontal of Argentina and Chile. Ages from the Veladero North area are 2 sigma uncertainty, remaining ages are reported as originally published. Shaded boxes outline the expected age by magmatic unit, see also Figure 2-13. Arrow indicates single sample analyzed by different methods.

likely that it extends farther east than the Colangüil plutons. The age of the Guanaco Sonso Formation, considering volcanic and intrusive facies together, is comparable to the Rb-Sr cooling dates obtained in the Colangüil Granodiorites and Granites. Whether the Colangüil plutons are time equivalent to the Guanaco Sonso Formation or wheter they are older, unrelated rocks that have been thermally disturbed during the emplacement of the extensive rhyolitic sequence, needs to be defined using higher precision dating techniques.

Los Tilos Formation (modified name after Los Tilos Sequence of Martin *et al.*, 1999) yielded a biotite K-Ar age of 235 ± 5 Ma that U-Pb geochronological method fails to replicate (Martin *et al.*, 1999). However, the $^{208}Pb/^{206}Pb$ isotopic compositions of Los Tilos and Guanaco Sonso zircons are noticeably dissimilar (0.055 to 0.067 and 0.065 to 0.159 respectively; Martin *et al.* (1999) data), supporting the likelihood of diverse sources and consequently different age for the two formations.

Regional correlation

The Cordillera Frontal of Chile and Argentina is dominated by north-trending Tertiary thrust faults and back-thrusts that juxtapose late Paleozoic and Miocene or younger rocks and obscure pre-Tertiary structures (Martin *et al.*, 1995; Mpodozis and Ramos, 1989). In a generalized cross-section, Tertiary deformation and subsequent erosion results in rocks packages that decrease in age towards the east whereas deeper portions are exposed towards the west. Consequently, crosscutting relationships and relative stratigraphy are best established along strike. Recognition of the intrusive units in the region relies on textural and compositional similarities, implying that defined lithological characteristics are unique and representative of each magmatic episode (for example Nasi *et al.*, 1985). Potassium-argon and Rb-Sr geochronological studies indicate that magmatism in this part of the Andes was apparently continuous for 130 m.y. Recent studies, relying on the precision of U-Pb and ^{40}Ar-^{39}Ar geochronometers, suggest

that the late Paleozoic to Mesozoic magmatic activity was not continuous, but rather occurred during distinct episodes much like the history that characterizes the modern Andes (e.g. Martin *et al.*, 1999).

Different geochronological methods have been used to define the timing of magmatism throughout the Cordillera Frontal of Argentina and Chile. The results by unit and method are summarized in Table 2-2. Whole-rock and biotite K-Ar geochronological studies (Nasi *et al.*, 1985; Mpodozis and Cornejo, 1988; Martin *et al.*, 1995, 1999; Heredia *et al.*, 2002) were used in initial geochronological research and constitute the majority of the available data.

The assumption that the age produced by whole-rock K-Ar analysis is the age of crystallization needs to be evaluated. In the same way, and because of closure temperatures near 300°C (Harrison *et al.*, 1985), biotite K-Ar dates in intrusive rocks must be interpreted with caution in regions of multi-episodic intrusive history. Moreover, hornblende closure temperatures in the range from 450°C to 500°C (Harrison, 1981) might explain the observation that older K-Ar ages are commonly produced by hornblende than biotite from the same rock (e.g. NBT-302: hornblende 256 ± 7 Ma vs. biotite 245 ± 4 Ma, Nasi *et al.*, 1995; see Table 2-2 and Figure 2-12 for other pairs). Uranium-lead geochronological studies using magmatic zircons reproduce within uncertainty amphibole K-Ar ages but fail to duplicate biotite data from the same unit. Of interest is the fact that biotite is commonly the same age as that of younger intrusive and volcanic rocks dated by the U-Pb zircon method (Figure 2-12).

Similar patterns that reveal a discrepancy between K-Ar and U-Pb data have been seen in other convergent margin batholiths, for example in the Sierra Nevada (Chen and Moore, 1982) or the Whitsunday Volcanic Province in Australia (Bryan *et al.*, 2000; Allen *et al.*, 1998). In some of those cases, the ages of the micas may not always be correct and geochronometers that are more robust are required to establish a precise magmatic timing. In the Cordillera Frontal between 28° 30'S and 31° 30'S, revision of available U-

Pb and ^{40}Ar-^{39}Ar geochronologic data suggest three peaks of intrusions and two diachronous volcanic periods (Figure 2-13). The following interpretation assumes that, although some rocks may have been inadequately assigned to a specific unit, petrology and field evidence sustain the unit subdivision. From oldest to youngest the plutonic episodes are represented by: Late Carboniferous (320 Ma to 280 Ma) Guanta and Cochiguás Units (Elqui Superunit), Late Permian-Early Triassic (270 Ma to 235 Ma) Chollay-El León Unit (Ingaguás Superunit) and Late Triassic – Early Jurassic (220 Ma to 190 Ma) Los Carricitos and Colorado Units (Ingaguás Superunit). No U-Pb or ^{40}Ar-^{39}Ar data are available from the Colangüil Batholith. However, as the dates of the Granodiorites and Granites are 270 Ma to 262 Ma and 261 Ma to 255 Ma respectively, those units have been preliminary assigned to the Chollay-El León Unit. The Permian (275 Ma to 250 Ma) Guanaco Sonso Formation and the poorly constrained Triassic (225 Ma to 210 Ma) Los Tilos Formation constitute two apparently independent volcanic episodes.

Biotite K-Ar dates form a group around 260-250 Ma, including plutons with Carboniferous U-Pb and hornblende K-Ar ages. Moreover, the Late Carboniferous sedimentary Hurtado Formation yields a whole rock K-Ar date of 254 ± 8 Ma (Martin *et al.*, 1995). These observations suggest the likelihood of a widespread Permian thermal event that disturbed the low temperature chronometers, and the initial isotopic composition of older rocks. Probably the same event partially mobilized Rb-Sr isotopes and therefore the dates determined by Rb-Sr method may reflect cooling ages if the isotopic system was completely homogenized at that time. The age of the thermal resetting event is similar to the age of the widespread volcanic rocks from the Guanaco Sonso Formation, and suggests a causal link to the widespread Permian magmatism.

The reassessment of the geochronological data suggest that plutonic units with distinct geochemical characteristics might have been emplaced in a relatively short period of time (e.g. Guanta and Cochiguás Units or Los Carricitos and Chollay-El León

Units; see Figure 2-12). Conversely, plutonic units with similar geochemical signature occur from Late Carboniferous to Late Triassic (e.g. Guanta and Chollay Units; data Mpodozis and Kay, 1992), implying a complicated petrotectonic interpretation.

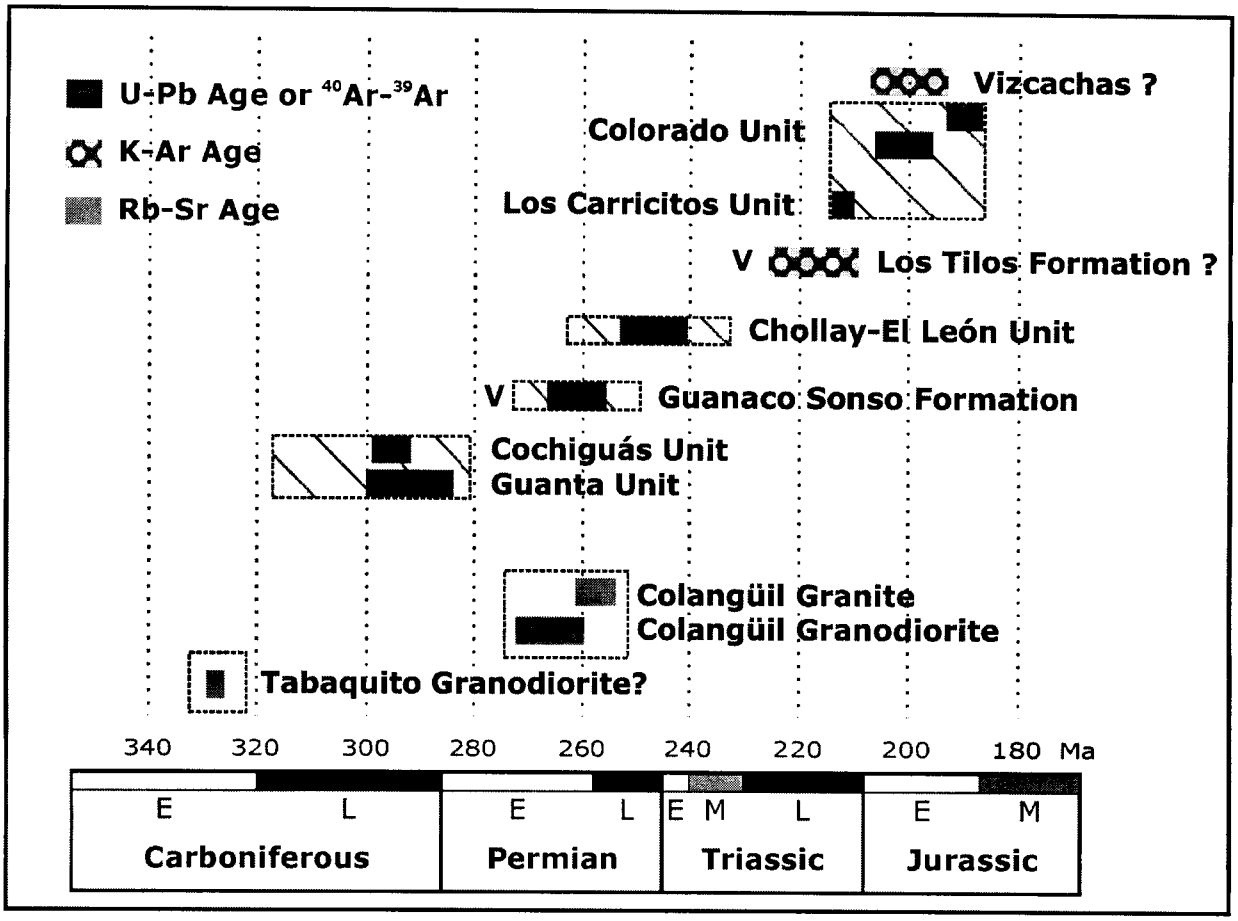

Figure 2-13: Summary of late Paleozoic to early Mesozoic magmatic episodes from the Cordillera Frontal of Argentina and Chile.

Conclusions

In the Veladero North area, the Permian volcanic sequence is assigned to the Guanaco Sonso Formation, the oldest formation in the Choiyoi Group. The sequence is formed by a succession of rhyolitic to dacitic out-flow tuffs, interfingered volcaniclastic rocks and shallow intrusives lithologically similar to the volcanic rocks. All these rocks were emplaced between 275 Ma and 250 Ma. Although K-Ar geochronometers indicate that the Guanaco Sonso Formation is coeval to the (270 Ma to 235 Ma) Chollay-El León plutonic event, U-Pb studies suggest that both units are diachronous.

Revision of geochronologic studies in the Cordillera Frontal indicates that the Los Tilos Formation (Choiyoi Group) was emplaced in the 225 Ma to 210 Ma range. Available data also suggest that a 25 m.y. volcanic gap exists between the two volcanic units that form the Choiyoi Group implying that the emplacement of the volcanic rocks from the granite-rhyolite province was probably discontinuous.

The intrusive rocks from the Granite-rhyolite province have been grouped into the Elqui and Ingaguás Superunits. Plutons from the Guanta and Cochiguás Units represent the largest part of the Elqui Superunit and, according to U-Pb geochronology, they have been emplaced between 300 Ma and 280 Ma. Chollay-El León intrusives are attributed to the oldest section of the Ingaguás Superunit. The Los Carricitos and El Colorado Units are also part of the Ingaguás Superunit and the plutons correspond to a younger and unrelated magmatic episode that spans from 220 Ma to 190 Ma.

The Rb-Sr ages of the Granites and Granodiorites from the Colangüil Batholith overlap with the emplacement of the Guanaco Sonso Formation but it is otherwise older than the estimated age of the Ingaguás Superunit. The single Early Carboniferous Rb-Sr date from the Tabaquito Granodiorite may indicate that this Unit groups the oldest plutons in the Cordillera Frontal. Future geochronologic studies are required to establish a precise timing of the emplacement of the Colangüil Batholith.

References

Bell, C.M., 1987, The late Paleozoic evolution of the Gondwanaland continental margin in northern Chile, in McKenzie, G.D., *ed.*, Gondwana Six; Structure, tectonics, and geophysics. Volume 40: Geophysical Monograph: Washington, DC, United States, American Geophysical Union, p. 261-270.

Bell, M.C., 1985, The Chinches Formation; an Early Carboniferous lacustrine succession in the Andes of northern Chile: Revista Geológica de Chile, v. 24, p. 29-48.

Bissig, T., 2001, Metallogenesis of the Miocene El Indio-Pascua gold-silver-copper Belt, Chile/Argentina: geodynamic, geomorphological and petrochemical controls on epithermal mineralization [Ph.D. thesis]: Kingston, Queen's University.

Caminos, R., 1979, Cordillera Frontal, in Castellanos, T.G., Sersic, J.L., Amuchastegui, S., Caputto, R., Cocucci, A.E., Fuchs, G.L., Gordillo, C.E., and Melo, C.R., *eds.*, Segundo simposio de geología regional Argentina: Córdoba, Argentina, Academia

Nacional de Ciencias, p. 397-453.

Chen, J.H., and Moore, J.G., 1982, Uranium-Lead Isotopic Ages from the Sierra Nevada Batholith, California: Journal of Geophysical Research, v. 87 B6, p. 4761-4784.

Cobbing, E.J., and Pitcher, W.S., 1972, The Coastal Batholith of central Perú: Journal of the Geological Society of London, v. 128, p. 421-460.

Coira, B., and Koukharsky, M., 1976, Efusividad tardío-Hercínica en el borde oriental de la Cordillera Frontal, zona de Arroyo de Tigre, provincia de Mendoza, República Argentina, in Charrier, G.R., *ed.*, Primer congreso geológico Chileno, Volume 1: Actas - Congreso Geológico Chileno: Antofagasta, Chile, Universidad del Norte Chile, Departamento de Geociencias, Facultad de Ciencias, p. F.105-F.123.

Cortés, J.M., 1985, Vulcanitas y sedimentitas lacustres en la base del Grupo Choiyoi al sur de la estancia Tambillos, Provincia de Mendoza, República Argentina: Actas - 4 Congreso Geológico Chileno, v. 4, p. 1.

Deyell, C.L., 2001, Alunite and high sulfidation gold-silver-copper mineralization in the El Indio-Pascua belt, Chile-Argentina [Ph. D. thesis]: Vancouver, Mineral Deposit Research Unit. University of British Columbia. Canada.

González Bonorino, G., 1991, Late Paleozoic orogeny in the northwestern Gondwana continental margin, western Argentina and Chile: Journal of South American Earth Sciences, v. 4, p. 131-144.

Groeber, P., 1946, Observaciones Geológicas a lo largo del meridiano 70; 1, Hoja Chos Malal: Revista de la Sociedad Geológica Argentina, v. 1, p. 177-208.

Harrison, T.M., 1981, Diffusion of ^{40}Ar in hornblende: Contributions to Mineralogy and Petrology, v. 78, p. 324-331.

Harrison, T.M., Duncan, I., and McDougall, I., 1985, Diffusion of ^{40}Ar in biotite; temperature, pressure and compositional effects: Geochimica et Cosmochimica Acta, v. 49, p. 2461-2468.

Heredia, N., Rodríguez Fernández, L., R, Gallastegui, G., Busquets, P., and Colombo, F., 2002, Geological setting of the argentine Frontal Cordillera in the flat-slab segment (30°00'- 31°30' S latitude): Journal of South American Earth Sciences, v. 15, p. 79-99.

Hervé, F., 1982, Condiciones de formación de complejos metamórficos chilenos a partir de la química de anfícbolas en metabasitas, Tercer Congreso Geológico Chileno, Volume 1: Congreso Geologico Chileno, Servicio Nacional de Geología y Minería, p. D93-D115.

Hervé, F., Godoy, E., Parada, M.A., Ramos, V., Rapela, C.W., Mpodozis, C., and Davidson, J., 1987, A general view on the Chilean-Argentine Andes, with emphasis on their early history, in Monger, J.W.H., and Francheteau, J., *eds.*, Circum-Pacific orogenic belts and evolution of the Pacific Ocean basin., Volume 18: Geodynamics Series: Washington, DC, United States, American Geophysical Union, p. 97-113.

Kay, S.M., Ramos, V.A., Mpodozis, C., and Sruoga, P., 1989, Late Paleozoic to Jurassic silicic magmatism at the Gondwana margin; analogy of the middle Proterozoic in North America ?: Geology (Boulder), v. 17, p. 324-328.

Llambías, E.J., and Sato, A.M., 1993, El grupo Choiyoi, Provincia de San Juan: equivalente efusivo del Batolito de Colangüil, Actas del décimo segundo Congreso Geológico Argentino y segundo Congreso de Exploración de Hidrocarburos, Volume 4: Buenos Aires, Asociación Geológica Argentina, p. 156-165.

Llambías, E.J., and Sato, A.M., 1995, El Batolito de Colangüil: Transición entre orogenesis y anarogénesis: Revista de la Asociación Geológica Argentina, v. 50, p. 111-131.

Llambías, E.J., Sato, A.M., and Castro, C.E., 1990, Relaciones entre el grupo Choiyoi y el Batolito de Colangüil, Actas del décimo primer Congreso Geológico Argentino, Volume 1: San Juan, Asociación Geológica Argentina, p. 79-82.

Llambías, E.J., and Sato, A.M., 1990, El Batolito de Colangüil (29-31 ° S), Cordillera Frontal de Argentina; estructura y marco tectónico: Revista Geológica de Chile, v. 17, p. 89-108.

Llambías, E.J., and Sato, A.M., 1990, El Batolito de Colangüil (29-31 S), Cordillera Frontal de Argentina; estructura y marco tectónico: Revista Geológica de Chile, v. 17, p. 89-108.

Llambías, E.J., Sato, A.M., Puigdomenech, H.H., and Castro, C., 1987, Neopaleozoic batholiths and their tectonic setting; frontal range of Argentina between 29 ° and 31 ° S, in Aceñolaza, F.G., *ed.*, Actas del décimo Congreso Geológico Argentino, Volume 4: Actas del Congreso Geológico Argentino. 9, Vol: Buenos Aires, Argentina, Asociación Geológica Argentina, p. 92-95.

Macfarlane, A., 1999, Isotopic studies of northern andean crustal evolution and ore metal sources, in Skinner, B.J., *ed.*, Geology and ore deposits of the central andes, Volume Special publication number 7, Society of Economic Geologists, p. 195- 217.

Malizia, D., Limarino, C.O., Sosa Gomez, J., Kokot, R., Nullo, F.E., and Gutiérrez, P.R., 1997, Hoja Geológica Cordillera del Zancarrón (Provincia de San Juan) N° 3169-26 y 25: Buenos Aires, Servicio de Geología y Minería de Argentina (SEGEMAR), 197 p.

Martin, M.W., Clavero, J., Mpodozis, C., and Cuitiño, L., 1995, Estudio geológico regional de la franja El Indio Cordillera de Coquimbo, Servicio Nacional de Geología y Minería, Compañía Minera San José, 238 p.

Martin, M.W., Clavero, R.J., and Mpodozis, C., 1999, Late Paleozoic to Early Jurassic tectonic development of the high andean Principal Cordillera, El Indio region, Chile (29-30°S): Journal of South American Earth Sciences, v. 12, p. 33-49.

Martin, M.W., Clavero, R.J., and Mpodozis, M.C., 1995, Tertiary geologic development of the high Andean El Indio gold belt, Chile, Geological Society of America, 1995 annual meeting., Volume 27: Abstracts with Programs - Geological Society of America: Boulder, CO, United States, Geological Society of America (GSA), p. 409.

Mirré, J.C., 1966, Geología del valle del rio de los Patos (entre Barreal y Las Hornillas): Revista de la Asociación Geológica Argentina, v. 21, p. 211-231.

Mpodozis, C., and Cornejo, P., 1988, Hoja Pisco Elqui, IV Región de Coquimbo: Santiago, Servicio Nacional de Geología y Minería, 164 p.

Mpodozis, C., and Kay, S.M., 1990, Provincias magmáticas ácidas y evolución tectónica de Gondwana; Andes chilenos, 28-31 ° S: Revista Geológica de Chile, v. 17, p. 153-180.

Mpodozis, C., and Kay, S.M., 1992, Late Paleozoic to Triassic evolution of the Gondwana margin; evidence from Chilean Frontal Cordilleran batholiths (28 ° S to 31 ° S); with Suppl. Data 92-22: Geological Society of America Bulletin, v. 104, p. 999-1014.

Mpodozis, C., and Ramos, V.A., 1989, The Andes of Chile and Argentina, in Ericksen, G.E., Pinochet, M.T.C., and Reinemund, J.A., *eds.*, Geology of the Andes and its relation to hydrocarbon and mineral resources.: Circum-Pacific Council for Energy and Mineral Resources, Earth Science Series: Houston, TX, United States, Circum-Pacific Council for Energy and Mineral Resources, p. 59-90.

Mpodozis, C., and Ramos, V.A., 1990, The Andes of Chile and Argentina, in Ericksen,

G.E., Pinochet, M.T.C., and Reinemund, J.A., *eds.*, Geology of the Andes and its relation to hydrocarbon and mineral resources.: Circum-Pacific Council for Energy and Mineral Resources, Earth Science Series: Houston, TX, United States, Circum-Pacific Council for Energy and Mineral Resources, p. 59-90.

Nasi, C.P., Moscoso, R.D., and Maksaev, V.J., 1990, Hoja Guanta, IV Región de Coquimbo: Santiago, Servicio Nacional de Geología y Minería, 140 p.

Nasi, P.C., Mpodozis, M.C., Cornejo, P.P., Moscoso, D.R., and Maksaev, J.V., 1985, El Batolito Elqui-Limarí (Paleozoico Superior-Triásico); características petrográficas, geoquímicas y significado tectónico: Revista Geológica de Chile, v. 25-26, p. 77-111.

Pankhurst, R.J., Millar, I.L., and Hervé, F., 1996, A Permo-Carboniferous U-Pb age for the part of the Guanta unit of the Elqui-Limarí batholith at Rio del Tránsito, Northern Chile: Revista Geológica de Chile, v. 23, p. 35-42.

Parada, M.A., 1990, Granitoid plutonism in central Chile and its geodynamic implications; a review, in Kay, S.M., and Rapela, C.W., *eds.*, Plutonism from Antarctica to Alaska., Volume 241: Special Paper - Geological Society of America: Boulder, CO, United States, Geological Society of America (GSA), p. 51-66.

Parada, M.A., Levi, B., and Nystrom, J.O., 1991, Geochemistry of the Triassic to Jurassic plutonism of central Chile (30 to 33 ° S); petrogenetic implications and tectonic discussion, in Harmon, R.S., and Rapela, C.W., *eds.*, Andean magmatism and its tectonic setting, Volume Special Paper 265: Boulder, CO, Geological Society of America (GSA), p. 99-112.

Petersen, U., 1999, Magmatic and metallogenic evolution of the central andes, in Skinner, B.J., *ed.*, Geology and ore deposits of the central andes, Volume Special publication number 7, Society of Economic Geologists, p. 109-153.

Poma, S., and Ramos, V.A., 1994, Las secuencias básicas iniciales del Grupo Choiyoi, Cordón del Portillo, Mendoza, sus implicancias tectónicas, in Campos, E., and Cecioni, A., *eds.*, 7 congreso geologico chileno; actas, Volume 2: Actas - Congreso Geológico Chileno. 7, Vol: Antofagasta, Chile, Universidad del Norte Chile, Departamento de Geociencias, Facultad de Ciencias, p. 1162-1166.

Ramos, V.A., 1988, Late Proterozoic-early Paleozoic of South America: a collisional history: Episodes, v. 11, p. 168-174.

Ramos, V.A., Jordan, T.E., Allmendinger, R.W., Kay, S.M., Cortes, J.M., and Palma, M.A., 1984, Chilenia: un terreno alóctono en la evolución Paleozoica de los Andes centrales, Actas del Noveno Congreso Geológico Argentino, Volume 2: Bariloche, Asociación Geológica Argentina, p. 84-106.

Ramos, V.A., Jordan, T.E., Allmendinger, R.W., Mpodozis, M.C., Kay, S.M., Cortes, J.M., and Palma, M., 1986, Paleozoic terranes of the central Argentine-Chilean Andes: Tectonics, v. 5, p. 855-880.

Rapalini, A.E., 1989, Estudio paleomagnético del volcanismo permotriásico de la región andina de la Republica Argentina. Consecuencias tectónicas y geodinámicas [Ph. D. thesis]: Buenos Aires, Universidad de Buenos Aires.

Rapalini, A.E., and Vilas, J.F.A., 1991, Tectonic rotations in the late Palaeozoic continental margin of southern South America determined and dated by palaeomagnetism: Geophysical Journal International, v. 107, p. 333-351.

Ribba, L., Mpodozis, C., Hervé, F., Nasi, C., and Moscoso, R., 1988, El basamento del valle del Transito, Cordillera de Vallenar; eventos magmáticos y metamórficos y su relación con la evolución de los Andes chileno-argentinos: Revista Geológica de Chile, v. 15, p. 129-149.

Rodríguez Fernández, L.R., Heredia, N., Espina, R.G., and Cegarra, M.I., 1997,

Estratigrafía y estructura de los Andes centrales argentinos entre los 30° y 31° de latitud sur, in Busquets, P., Colombo, F., Pérez, E.A., and Rodríguez, F.R., *eds.*, Geología de los Andes centrales argentino-chilenos, Volume 32: Acta Geológica Hispánica: Barcelona, Spain, Instituto Nacional de Geología, p. 51-75.

Rolleri, E.O., and Criado Roque, P., 1969, Geología de la provincia de Mendoza, Actas de las Jornadas Geológicas Argentinas, Volume 2, Asociación Geológica Argentina, p. 1-46.

Sato, A.M., and Llambías, E.J., 1993, El Grupo Choiyoi, Provincia de San Juan: Equivalente efusivo del Batolito de Colangüil, in Anonymous, *ed.*, Actas del Décimo Segundo Congreso Geológico Argentino y Segundo Congreso de Exploración de Hidrocarburos, Volume 4: Actas del Congreso Geológico Argentino. 12, Vol, Asociación Geológica Argentina, p. 157-165.

Stipanicic, P., Rodrigo, F., Baulies, O.L., and Martínez, C.G., 1968, Las formaciones presenonianas en el denominado Macizo Nordpatagónico y regiones adyacentes: Revista de la Asociación Geológica Argentina, v. 23, p. 67-98.

Taylor, S.R., and McLennan, S.M., 1985, The continental crust: its composition and evolution: Oxford, Blackwell, 312 p.

Thiele, C.R., 1964, Reconocimiento geologico de la Alta Cordillera de Elqui: Santiago, Universidad de Chile, Departamento de Geología, 73 p.

Vilas, J.F.A., and Valencio, D.A., 1982, Implicaciones geodinámicas de los resultados paleomagnéticos de formaciones asignados al Paleozoico tardío-mesozoico temprano del Centro-Oeste Argentino, Quinto congreso latinoamericano de geología, Volume 3: Buenos Aires, Argentina, Serv. Geol. Nac., p. 743-758.

Winchester, J.A., and Floyd, P.A., 1977, Geochemical discrimination of different magma series and their differentiation products using immobile elements: Chemical Geology, v. 20, p. 325-343.

Chapter 3

Geological framework of the Veladero North area, Cordillera Frontal, Argentina.

Abstract

Located in the northern part of the El Indio-Pascua Belt, the Veladero North area is underlain by a north-trending fold and thrust belt that superposes late Paleozoic and Oligocene rocks over early Miocene rocks. The deformed rocks are unconformably covered and intruded by middle Miocene rocks. Field mapping and U-Pb geochronology indicate that the Tertiary volcanic rocks are equivalent in age and lithology to region-scale units previously defined in Chile (Bissig *et al.*, 2001). In the study area the recognized units include: dacite, andesite and volcaniclastic rocks from the (26 Ma to 23 Ma) Tilito Formation; heterolitic breccia, tuff, sandstone and dacite from the (17 Ma to 14 Ma) Cerro de las Tórtolas Formation and Infiernillo Unit; biotite-phyric dacites from the (12 Ma to 11 Ma) Vacas Heladas Formation and rhyolite from the (2 Ma) Cerro de Vidrio Formation.

Geologic and geochronologic data together with the position of regionally defined erosional surfaces indicate multiple episodes of deformation in the study area. At least two distinct periods of shortening, one pre- and other post- ~16 Ma, are characterized by folding and thrusting. Shortening is followed by a post-11 Ma deformation, which reactivated pre-existing faults.

Gold mineralization is largely hosted in volcanic and volcaniclastic rocks from the Cerro de las Tórtolas Formation. Limited published information suggests that the age of the hydrothermal alteration (and likely the mineralization) of the Veladero North deposit is 5 m.y. younger than the ~16 Ma host-rock.

Introduction

The Veladero North and Pascua-Lama high-sulfidation deposits at the northern end of the El Indio Belt contain gold reserves over 30 million ounces that were deposited in association with Miocene volcanic and plutonic activity. Together, the deposits represent one of the largest undeveloped gold and silver mining districts in the world (Barrick data, 2002). The deposits lie along a 7-km long west-northwest trending zone that straddles the Argentina-Chile international border at 29°30′ S in the Cordillera Frontal morphostructural province of the Central Andes (Figure 3-1). The stratigraphy, geologic and tectonic evolution of the Chilean part of the El Indio Belt is well documented (Maksaev *et al.*, 1984; Nasi *et al.*, 1990; Martin *et al.*, 1995, 1997a,b; Bissig *et al.*, 2001). Furthermore, known deposits such as El Indio, Tambo and Pascua-Lama have been studied in detail (Jannas *et al.*, 1999; Deyell, 2001; Chouinard, in prep.). In stark contrast, the geologic and tectonic history of the Argentinan side of the El Indio Belt is poorly defined (Malizia *et al.*, 1997; Marín and Nullo, 1988; Nullo and Marín, 1990), and the setting of the Veladero North deposit is only known from a reconnaissance study (Jones *et al.*, 1999).

This chapter, which builds upon the Paleozoic framework in Chapter 2, provides the first well constrained Miocene geologic and tectonic history of the area. The work utilizes previous geologic studies (Bissig, 2001; Jones *et al.*, 1999; Malizia *et al.*, 1997; Martin *et al.*, 1995) and incorporates data from the Chilean side of the Belt. The discussion is focused on major late Tertiary volcanic and volcanosedimentary units that surround the Veladero North high-sulfidation deposit. Permian rocks, although volumetrically important in the study area, are not fully described in this chapter. Understanding the local geology is critical in order to evaluate the relationship, if any, between gold mineralization and Tertiary magmatism. In detail, the diatreme model currently being used in mining exploration (e.g. Jones *et al.*, 1999) needs to be tested against new geological information.

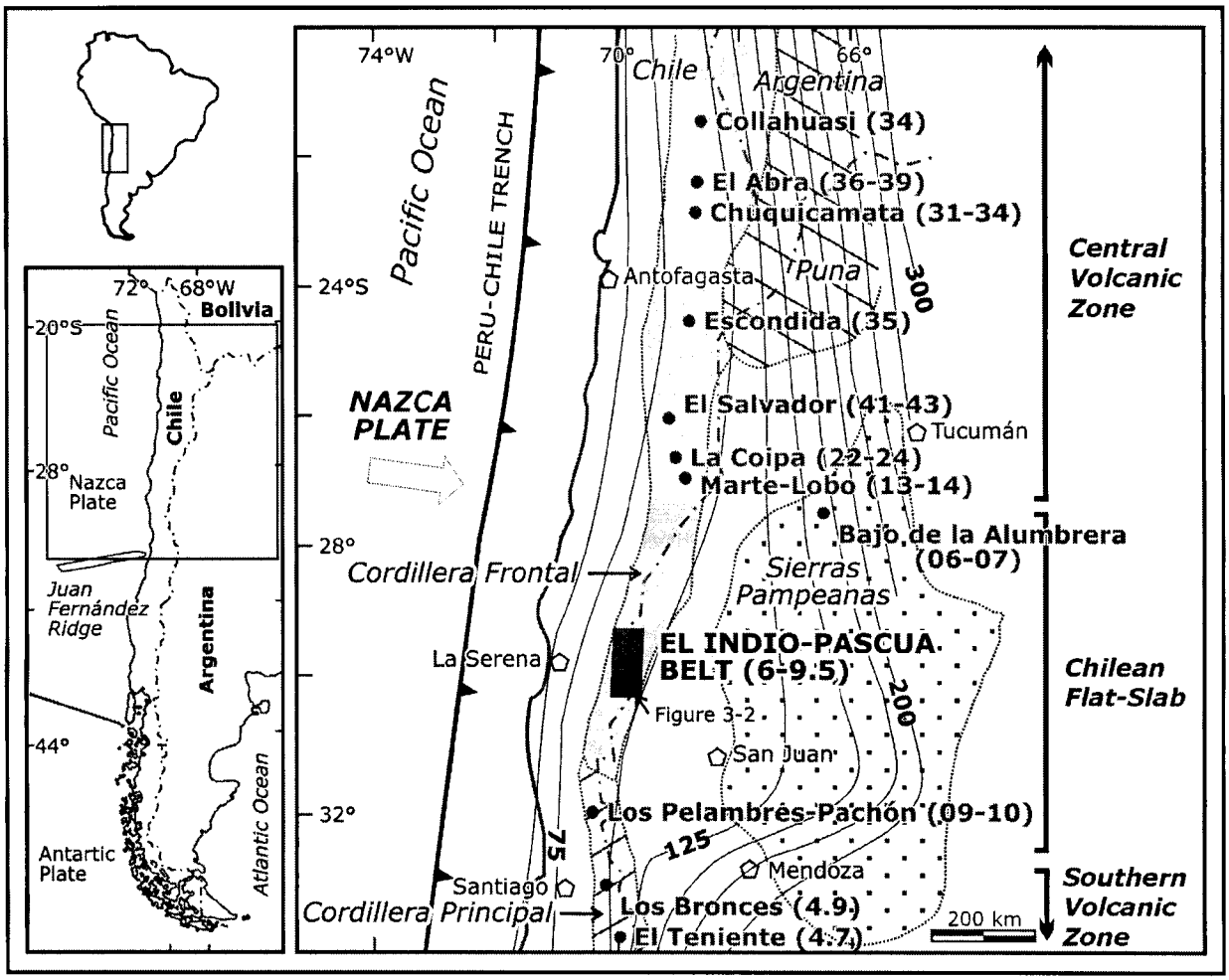

Figure 3-1: Southern South America Andes. Location of the El Indio-Pascua Belt and major Tertiary mineralization districts. Age of mineralization is shown in million years between brackets. Based on Bissig (2001) and Dilles and Camus (2001). Represented depth contour lines (25 Km interval) of the Wadati-Benioff zone are from Cahill and Isacks (1992) and Andean Magmatic segments from Kay et al. (1991). Morphostructural elements are simplified from Hervé et al. (1987).

Geologic setting of the El Indio Belt

Mining, exploration and new mineralization discoveries have successively extended the north-south dimension of the El Indio Belt to an approximately 150-km long strip that has recently been referred as the El Indio-Pascua Belt (e.g. Deyell, 2001). The belt is confined between two reverse faults, the Baños del Toro fault in the west and the Colangüil fault in the east (Figure 3-2). The opposite dipping Miocene thrust faults place late Paleozoic rocks over late Paleozoic to early Mesozoic igneous and sedimentary units which are unconformably overlain by a thick succession of Tertiary volcanic and volcaniclastic rocks. Late Paleozoic to pre-Miocene rocks form the effective basement to

the Au deposits and prospects, which are genetically related to the Miocene volcanic complexes (e.g. Martin *et al.*, 1995).

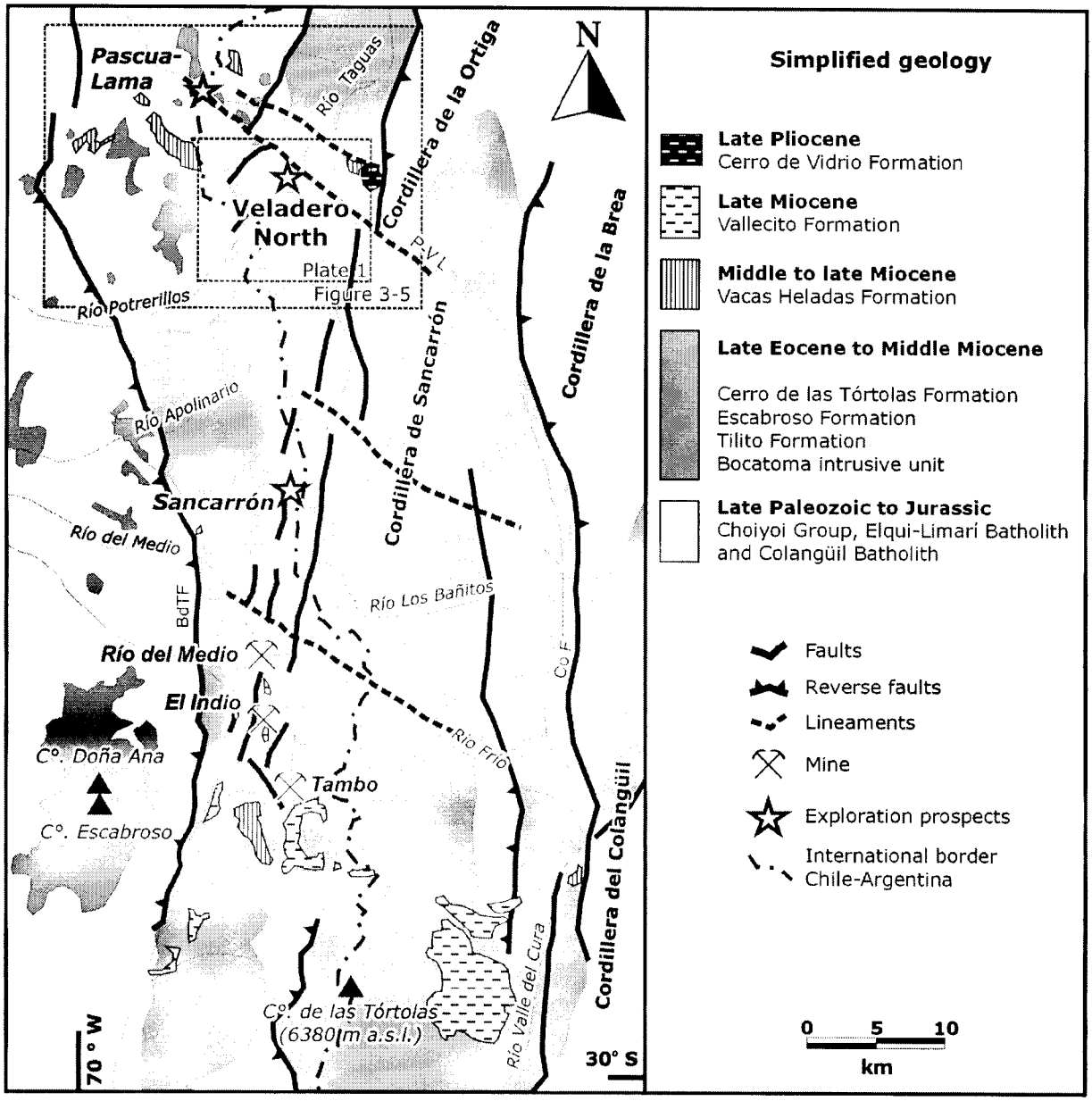

Figure 3-2: Regional Geology of the El Indio-Pascua Belt and location of major deposits and mines modified from Bissig et al. (2001). Abbreviations: BdTF = Baños del Toro Fault, P-V L = Pascua-Veladero Lineament, Co F = Colangüil Fault.

The El Indio-Pascua Belt lies within the Cordillera Frontal morphostructural unit of Argentina and Chile, as defined by Hervé *et al.* (1987). Geological studies of the Cordillera Frontal of Chile and Argentina have proceeded at a different pace in each country after the initial reconnaissance of Groeber (1946, 1951). Regional scale Tertiary

rock units were first outlined in Chile (Thiele, 1964) where further mapping and geochronological studies established a more detailed volcanic stratigraphy (Maksaev *et al.*, 1984; Martin *et al.*, 1995, 1997a). In Argentina, the geology of the eastern flank of the Cordillera Frontal is poorly known, as geological studies are usually focused on relatively small and separate areas (Ramos *et al.*, 1987, 1989; Litvak *et al.*, 2002; Nullo, 1988; Godeas *et al.*, 1993; Jones *et al.*, 1999). The lack of geochronological studies (Marín and Nullo, 1988; Nullo and Marín, 1990) or imprecise K-Ar whole-rock determinations (Malizia *et al.*, 1997) hindered the development of a coherent regional stratigraphy. Instead, the rock units were either correlated to Chilean formations according to their composition and lateral continuity, or new formation names were assigned to poorly time-constrained or isolated rock entities. Bissig *et al.* (2001) refined the volcanic stratigraphy on the Argentinan side of the El Indio Belt in the first attempt to reconcile Chilean and Argentinan stratigraphic columns in the region (Figure 3-4). These formation names and paleosurfaces or unconformities separating them have been adopted herein as the geologic framework recognized at Veladero North supports the sequence established by Bissig *et al.* (2001).

The El Indio Belt lies in a region of active magmatism and shortening deformation from the Eocene to late Miocene (e.g. Kay and Mpodozis, 2001). Magmatism continued to early Pliocene (Bissig *et al.*, 2001). The limited Eocene to early Oligocene magmatism and deformation in the 29°S-30°S is attributed to a relatively slow, oblique convergence tectonic setting between the Farallón and South American plates (Pilger, 1984; Pardo-Casas and Molnar, 1987; Somoza, 1998 and Figure 3-3).

The pattern of magmatism and deformation have changed over time, and have been proposed to reflect changes from normal to a "flat" subduction stage over almost 25 m.y. (Kay and Abruzzi, 1996; Kay, 1991; Kay *et al.*, 1987, 1988; Kay and Mpodozis, 2001, 2002; Isacks, 1988; Mpodozis and Ramos, 1989) (Figure 3-3).

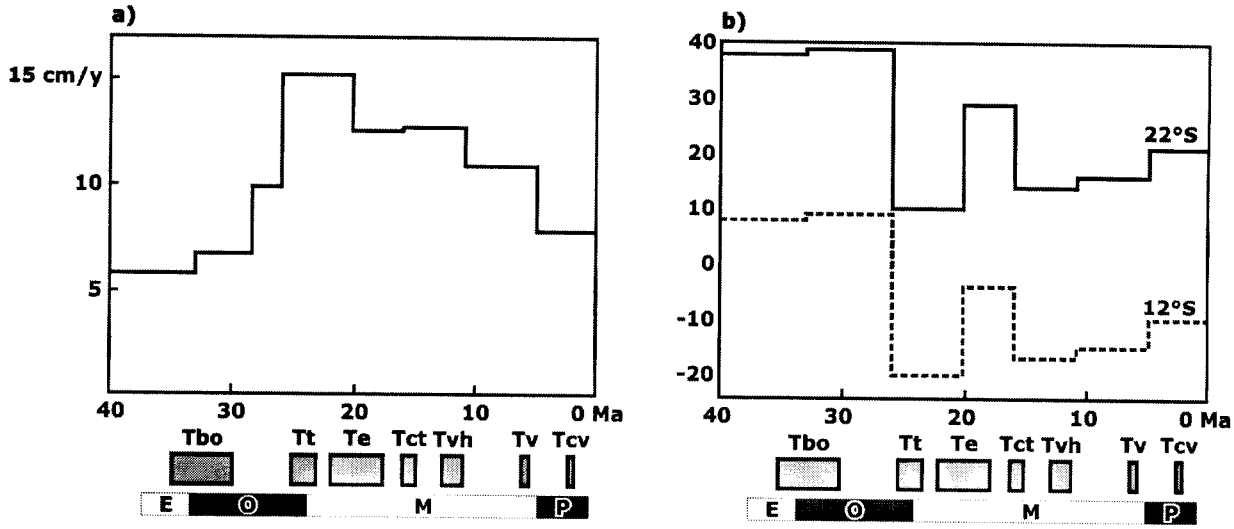

Figure 3-3: Mean convergence rate (a) and obliquity (b) between the Nazca and South America plates during the last 40 m.y. Positive values indicate dextral convergence. (Somoza, 1998). Grey boxes represent the time span of the Tertiary volcanic and intrusive units of the El Indio-Pascua Belt. Abbreviations: E=Eocene, O=Oligocene, M=Miocene, P=Pliocene, Tbo=Bocatoma Intrusive Unit, Tt=Tilito Formation, Te=Escabroso Formation, Tct=Cerro de las Tórtolas Formation, Tvh=Vacas Heladas Formation, Tv=Vallecito Formation and Tcv=Cerro de Vidrio Formation.

With the break-up of the Farallón plate into the Nazca and Cocos plates around 25 Ma, an increase in the relative subduction rate (~15 cm/year) and the beginning of normal convergence between the Nazca and South American plates coincided with the onset of the most current phase of Andean volcanism and deformation (Pilger, 1984; Pardo-Casas and Molnar, 1987; Somoza, 1998; Mpodozis and Ramos, 1989 and Figure 3-3). Crustal thickness increased from 40-45 km at the moment of emplacement of the voluminous Tertiary volcanic units, to approximately 65 km at the waning stages of volcanism in response to shortening in the upper Miocene (Kay and Abbruzzi, 1996, Ramos *et al.*, 1989; Allmendinger *et al.*, 1990). At *ca.* 12 Ma, a shallow-subduction geometry (<<30°) beneath the Andes resulted in the formation of a magmatic gap between the Central and Southern Volcanic Zone between 28°S and 33°S (Barazangi and Isacks, 1976; Kay *et al.*, 1999 and references therein). The present amagmatic gap and shallow subduction geometry is interpreted to have resulted from either of two mechanisms. One, the geometry resulted from a progressive and continuous flattening of the oceanic slab since 26 Ma (Kay *et al.*, 1987, 1988, 1991, 1999; Kay and Abbruzzi, 1996) related to the shape of the overriding South American plate (Isacks, 1988; Cahill

and Isacks, 1992) or, two, it is linked to the subduction of the Juan Fernández Ridge (Pilger, 1981, 1984; Yañez *et al.*, 2001; Kay and Mpodozis, 2002). The El Indio-Pascua Belt occupies the centre of the present-day amagmatic segment of the Andes between the volcanically active Central and Southern Volcanic Zones (e.g. Jordan *et al.*, 1983).

Late Paleozoic to Jurassic basement rocks

Late Paleozoic to middle Mesozoic volcanic, sedimentary and plutonic units are the dominant rocks in the composite basement of the El Indio Belt (Martin *et al.*, 1999; Jannas *et al.*, 1999; Bissig *et al.*, 2001). Carboniferous (?) shallow marine sandstones, schist and gneisses of restricted occurrence are the oldest rocks and lie in the hanging wall of the Baños del Toro Fault. East of that fault, Permian to Early Jurassic granitoids from the Elqui-Limarí Batholith and volcanic rocks of the Choiyoi Group form the basement to the Tertiary volcanic sequence. The Choiyoi Group, subdivided into the Permian rhyolitic Guanaco Sonso Formation and the Middle Triassic-Early Jurassic bimodal Los Tilos Formation, represent the oldest volcanic-related products in the region. The rhyolitic to dacitic ash-flow tuff and interbedded volcaniclastic rocks of Guanaco Sonso Formation are a major component of the El Indio Belt. These rocks, especially where hydrothermally altered, are locally very difficult to distinguish from altered Miocene volcanic rocks (Martin *et al.*, 1995; Bissig *et al.*, 2001).

Tertiary stratigraphy of the El Indio Belt

Eocene to early Oligocene rocks

The Eocene to early Oligocene Bocatoma Intrusive Unit (Mpodozis and Cornejo, 1988) and the Tobas del Valle del Cura Formation (Malizia *et al.*, 1997) form the oldest Tertiary units of the El Indio Belt.

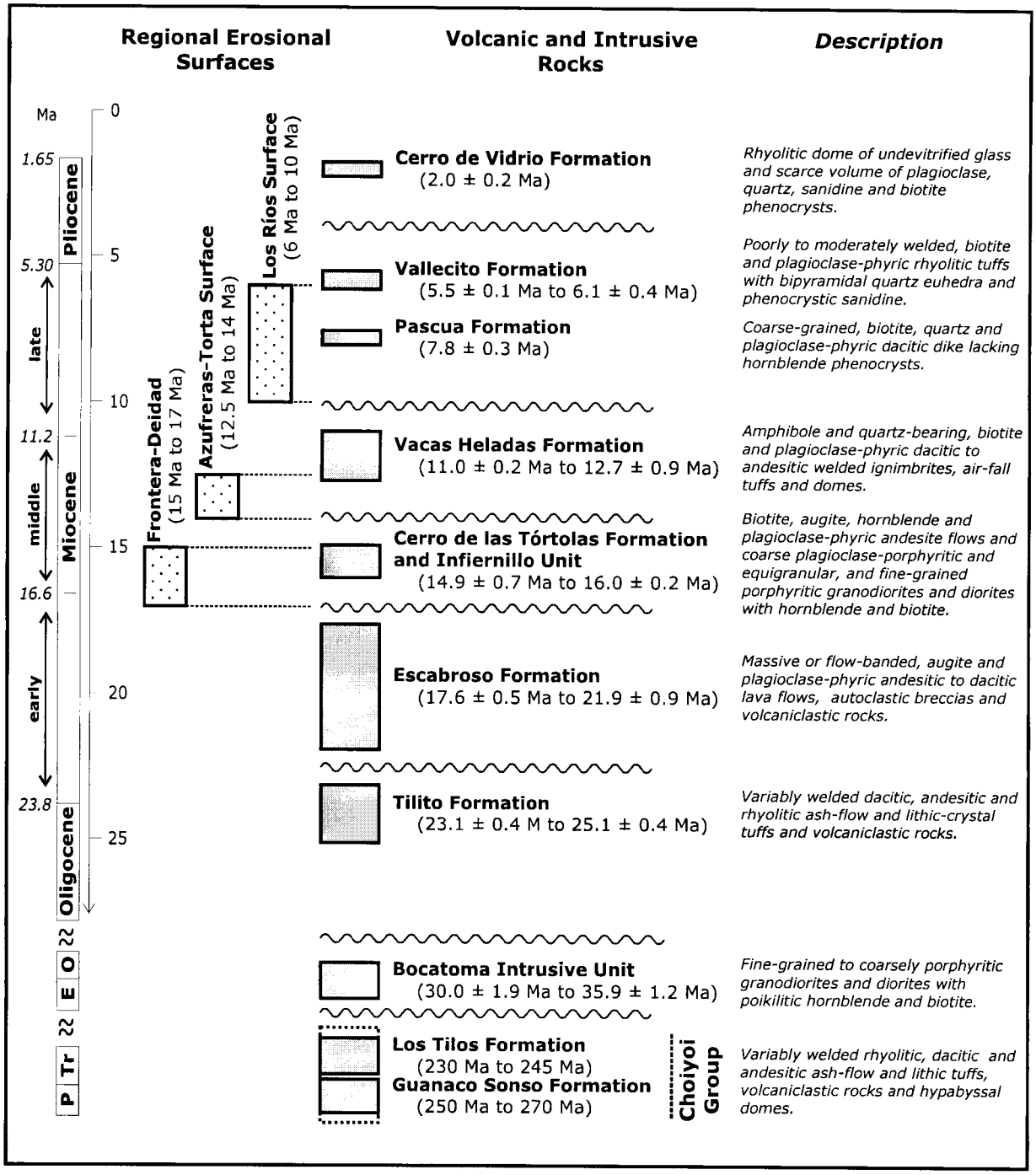

Figure 3-4: El Indio-Pascua Belt stratigraphy compiled from Martin et al. (1999) and Bissig et al. (2001). Abbreviations: P=Permian, Tr=Triassic, E=Eocene and O=early Oligocene. Choiyoi Group Formation names as in Chapter 2. The relative position of the Erosional Surfaces of the region is represented from higher altitude in the leflt side to lower altitude in the right side. Lithology from each unit is from the most representative rock types. Absolute ages extracted from Geology (1983) Time Scale.

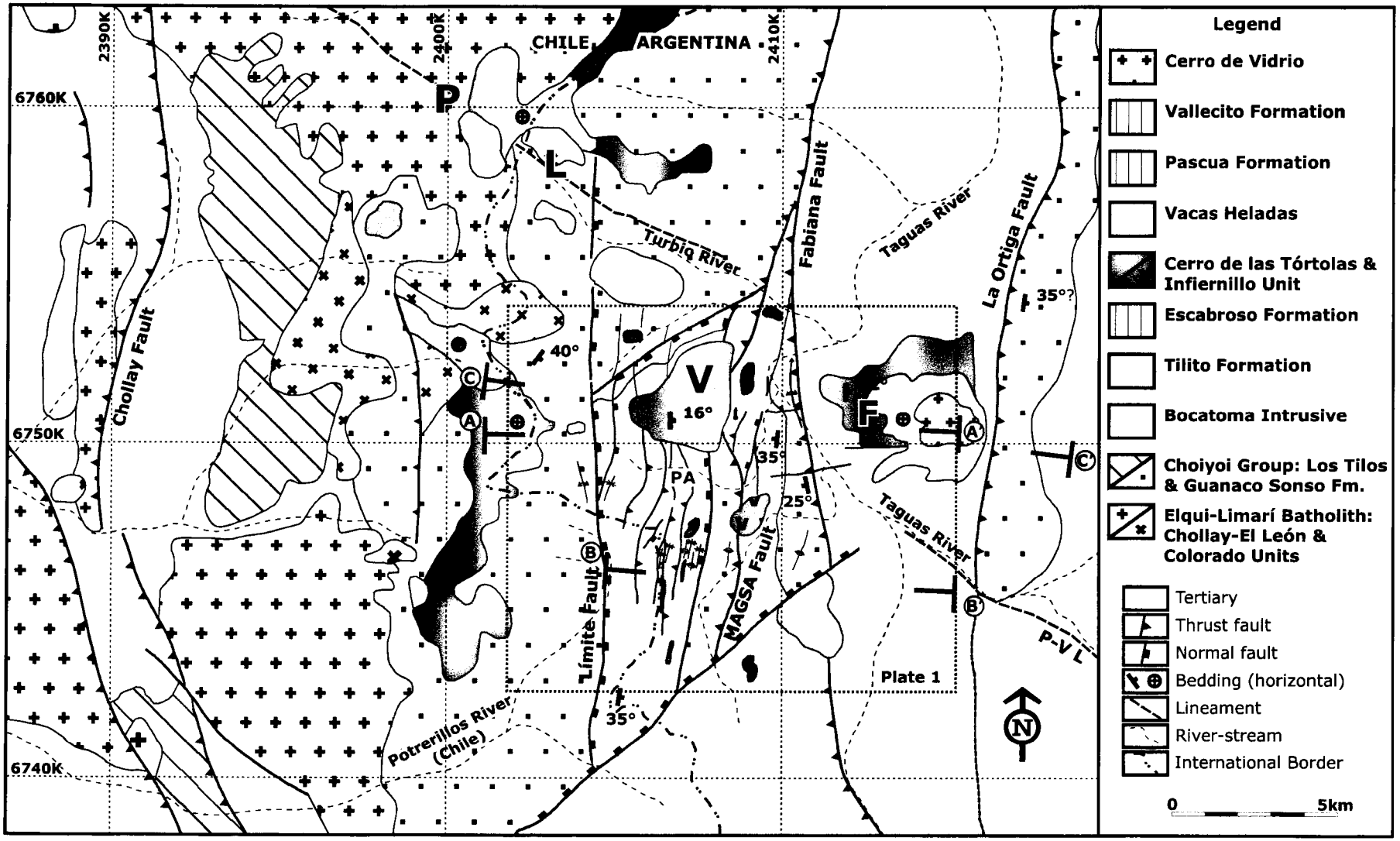

Figure 3-5: Veladero North-Pascua district geology. Compiled from Bissig et al. (2001), Deyell (2001), Martin et al. (1999) and field observations. Vallecito, Pascua and Escabroso Formations are not exposed in the map area. See Figures 3-19 and 3-20 for sections A-A' and B-B'. Section C-C' is shown in Figure 3-21. Abbreviations: V=Veladero North mineralization area, L=Lama, P=Pascua, F=Fabiana, P-V L=Pascua-Veladero Lineament, PA= Potrerillos River (Argentina). Reference grid is Gauss-Krugger (faja 2).

The Bocatoma Unit consists of fine to coarse-grained, hornblende-biotite-rich granodiorite and diorite stocks and dacite to andesite porphyries (Mpodozis and Cornejo, 1988; Martin *et al.*, 1995; Bissig *et al.*, 2001). The 36 Ma to 30 Ma small stocks, less than 2 km in diameter, intrude Paleozoic rocks. They are compositionally and texturally similar to intrusive phases of the Miocene Escabroso Formation and Infiernillo Unit and can be confused with those rocks in the field.

The Eocene to Oligocene (45 Ma to 34 Ma) Tobas Valle del Cura Formation, found only in Argentina, consists of andesitic flows interbedded within a predominately clastic sequence formed by sandstone and conglomerate (Malizia *et al.*, 1997).

Late Oligocene to late Pliocene rocks

Miocene volcanic and subvolcanic intrusions dominate the Tertiary stratigraphic sequence. The Tilito Formation (Martin *et al.*, 1997) is the most voluminous Cenozoic unit of the El Indio Belt, being locally as thick as 1200 m. The variably welded dacitic to rhyolitic ash-flow tuffs, volcano-sedimentary rocks and basaltic to andesitic lava flows were erupted between 25.1 ± 0.4 Ma and 23.1 ± 0.4 Ma (Bissig *et al.*, 2001).

The Escabroso and Cerro de las Tórtolas Formations unconformably overlie the Tilito Formation whereas the Infiernillo Unit intrude these rocks. These rocks represent the magmatic products of a volcanic arc active during that time span. The age of the Escabroso Formation is between 21.9 ± 0.9 Ma and 17.6 ± 0.5 Ma whereas the Cerro de las Tórtolas Formation and Infiernillo Unit is 16.0 ± 0.2 Ma to 14.9 ± 0.7 Ma (Bissig *et al.*, 2001). Andesitic to dacitic lava flows, autoclastic breccias, conglomerates, sandstones and minor ash-flow tuff form the extrusive phases of the Escabroso and Cerro de las Tórtolas Formations. Andesitic to dacitic porphyries that grade into equigranular stocks form the intrusive phases. Similar intrusive rocks form the (16.0 Ma to 14.9 Ma) Infiernillo Unit and these rocks represent the subvolcanic equivalent of the volcanic rocks of the Cerro de las Tórtolas Formation. Volcanic rocks from these two

units are petrologically and geochemically indistinguishable; they are assigned to the respective unit based on their ages (Martin *et al.*, 1995, 1997).

The 12.7 ± 0.9 Ma to 11.0 ± 0.2 Ma Vacas Heladas Formation unconformably overlie the older rocks in the El Indio-Pascua Belt (^{40}Ar-^{39}Ar data, Bissig *et al.*, 2001). Amphibole-, biotite- and quartz-phyric dacitic to andesitic welded ignimbrite, subvolcanic rocks of the same composition and reworked tuffs form the Vacas Heladas Formation (Martin *et al.*, 1995; Bissig *et al.*, 2001). The flat-lying volcanic rocks commonly form the highest ridges, and are associated with small eruptive centres scattered throughout the region. Age equivalent dacitic to andesitic dome complexes and contemporaneous ignimbrites extend to the eastern flank of the Cordillera Frontal and in the Precordillera, they record the eastward widening of the magmatic arc (Kay *et al.*, 1988; Kay and Abbruzzi, 1996), a common phenomenon that extended virtually as far north as southern Perú (e.g. Jordan *et al.*, 1983; Clark *et al.*, 1992).

Magmatic activity in the region markedly decreased after *ca.* 12 Ma and ceased by late Pliocene. A series of small units formed isolated entities along the El Indio-Pascua Belt. The Pascua Formation, as defined by Bissig *et al.* (2001), includes 7.8 ± 0.3 Ma dacitic dykes that crosscut the Vacas Heladas Formation. Dacitic tuffs of the same age, previously assigned to the Vallecito Formation at the southern end of the Valle del Cura in Argentina, are also included in the Vacas Heladas Formation. This rhyolitic tuff has ages of 6.1 ± 0.4 Ma to 5.5 ± 0.1 Ma (Bissig *et al.*, 2001; Ramos *et al.*, 1989) and contain subordinate sandstone and conglomerate. The latter tuff unit is related to a single volcanic centre although sedimentary rocks of the same age are very likely present throughout the El Indio-Pascua Belt.

A 2.1 ± 0.5 Ma (Bissig *et al.*, 2001) rhyolite dome located 4 km to the east of the Veladero North area (Figure 3-5 and Plate 1) is the youngest volcanic feature of the region. Dark grey glass with scarce plagioclase, quartz, sanidine and biotite phenocrysts form the dome that constitutes the Cerro de Vidrio Formation. Bissig and others (2002)

document the petrography, geochronology and goechemistry of the 3-km^2 obsidian dome that form this unit.

Structure

Multiple episodes of deformation during the Oligocene to Recent (Andean Orogeny) formed the north striking, east- and west-dipping high angle reverse faults, associated folds and subordinate normal faults that define the structural architecture of the El Indio-Pascua Belt (Martin *et al.*, 1995; Maksaev *et al.*, 1984; Nasi *et al.*, 1990; Mpodozis and Cornejo, 1988; Moscoso and Mpodozis, 1988, Malizia *et al.*, 1997). Late Paleozoic to early Mesozoic structures, such as the northern portion of the Chollay fault in Figure 3-5, are strongly overprinted by younger deformation events (Mpodozis and Ramos, 1989; Heredia *et al.*, 2002; Martin *et al.*, 1995). Triassic and Jurassic (?), northwest trending extensional structures controlled the position of relatively small pull-apart basins such as the Cuyo Basin, which are best preserved in southern part of the Cordillera Frontal (Ramos and Kay, 1991, Uliana *et al.*, 1989). In the El Indio Belt, tectonic inversion of Mesozoic faults is represented by northwest striking lineaments such as the Pascua-Veladero lineament (Jones *et al.*, 1999; Figure 3-2). Shortening deformation appears coeval with the initial stages of the Andean orogeny, and very likely limited the emplacement of the Tertiary volcanic units. The deformation front migrated progressively from west to east to the present location at the base of the Sierras Pampeanas, 600 km east off the trench, east of the Veladero North area (Jordan *et al.*, 1983; Ramos *et al.*, 1996; Cristallini *et al.*, 2000; Martin *et al.*, 1995).

Tertiary volcanic units provide important temporal constraints on the timing of the episodic deformation within the El Indio Belt. East of the Baños del Toro Fault, an angular unconformity and a regolith horizon between the (25.1 Ma to 23.1 Ma) Tilito and (21.9 Ma to 17.6 Ma) Escabroso Formations record regional Early Miocene deformation (Martin *et al.*, 1997; Bissig *et al.*, 2001). High-angle reverse faults and associated folds developed in the Tilito and Escabroso Formation rocks and unconformably overlain by

sub-horizontal strata from the (16.0 Ma to 14.9 Ma) Cerro de las Tórtolas Formation demonstrate a middle Miocene, east-west shortening event (Martin *et al.*, 1997).

Remanent late Miocene landforms

Bissig *et al.* (2002) defined a succession of geomorphological features throughout the El Indio-Pascua Belt as remnants of extensive pediplains. The moderately dissected planar landforms formed throughout the late Miocene when semi-arid climatic conditions dominated the region. Three erosional surfaces, vertically separated by 200 m to 400 m resulted from the episodic uplift of the Cordillera Frontal. From oldest to youngest, thus from highest to lowest in altitude, the surfaces are: Frontera-Deidad, Azufreras-Torta and Los Ríos. The 17 Ma to 15 Ma Frontera-Deidad Surface eroded intrusive bodies assigned to the Escabroso Formation, whereas volcanic rocks of the Cerro de las Tórtolas Formation were deposited over the erosional surface. The same relationship is documented for the 14 Ma to 12.5 Ma Azufreras-Torta surface as the Vacas Heladas Formation unconformably overlie along the surface cut across the Infiernillo Unit intrusives.

The Los Ríos Surface is the youngest geomorphic feature dissected after the (~11 Ma) Vacas Heladas Formation and before the emplacement of the (~6 Ma) Vallecito Formation ignimbrites (Figure 3-4). It commonly lies in the present valleys within the Cordillera.

Miocene volcanic framework of the Veladero North area

The Veladero North area is underlain by a Miocene fold and thrust system that superposes late Paleozoic Guanaco Sonso Formation and Oligocene Bocatoma Unit rocks over early Miocene rocks. The deformed rocks are unconformably covered and intruded by middle Miocene rocks (Plate 1 and Figure 3-5). The Tilito, Cerro de las Tórtolas-Inifernillo, Vacas Heladas and Cerro de Vidrio Formations have been recognized in the area. Rocks of the same age as the Escabroso Formation have not been identified.

Tilito Formation

Volcanic, intrusive and sedimentary rocks assigned to the Tilito Formation underlie as much as 50% of the map area on Figure 3-5. Three packages bounded by thrust and normal faults or unconformities with underlying Paleozoic rocks are recognized (Plate 1). Each package consists of a unique stratigraphic sequence not repeated in adjacent packages. Andesitic porphyry, dikes and plugs intrude the volcanic and volcaniclastic rocks, and may represent subvolcanic equivalents to the extrusive volcanic rocks. From east to west, the structural packages are located along and east of the Río Taguas valley (Río Taguas structural package), at the eastern flank of the Veladero deposit (East Veladero structural package) and at the base and south of the Cerro Pelado (West Veladero structural package).

Río Taguas structural package

Dark green andesitic rocks, brown volcaniclastic conglomerate and breccias and minor block and ash deposits form a sequence that crops out in the Taguas valley, along the access road to the Veladero North project. The rocks extend towards the east and south outside of the map area. The Fabiana fault defines the western limit of the structural package. It is a steep, west-dipping thrust fault that superposes late Paleozoic rocks over Miocene andesite along the Río Taguas. Middle Miocene Cerro de las Tórtolas and Vacas Heladas Formations unconformably cover the andesitic rocks east of the Fabiana fault (Plate 1).

The volcanic rocks are plagioclase- and biotite-phyric, hornblende, clinopyroxene (augite ?) and quartz-bearing, matrix-supported andesites that form coherent packages without visible bedding or foliation. The matrix is generally altered to clay minerals and partially devitrified. In hand specimen, the rocks are weakly magnetic due to the abundant fine-grained opaque minerals that are a common component of the matrix. Dark green monomict breccias with andesitic matrix and andesite blocks larger than 1 m

in diameter are subordinate to the andesitic lava previously described. Volcaniclastic conglomerate dominate the sequence (Figure 3-6a). The sequence likely represents the remanents of a dome field and surrounding volcaniclastic apron deposits.

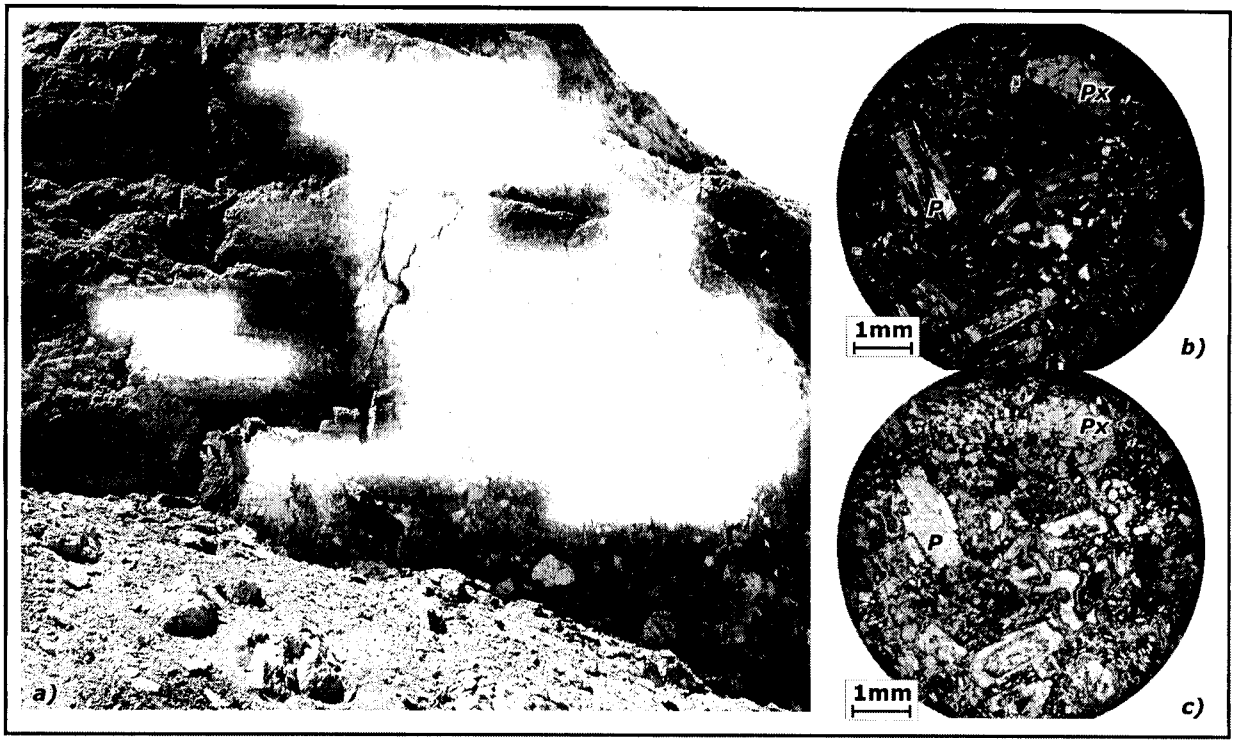

Figure 3-6: Tilito Formation rocks from the Río Taguas structural package. a) Volcaniclastic beds interbedded within monomict andesitic conglomerates. b) and c) Andesitic matrix in thin-section: Crystals and fragments of plagioclase (P), Pyroxene (Augite?) (Px) in a fine-grained, altered matrix. b) Transmitted cross-polarized light. c) Transmitted plane-polarized light.

Dark green porphyritic andesite intrudes the volcaniclastic sequence. The texture of these rocks varies from aphanitic to coarsely porphyritic. Their composition and irregular contacts suggest a syn-volcanic intrusive origin. Magmatic zircon geochronology indicates that the age of one of those porphyritic andesites is 25 ± 1.4 Ma (Figure 3-10a Sample DC-128b, SHRIMP data, Table 3-1). That age is consistent with the structural package being equivalent to the oldest part of the Tilito Formation rocks. Previously reported whole-rock K-Ar date of 20 ± 1 Ma from a sample located 500 m east of DC-128b (Malizia *et al.*, 1997) is a minimum age, most likely due to the overimposed propylitic alteration.

East Veladero structural package

Green and brown andesitic lithic tuffs, dark green volcaniclastic flows volcaniclastic conglomerates, and minor dacitic tuffs compose this unit. Welding defined by pumice fiammes with an aspect ratio of 10:1 (Figure 3-7) is a distinct feature of this sequence around Veladero North. The western margin of the East Veladero package is represented by a west-dipping thrust that places Permian Guanaco Sonso Formation over Tertiary units. The eastern boundary is an angular unconformity with late Paleozoic rocks. The Tertiary rocks dip more steeply than the underlying rocks. The tuff and conglomerate form a northerly striking unit that extends from the northern to the southern limit of the map area (Plate 1).

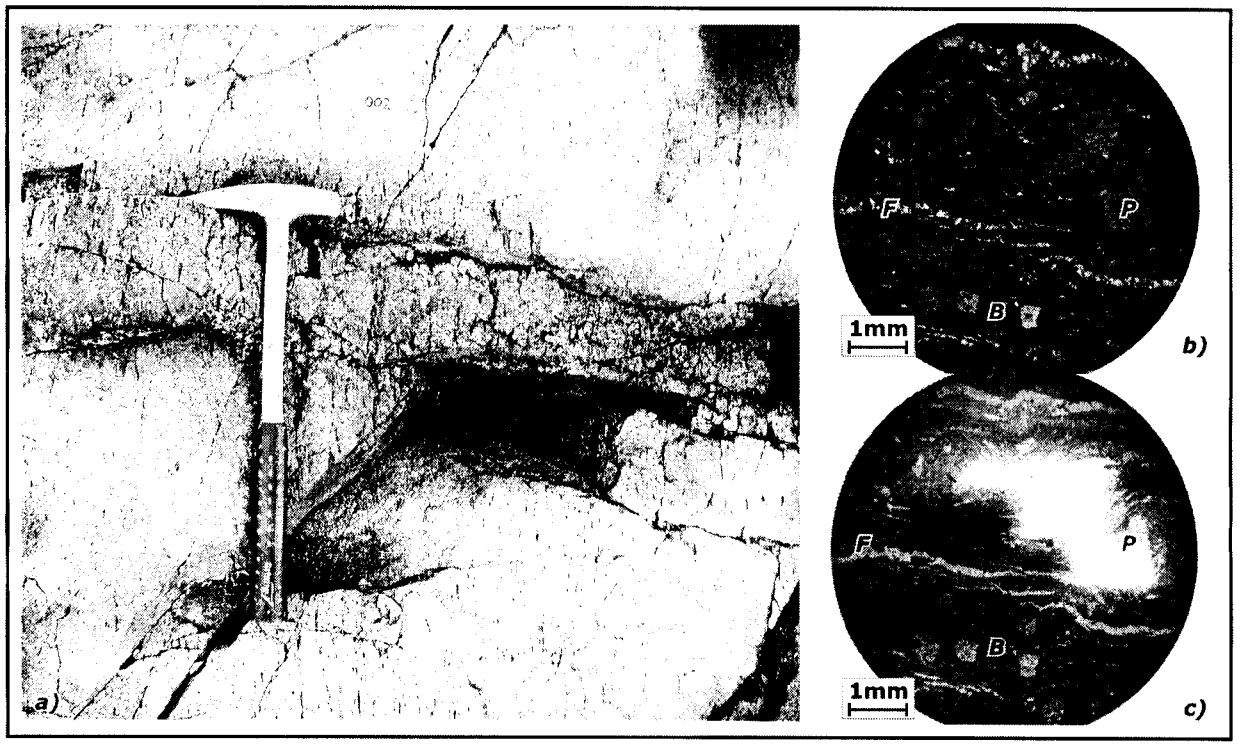

Figure 3-7: a) Tilito Formation rocks in the eastern flank of the Veladero North area. Fiammes and flow features are characteristic of this structural package. Fiammes are sub-vertical in the photographed outcrop. Welded dacite: Crystals and fragments of plagioclase (P), biotite (B) and recrystallized, deformed lithic fragments (F). b) Transmitted cross-polarized light. c) Transmitted plane-polarized light.

In detail, the volcanic rocks are carbonate-, clay- and chlorite- altered, crystal-rich andesites with as much as 40% lithic volcanic fragments. Plagioclase (40%), biotite and amphibole (30%), rare relict clinopyroxene (?), opaque minerals (30%) and small

amounts of quartz form phenocrysts. In the clay-altered aphanitic matrix, some flow or welding textures have been preserved (Figure 3-7). In the southern part of the study area, dark green, microphenocrystic plagioclase-bearing andesitic rocks with a preferred orientation of crystals and clasts are interpreted as volcaniclastic debris-flows. Very fine-grained to aphanitic intrusive andesites cannot be clearly distinguished from those flows except where contact relations are exposed.

Outcrops of welded andesitic tuff with sparse lithic fragments located 10 m above the unconformity with late Paleozoic rocks represent the lowest stratigraphic exposures of the Tilito Formation in the study area (Sample DC-120, Plate 1). Conventional U-Pb geochronology indicates that the ^{206}Pb-^{238}U age of the rock is 24.5 ± 0.2 Ma (Table 3-2, Figure 3-11a and Appendix for discussion). An east-dipping thrust places dacitic tuffs over the welded andesitic rocks at the Cerro Blanco, east of the Veladero mineralization area. Those dacitic rocks yield a conventional U-Pb age of 22.8 ± 1.7 Ma (Sample DC-111, Table 3-2 Figure 3-11b and Appendix).

West Veladero structural package

Light brown and purple welded dacitic to andesitic tuff, quartz-phyric dacite, red conglomerate and sandstone and minor dark grey basaltic andesite flows form the west Veladero structural package of the Tilito Formation. Most rocks assigned to this package lie south of the Potrerillos River valley. On the northern flank of that valley, the rocks that underlie the Cerro de las Tórtolas Formation (see below) in the Cerro Pelado area and that comformably cover the Guanaco Sonso Formation are also included in the same stratigraphic sheet. In both areas, dacitic ash-flow tuffs overlie red conglomerates or sandstones, and very likely represent similar stratigraphic levels. They provide an important stratigraphic link across the Potrerillos River valley. Two oppositely dipping faults that strike north define the east and west limits of the structural package (Plate 1). Along both faults, the observed stratigraphic relationship consists of younger rocks

over older, implying a normal displacement. Previous history of the fault is poorly constrained but the steep dip observed in the rocks is elsewhere seen in association with reverse faults (e.g. Martin *et al.*, 1995). Tight folds in the sedimentary rocks adjacent to the eastern fault require a component of shortening along the package-bounding faults (see below). Thus, although the younger-over-older stratigraphic relationship suggests normal displacement, it seems likely that the faults also had significant reverse movement.

The dominant rock types of this package are advanced argillic altered, welded, crystal-rich dacitic to andesitic ash-flow tuffs. Plagioclase, biotite and amphibole are the dominant phenocrysts; clinopyroxene is a common mineral in the andesitic rocks. Quartz phenocrysts are reabsorbed and in hand sample they appear as rounded, clear eyes (Figure 3-8). The felsic rocks from the Tilito Formation are very similar to the Permian Guanaco Sonso rhyolitic tuffs, although in the Permian rocks the quartz phenocrysts are more abundant and clinopyroxene is lacking. Where both Tertiary and Paleozoic rhyolitic tuffs are moderately to intensely altered it is very difficult to differentiate between them.

Red conglomerates and sandstones with interbedded volcaniclastic horizons are relatively common in the Tilito Formation. In the Portezuelo Sur area, the conglomerates contain rounded clasts, less than 25 cm in diameter, derived from volcanic rocks similar to the Guanaco Sonso Formation. Cross beds and channels are common features. Dacitic ash-flow tuffs (e.g. sample DC-163) overlie the sedimentary rocks. In the area located to the south of the Potrerillos Valley, folded sandstones and subordinate conglomerates with clasts compositionally identical to the Permian rocks, form a ~2 km long, north-south striking belt. The sandstones grade transitionally into purple volcaniclastic rocks and dacitic volcanic flows (e.g. sample DC-249).

Isolated, dark grey basaltic andesite lava flows with columnar joints are a minor rock type of the Tilito Formation. The rock is glassy and only plagioclase phenocrysts are visible. In thin section, the texture is microporphyritic; the matrix is very fine and

represents 60% of the rock. Plagioclase (80%), clinopyroxene (20%) and opaque minerals are the only phenocrysts.

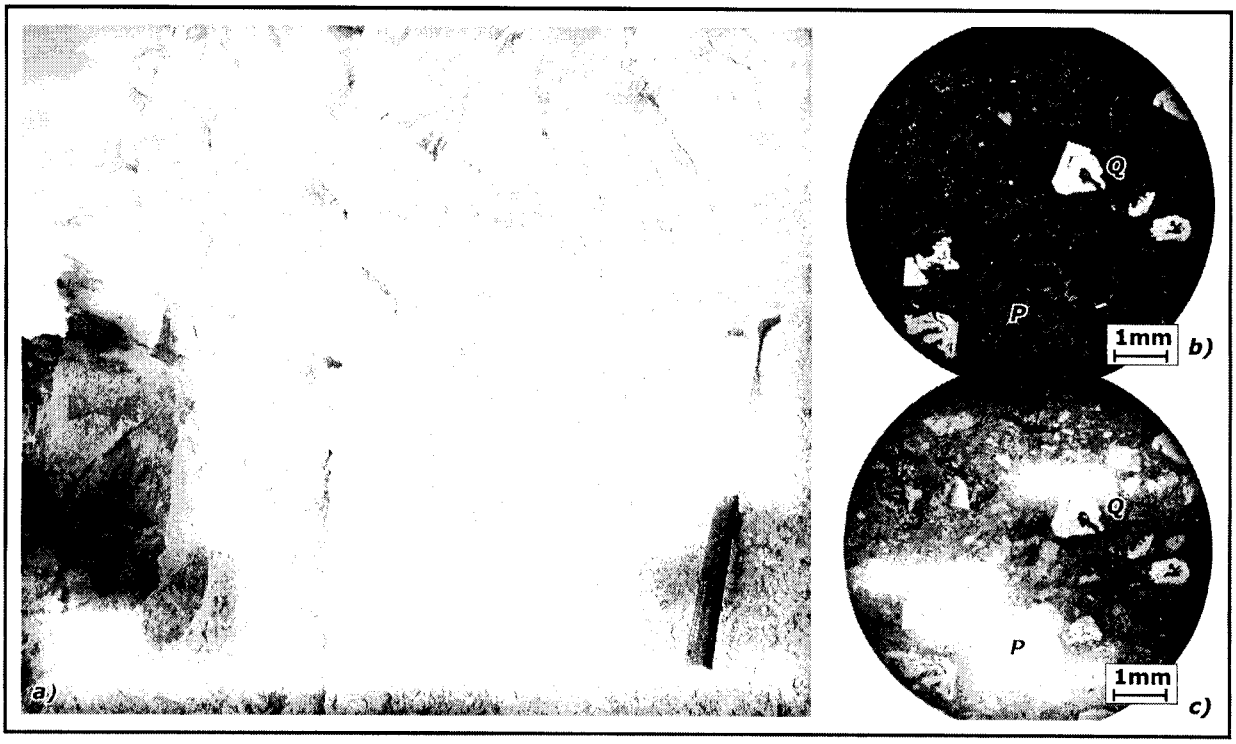

Figure 3-8: Tilito Formation rocks from the West Veladero structural package. a) Welded, dacitic flow tuffs cover volcaniclastic conglomerates. Dacitic tuff in b) transmitted cross-polarized light and c) transmitted plane-polarized light: Intensely altered crystals and fragments of plagioclase (P) and embayed quartz phenocrysts (Q) in a fine-grained, altered matrix. Relict welding is preserved.

The age of the West Veladero structural package on either side of the Potrerillos River is defined by samples DC-163 and DC-249 (Plate 1). The first sample (DC-163) is from the dacitic ash-flow tuffs located in the western margin of the mineralization zone in Veladero North area and immediately above the conglomerates. The second sample (DC-249) is from rocks of similar composition that overlie a sequence of tuffaceous sandstones and red conglomerates south of the Potrerillos River valley. Numerous zircon crystals and fragments were recovered from sample DC-163. SHRIMP analysis of elongate grains (typically magmatic) yield weighted mean ^{206}Pb-^{238}U age of 23 ± 1 Ma (Table 3-1 and Figure 3-10b). Preliminary results from conventional U-Pb geochronology show that the age of the same sample is constrained in the 22 Ma to 25 Ma range and that very likely the rock age is 23.5 ± 0.9 Ma (Table 3-2, Figure 3-11c and Appendix),

consistent with the limited data produced by SHRIMP. Sample DC-249 yield a preliminary U-Pb conventional age of 23.9 ± 0.2 Ma (Table 3-2, Figure 3-11d and Appendix) that is comparable to the age of the first sample.

Andesitic intrusive rocks equivalent to the Tilito Formation

Volcanic and volcaniclastic rocks from the Tilito Formation are intruded by dark green microporphyritic to aphanitic andesites, which likely represent the subvolcanic equivalent to the volcanic rocks. The intrusives range in plan view from several metres to as much as 100 metres in diameter. These rocks contain predominantly plagioclase phenocrysts, which are commonly altered to clays, as well as amphibole, biotite and minor clinopyroxene. The latter mineral is more abundant in these rocks than in the Infiernillo Intrusive Unit (see below), but otherwise both units have the same overall composition. The matrix is fine grained and opaque minerals are very abundant (Figure 3-9).

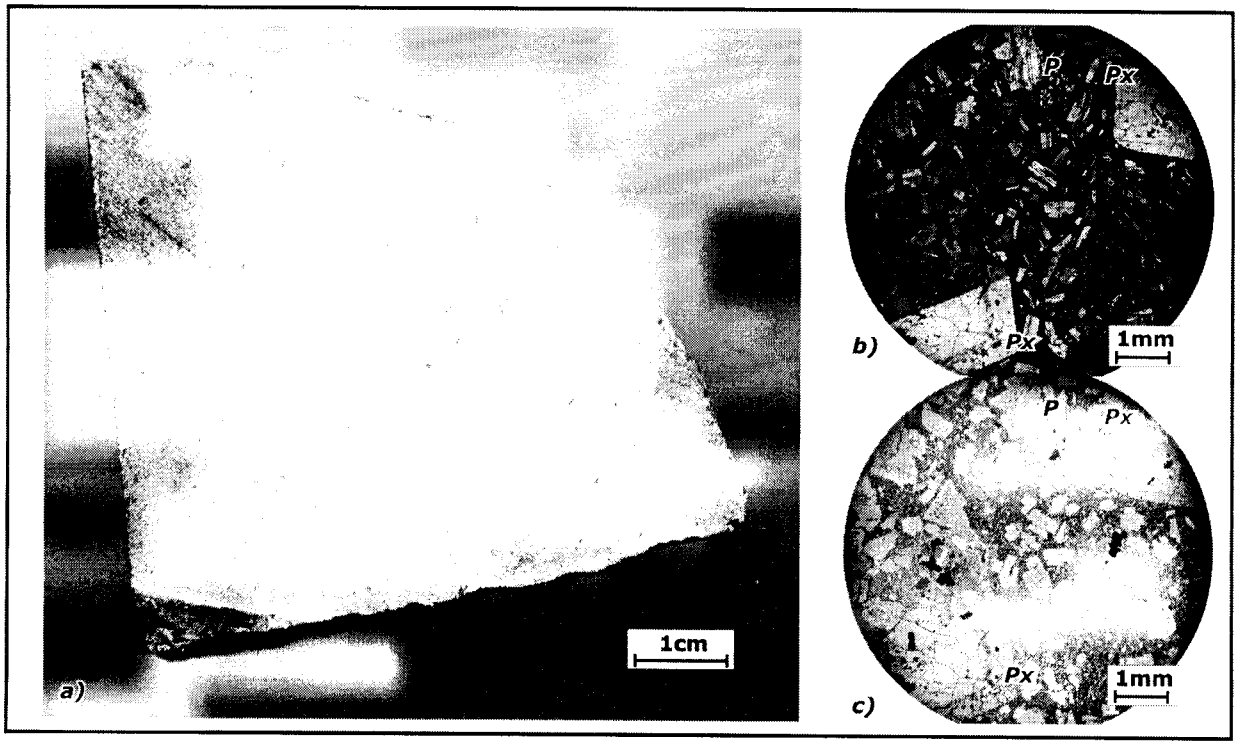

Figure 3-9: a) Hand specimen from the intrusive phase of the Tilito Formation. Porphyritic andesite in b) transmitted cross-polarized light and c) transmitted plane-polarized light: Altered crystals and fragments of plagioclase (P) and pyroxene (PX) phenocrysts in a fine-grained, altered matrix.

Table 3-1: Summary of SHRIMP analyses in the Veladero North area

Sample Spot Name	^{206}Pb [1] %	U (ppm)	Th (ppm)	$\frac{^{232}Th}{^{238}U}$	^{206}Pb [2] (ppm)	$\frac{^{206}Pb}{^{238}U}$ [2]	1σ %	Apparent Age (Ma, 1σ) $^{206}Pb/^{238}U$ [3]	
DC-128b									
DC128-1.1	0.0	116.1	134.5	1.196	0.36	0.003604	7.1	22.73	(1.7)
DC128-2.1	0.0	230.1	70.7	0.318	0.83	0.004222	5.4	26.49	(1.5)
DC128-3.1	2.8	2407	686.7	0.295	8.70	0.004089	3.1	27.08	(0.8)
DC128-4.1	0.0	400.5	355.4	0.917	1.38	0.004001	4.7	25.80	(1.2)
DC128-5.1	0.0	359.3	200.8	0.577	1.18	0.003819	4.6	24.26	(1.2)
DC128-6.1	0.0	305.5	205.0	0.693	0.94	0.003598	4.7	23.18	(1.1)
DC128-7.1	0.0	1013	643.7	0.657	3.19	0.003662	3.6	23.55	(0.9)
DC128-8.1	0.0	359.3	300.6	0.864	1.22	0.003943	5.4	25.25	(1.4)
DC-163									
DC163-1.1	29.4	237.1	387.3	1.688	0.91	0.003138	27.3	27.1	(1.7)
DC163-2.1	0.0	294.5	292.0	1.024	0.91	0.003590	5.4	21.9	(1.2)
DC163-3.1	31.3	388.6	662.4	1.762	2.06	0.004232	30.0	22.3	(2.8)
DC163-4.1	57.7	302.2	260.0	0.889	1.09	0.001778	75.1	23.5	(1.6)
DC163-5.1	0.0	592.0	519.0	0.906	1.80	0.003532	5.9	22.7	(1.3)
DC163-6.1	42.9	211.8	177.6	0.866	0.69	0.002177	20.3	21.2	(1.6)
DC163-7.1	34.1	689.9	1179.0	1.766	2.36	0.002620	22.3	21.8	(1.1)
DC163-8.1	0.0	212.6	190.4	0.925	0.76	0.004180	6.4	25.6	(1.7)
DC-375									
DC375-1.1	112.4	120.5	132.0	1.131	0.47	-0.00056	301.3	20.31	(2.1)
DC375-2.1	27.6	913.4	954.9	1.080	3.11	0.00287	5.3	15.01	(1.7)
DC375-3.1	0.0	389.1	379.0	1.006	1.00	0.00299	4.8	17.18	(0.9)
DC375-4.1	0.0	82.8	60.7	0.758	0.25	0.00352	12.8	17.77	(2.8)
DC375-5.1	0.0	131.2	121.3	0.955	4.63	0.04107	3.4	257.3	(8.8)
DC375-6.1	69.5	597.0	766.1	1.326	1.67	0.00099	93.7	15.03	(0.9)
DC375-7.1	0.0	292.7	352.0	1.242	0.69	0.00276	6.0	16.53	(1.0)
DC375-8.1	0.7	555.1	365.8	0.681	19.66	0.04094	2.7	259.0	(7.1)

[1] Common lead

[2] Radiogenic lead

[3] $^{206}Pb/^{238}U$ age using ^{207}Pb to correct for common lead

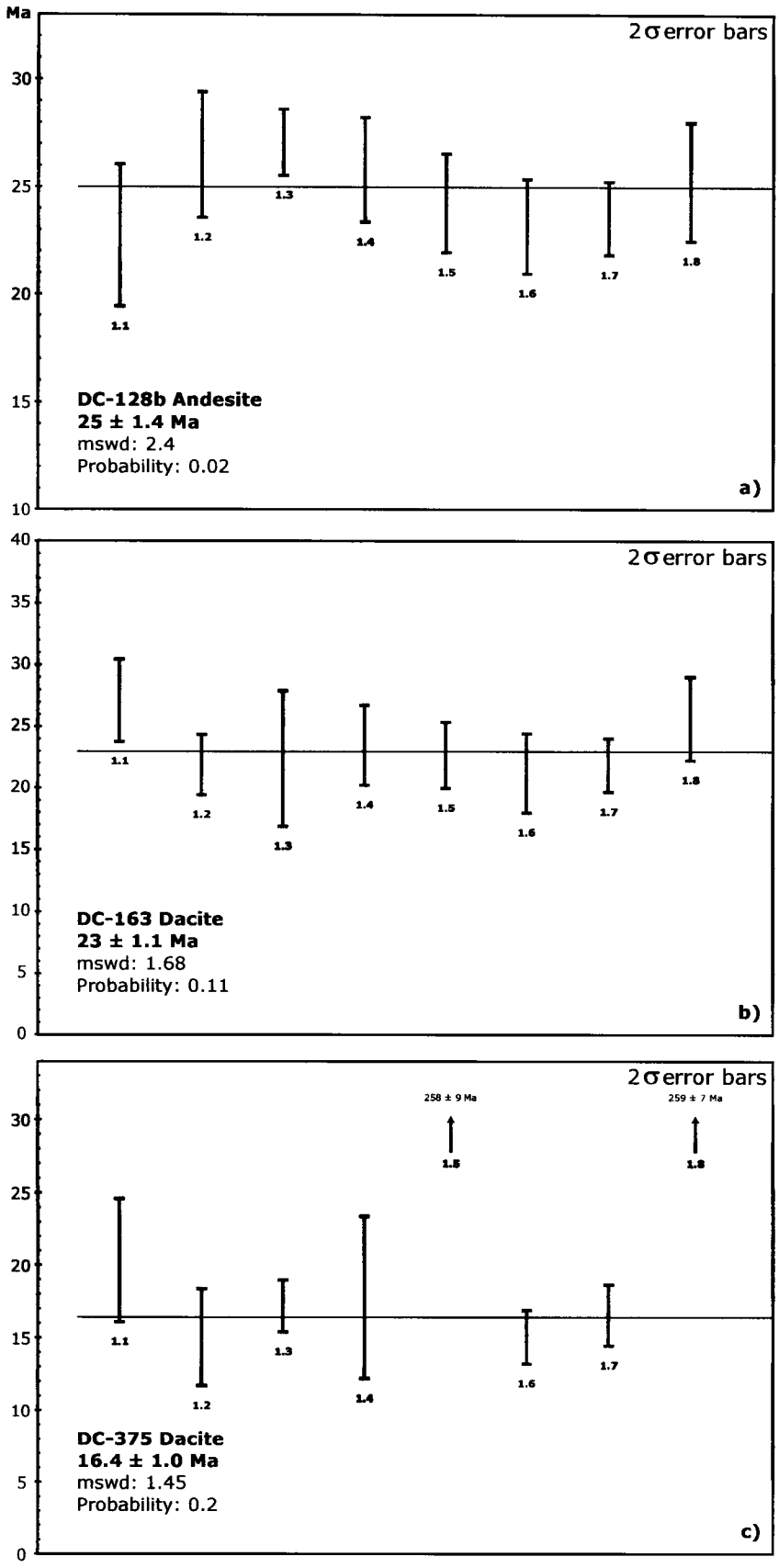

Figure 3-10: SHRIMP data of Veladero North samples. Reported age is a weighted mean of $^{206}Pb/^{238}U$ ages. See appendix and Table 3-1 for analytical data and results.

Table 3-2: Summary of U-Pb geochronology in the Veladero North area

Sample	Wt.	U[2]	Pb*[3]	$^{206}Pb/^{204}Pb$[4]	Pb[5]	^{208}Pb[3]	Isotopic Ratios (1σ, %)[6]			Apparent Age 2σ, Ma [6]		
Fraction[1]	(mg)	(ppm)	(ppm)		(pg)	%	$^{206}Pb/^{238}U$	$^{207}Pb/^{235}U$	$^{207}Pb/^{206}Pb$	$^{206}Pb/^{238}U$	$^{207}Pb/^{235}U$	$^{207}Pb/^{206}Pb$
DC-120 (◇)												
A vc, n2, s, p	0.128	406	2	105	147	19.7	0.003820 (0.24)	0.02519 (1.90)	0.04783 (1.70)	24.6 (0.1)	25.3 (1.0)	91.0 (84.6)
B vc, n2, s, s	0.170	294	1	485	26	14.1	0.003824 (0.18)	0.02370 (1.10)	0.04494 (0.99)	24.6 (0.1)	23.8 (0.5)	-58.6 (49.2)
C vc, n2, s, p	0.372	357	1	389	87	15.8	0.003826 (0.14)	0.02475 (0.57)	0.04691 (0.48)	24.6 (0.1)	24.8 (0.3)	44.8 (23.3)
D vc, n2, s, p	0.216	436	2	397	84	15.1	0.005302 (0.10)	0.03498 (0.54)	0.04785 (0.47)	34.1 (0.1)	34.9 (0.4)	92.1 (22.3)
E vc, n2, m, p	0.330	314	1	273	98	18.6	0.003795 (0.18)	0.02445 (0.76)	0.04672 (0.67)	24.4 (0.1)	24.5 (0.4)	34.8 (32.3)
F vc, n2, s, su	0.260	239	1	165	102	15.2	0.003792 (0.19)	0.02473 (1.20)	0.04730 (1.10)	24.4 (0.1)	24.8 (0.6)	64.2 (53.3)
G c, n2, s, p	0.188	406	2	443	45	16.4	0.003943 (0.11)	0.02555 (0.62)	0.04700 (0.56)	25.4 (0.1)	25.6 (0.3)	49.0 (26.9)
H c, n2, s, p	0.160	368	2	357	64	15.4	0.005816 (0.11)	0.03904 (0.63)	0.04869 (0.56)	37.4 (0.1)	38.9 (0.5)	133.0 (26.5)
I f, n2, n, pn	0.462	475	2	260	231	18.1	0.003971 (0.15)	0.02586 (0.73)	0.04724 (0.63)	25.5 (0.1)	25.9 (0.4)	61.4 (30.4)
DC-111 (◇)												
A m, n2, s, p	0.238	163	1	56	247	26.0	0.003782 (0.51)	0.02510 (4.00)	0.04814 (3.60)	24.3 (0.2)	25.2 (2.0)	106.2 (181)
B m, n2, s, p	0.128	141	1	31	341	27.6	0.003781 (1.50)	0.02813 (10.4)	0.05396 (9.50)	24.3 (0.7)	28.2 (5.8)	369.4 (494)
C m, n2, s, s	0.249	162	2	65	577	18.3	0.010310 (0.43)	0.07445 (3.00)	0.05237 (2.80)	66.1 (0.6)	72.9 (4.3)	301.7 (130)
D m, n2, n, n	0.365	145	1	36	689	27.3	0.003463 (1.20)	0.02747 (7.90)	0.05753 (7.10)	22.3 (0.5)	27.5 (4.3)	511.8 (347)
E f, n2, n, n	0.070	165	1	58	105	21.7	0.005657 (0.51)	0.03923 (4.00)	0.05030 (3.60)	36.4 (0.4)	39.1 (3.0)	208.9 (177)
F f, n2, n, n	0.044	201	1	26	266	26.3	0.003464 (2.60)	0.02451 (19.0)	0.05131 (17.4)	22.3 (1.1)	24.6 (9.2)	254.9 (650)
G f, n2, s, p	0.028	186	1	26	165	27.3	0.003755 (2.50)	0.03036 (16.2)	0.05863 (14.6)	24.2 (1.2)	30.4 (9.7)	553.3 (810)
DC-163 (◇)												
A vc, n2, s, s	0.026	615	7	2408	4	28.6	0.008520 (0.20)	0.05543 (0.40)	0.04718 (0.34)	54.7 (0.2)	54.8 (0.4)	58.5 (16.1)
B vc, n2, s, s	0.026	112	1	263	5	21.3	0.007178 (0.31)	0.05361 (2.00)	0.05417 (1.90)	46.1 (0.3)	53.0 (2.1)	378.3 (88.5)
C c, n2, s, p	0.146	147	1	89	74	25.8	0.003766 (0.30)	0.02543 (2.40)	0.04897 (2.20)	24.2 (0.1)	25.5 (1.2)	146.4 (105)
D c, n2, s, p	0.077	156	3	401	31	14.4	0.015419 (0.23)	0.10701 (1.20)	0.05034 (1.10)	98.6 (0.4)	103.2 (2.3)	210.5 (50.4)
E c, n2, s, p	0.065	150	3	109	114	18.9	0.016550 (0.23)	0.11721 (1.60)	0.05136 (1.50)	105.8 (0.5)	112.5 (3.5)	257.2 (67.8)
F m, n2, n, n	0.230	181	1	49	327	26.7	0.003762 (0.64)	0.02663 (4.70)	0.05134 (4.30)	24.2 (0.3)	26.7 (2.5)	256.3 (208)
G c, n2, n, n	0.261	199	1	70	230	25.6	0.003542 (0.39)	0.02356 (3.00)	0.04824 (2.70)	22.8 (0.2)	23.6 (1.4)	111.1 (132)
DC-249 (◇)												
A m, n5, s, s	0.343	26	<1	127	20	24.5	0.003716 (0.24)	0.02460 (2.10)	0.04801 (1.90)	23.9 (0.1)	24.7 (0.1)	99.6 (93.5)
B, m, n5, s, p	0.213	58	<1	136	40	23.2	0.006030 (0.21)	0.04317 (1.60)	0.05193 (1.40)	38.8 (0.2)	42.9 (1.3)	282.3 (67.0)
C f, n5, s, p	0.063	95	<1	116	16	25.7	0.004178 (0.29)	0.02562 (2.50)	0.04448 (2.30)	26.9 (0.2)	25.7 (1.3)	-83.9 (118)
D f, n5, s, p	0.012	112	<1	49	10	25.4	0.003606 (0.72)	0.01851 (11.3)	0.03722 (10.8)	23.2 (0.3)	18.6 (4.2)	540.5 (708)
E m, n5, s, p	0.024	134	1	284	5	18.8	0.006920 (0.26)	0.04507 (1.80)	0.04725 (1.70)	44.5 (0.2)	44.8 (1.5)	61.6 (81.3)
DC-374 (‡)												
B c, n2, s, an	0.062	22	<1	29	21	17.2	0.002443 (3.40)	0.01183 (23.8)	0.03510 (22.0)	15.7 (1.1)	11.9 (5.6)	700.4 (2010)
C m, n2, s, p	0.022	112	<1	62	8	26.7	0.002387 (1.60)	0.01532 (20.2)	0.04653 (19.3)	15.4 (0.5)	15.4 (6.2)	25.1 (700)
D m, n2, s, s	0.062	215	1	21	1626	34.2	0.004007 (17.9)	0.05095 (37.7)	0.09222 (29.6)	25.8 (9.2)	50.5 (37)	1471.9 (1998)
E m, n2, m, pan	0.012	241	2	140	13	12.5	0.008955 (0.34)	0.05791 (1.90)	0.04690 (1.70)	57.5 (0.4)	57.2 (2.1)	44.1 (85.1)

Table 3-2: Cont'd

Sample	Wt.	U[2]	Pb*[3]	$^{206}Pb/^{204}Pb$[4]	Pb[5]	^{208}Pb[3]	Isotopic Ratios (1σ, %)[6]			Apparent Age 2σ, Ma [6]		
Fraction[1]	(mg)	(ppm)	(ppm)		(pg)	%	$^{206}Pb/^{238}U$	$^{207}Pb/^{235}U$	$^{207}Pb/^{206}Pb$	$^{206}Pb/^{238}U$	$^{207}Pb/^{235}U$	$^{207}Pb/^{206}Pb$
DC-374 (‡)												
F f, n2, m, s	0.025	323	1	67	25	20.1	0.002415 (0.74)	0.01565 (3.80)	0.04700 (3.40)	15.5 (0.2)	15.8 (1.2)	49.4 (173)
G f, n2, n, n	0.025	343	2	30	220	19.9	0.004551 (3.30)	0.02176 (18.7)	0.03468 (16.8)	29.3 (1.9)	21.9 (8.1)	734.1 (749)
DC-265 (◇)												
A c, n2, s, eq	0.113	128	<1	76	42	20.4	0.002591 (0.41)	0.01593 (3.70)	0.04460 (3.40)	16.7 (0.1)	16.1 (1.2)	-77.6 (177)
B vc, n2, s, p	0.637	143	<1	99	185	20.1	0.002568 (0.32)	0.01629 (2.40)	0.04600 (2.10)	16.5 (0.1)	16.4 (0.8)	-2.3 (107)
C vc, n2, s, p	0.501	179	1	121	154	21.5	0.002751 (0.22)	0.01777 (1.60)	0.04686 (1.40)	17.7 (0.1)	17.9 (0.6)	42.3 (70.0)
D vc, n2, s, s	0.205	153	<1	122	50	20.8	0.002578 (0.37)	0.01455 (3.60)	0.04094 (3.40)	16.6 (0.1)	14.7 (1.1)	-291.0 (185)
E vc, n2, s, eq	0.208	125	<1	212	22	21.0	0.002604 (0.21)	0.01631 (1.40)	0.04543 (1.30)	16.8 (0.1)	16.4 (0.5)	-32.6 (65.0)
DC-304 (‡)												
A c, n2, n, n	0.137	541	1	36	596	20.1	0.002216 (2.10)	0.01452 (8.70)	0.04754 (7.50)	14.3 (0.6)	14.6 (2.5)	76.4 (321)
B m, n2, n, n	0.122	490	1	34	460	22.3	0.001908 (2.40)	0.01362 (8.90)	0.05177 (7.50)	12.3 (0.6)	13.7 (2.4)	275.4 (387)
C c, n2, s, p	0.444	366	2	242	190	14.8	0.004074 (0.19)	0.02759 (0.74)	0.04911 (0.60)	26.2 (0.1)	27.6 (0.4)	153.1 (28.4)
D c, n2, s, eq	0.240	514	2	193	132	14.0	0.002935 (0.23)	0.01966 (0.94)	0.04858 (0.78)	18.9 (0.1)	19.8 (0.4)	127.8 (37.1)
E c, n2, s, pan	0.134	531	3	82	358	15.2	0.005012 (0.63)	0.03513 (2.40)	0.05083 (2.00)	32.2 (0.4)	35.1 (1.6)	233.2 (95.0)
F c, n2, s, an	0.177	484	3	34	1711	17.2	0.004919 (2.40)	0.03543 (8.90)	0.05224 (7.60)	31.6 (1.5)	35.4 (6.2)	295.7 (313)
G f, n2, n, n	0.016	661	2	59	42	22.4	0.002552 (0.90)	0.01582 (4.20)	0.04497 (3.70)	16.4 (0.3)	15.9 (1.3)	57.5 (171)
H f, n2, n, n	0.013	801	2	57	32	23.7	0.001858 (0.93)	0.01173 (4.40)	0.04581 (3.90)	12.0 (0.2)	11.8 (1.0)	12.6 (179)

[1]Zircon fraction identifier
Zircons are non-magnetic on a Frantz magnetic separator at field strength of 1.8 A with: m5=magnetic at side slope of 5°, m2=magnetic at side slope of 2°
n2=non-magnetic at side slope of 2°, n1=non-magnetic at side slope of 1°
Grain size: vc=>134 μm, c=<134 μm and >104 μm, m=<104 μm and >74 μm, f=<74 μm.
Air abraded fractions are marked with s=strong, m=medium, n=non abraded.
Grain shape: el=elongate, eq=equant, eu=euhedral, p=prismatic, s=stubby, su=subhedral, an=anhedral, ta=tabular, ti=tips or n=needles
[2]U blank correction of 1 pg ± 20%; U fractionation corrections were measured for each run with a double ^{233}U-^{235}U spike (about 0.005/amu).
[3]Radiogenic Pb.
[4]Measured ratio corrected for spike and Pb fractionation of 0.0035/amu ± 20% (Daly collector) and 0.0012/amu ± 20% and laboratory blank Pb of 1-3 pg ± 20%.
Laboratory blank Pb concentrations and isotopic compositions based on total procedural blanks analyzed.
[5]Total common Pb in analysis based on blank isotopic composition.
[6]Corrected for blank Pb, U and common Pb. Common Pb corrections based on Pb isotopic compositions of feldspars of equivalent, non-altered rocks from Bissig et al.(2003)
Isotopic compositions have uncertainties of less than 0.1% (2σ).
(◇) Tilito Formation samples were corrected with Pb isotopic composition: $^{208}Pb/^{204}Pb$=38.509, $^{207}Pb/^{204}Pb$=15.605 and $^{206}Pb/^{204}Pb$=18.625.
(‡) Cerro de las Tórtolas Formation samples were corrected with Pb isotopic composition: $^{208}Pb/^{204}Pb$=38.503, $^{207}Pb/^{204}Pb$=15.595 and $^{206}Pb/^{204}Pb$=18.651.

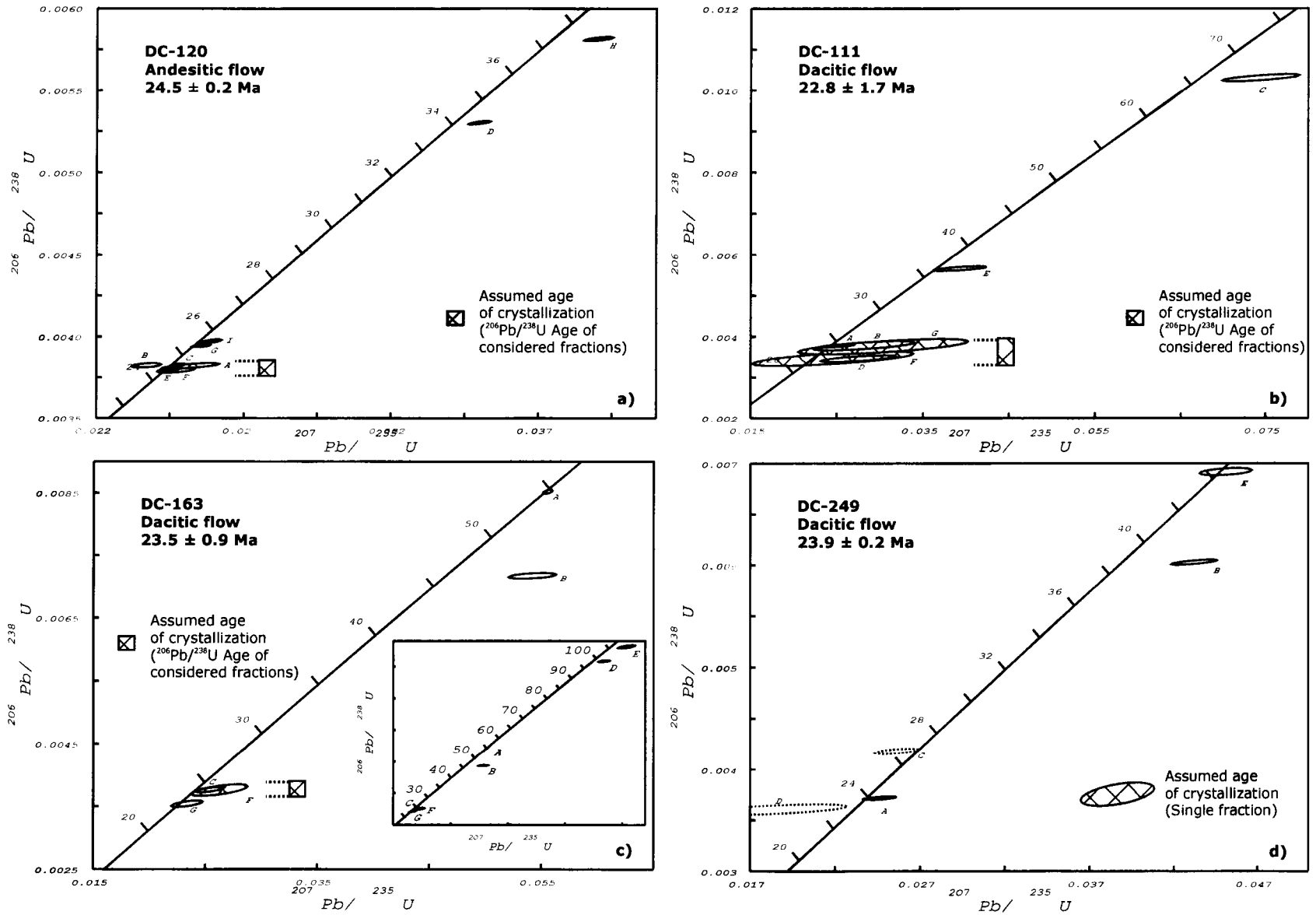

Figure 3-11: Concordia diagrams from Veladero North samples. See next page for details.

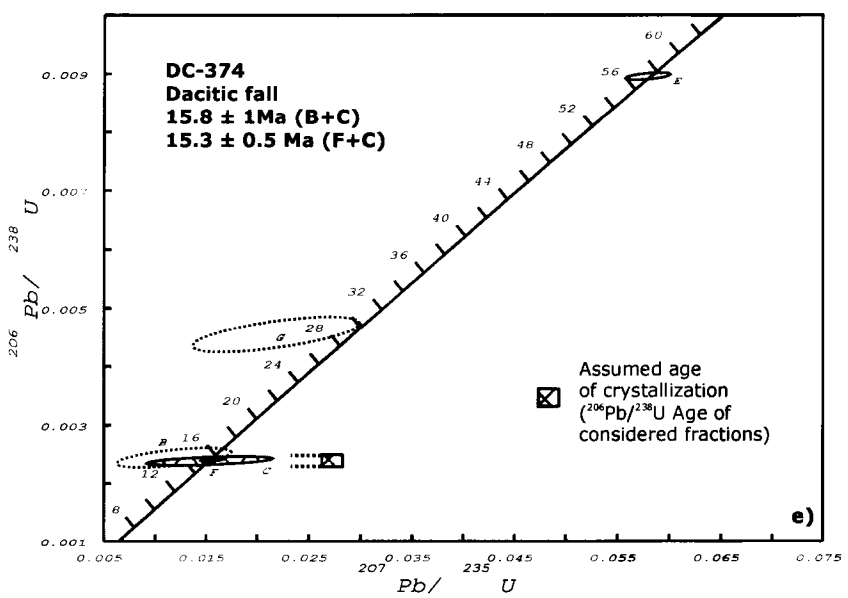

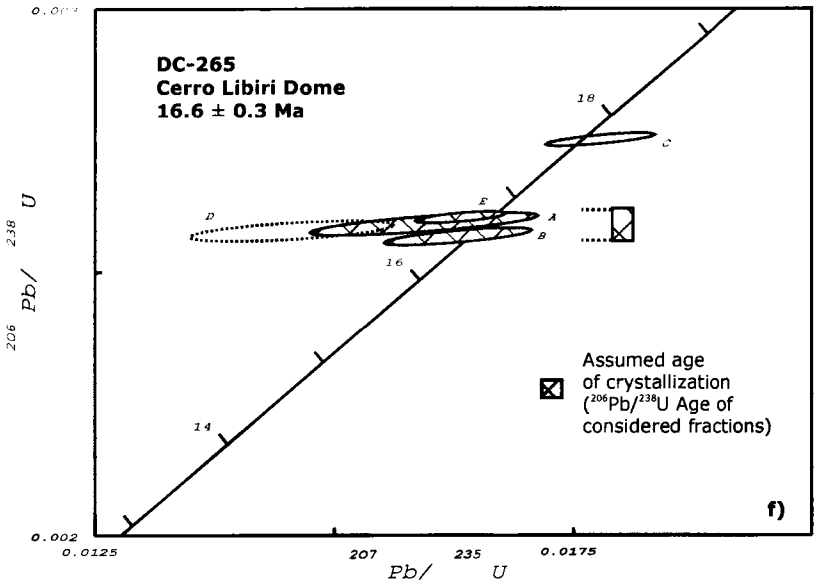

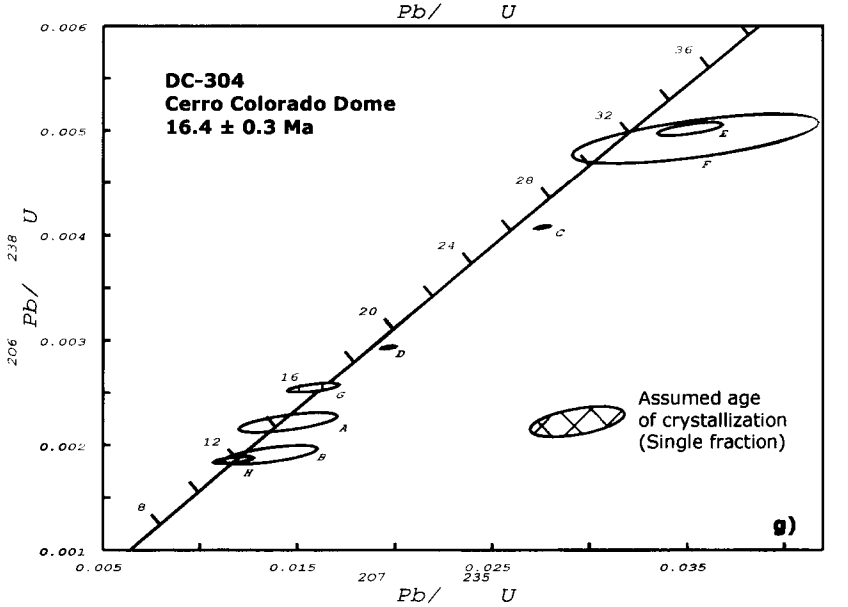

Figure 3-11: Concordia diagrams from Veladero North samples. Reported age of crystallization is $^{206}Pb/^{238}U$ age of indicated fractions. Uncertainty in age is based upon range of uncertainty of considered fractions and reflects maximum and minimum probable ages at 2 sigma level.See appendix for age determination and Table 3-2 for analytical data and results. Uncertainty ellipses shown at 2 sigma level.

Cerro de las Tórtolas Formation

Volcanic breccias, conglomerate, volcaniclastic and sedimentary rocks unconformably overlying Guanaco Sonso and Tilito Formations rocks have been assigned to the Cerro de las Tórtolas Formation. The Cerro de las Tórtolas Formation is present in three separate areas, Veladero, Turbio River and Fabiana (Plate 1). A tabular package along the east and northeast flank of the Cerro Pelado and next to its summit is the largest extent of the formation. Most of the Veladero North epithermal deposit is hosted in these rocks and consequently these rocks are referred hereafter as the Veladero section. A second section of the formation comprises a series of outcrops in the southern flank of the Turbio River and west of the Río Taguas. These rocks, known as the Turbio River section, are located to the northeast but are separated from the mineralized zone by rocks of the Tilito Formation. Flat-lying rocks in the Fabiana prospect area at the east side of the Río Taguas form the third section, these are referred to as Fabiana section (Plate 1).

Age-equivalent shallow intrusive, domes and their vent products, although intimately related, form the Infiernillo Intrusive Unit and will be described in a separate section.

Veladero Section

A diatreme model has been proposed to explain both the mineralization characteristics and the origin of the Veladero North deposit and the Veladero section (Jones *et al.*, 1999; Corbett, 1999). In this model, a volcanic pipe (diatreme) with sub-vertical margins cut through the basement rocks as a result of near-surface, phreato-magmatic eruptions localized along structural anisotropies. In the Veladero North area, two types of breccias were recognized. Bedded heterolitic breccias are considered to represent the subaerial volcanic products emplaced during and immediately after the explosive eruption. Milled breccias composed of rounded to sub-angular fragments in a

fine-grained predominant matrix (tuffisites) are considered to represent the vent facies.

Figure 3-12: a) Cerro de las Tórtolas Formation rocks from the Veladero Section. Bedded heterolitic breccias and interfingered fine-grained beds of volcaniclastic sandstone and tuff. b) DDH042 core (-125m) intercepts very well bedded sandstone and heterolitic breccias. Note the volcanic (VI) and juvenile dacitic fragments (JI) embedded in a fine-grained matrix.

East of Cerro Pelado, strongly altered heterolithic breccias in coarsely to well-bedded horizons form the upper part of the Cerro de las Tórtolas Formation. Breccia fragments are angular to subrounded, derived from quartz-bearing volcanic rocks, porphyritic intrusives or textureless sedimentary (?) rocks. The original composition and texture are, in most of the cases, completely obscured by superposed alteration. Near Amable, the matrix of the fragmental rocks is ash to lapilli-size material, and the breccias range from clast-supported to matrix-supported assemblages. Very well bedded volcaniclastic sandstones lacking fragments are also common (Figure 3-12a). Tabular clasts are aligned parallel to bedding, and in strongly silicified rocks, their presence can be used to define bedding. In general, the rocks are non-graded or they show a relatively narrow zone of normal grading, which suggests deposition during fluid flow. Along the Filo Federico ridge, the fragments are completely replaced by silica and they

are often difficult to distinguish from the matrix. There, the breccia texture appears to be massive, but whether this is primary or an effect of secondary silicification is uncertain. As a general rule, the fragment size increases towards the west and south, reaching a maximum of 45-50 cm near Cerro Pelado.

Tuff, volcaniclastic siltstone and sandstone form beds 1 to 10 cm thick throughout the bedded heterolitic breccias. The beds are also visible in drill core (DDH040 and DDH042) between 114 and 125 m below the surface (Figure 3-12b). These horizons set the minimum thickness of the Veladero section of the Cerro de las Tórtolas Formation. A thin (<3 cm) sandstone layer interbedded with heterolithic breccias was also observed 245 m below the surface (DDH040), but pervasive superimposed advanced argillic alteration obscures the primary protolith of these rocks. The rocks could be tuffaceous rocks in the Veladero section, or be part of the composite Permian Guanaco Sonso and Tilito basement that underlies the Veladero section.

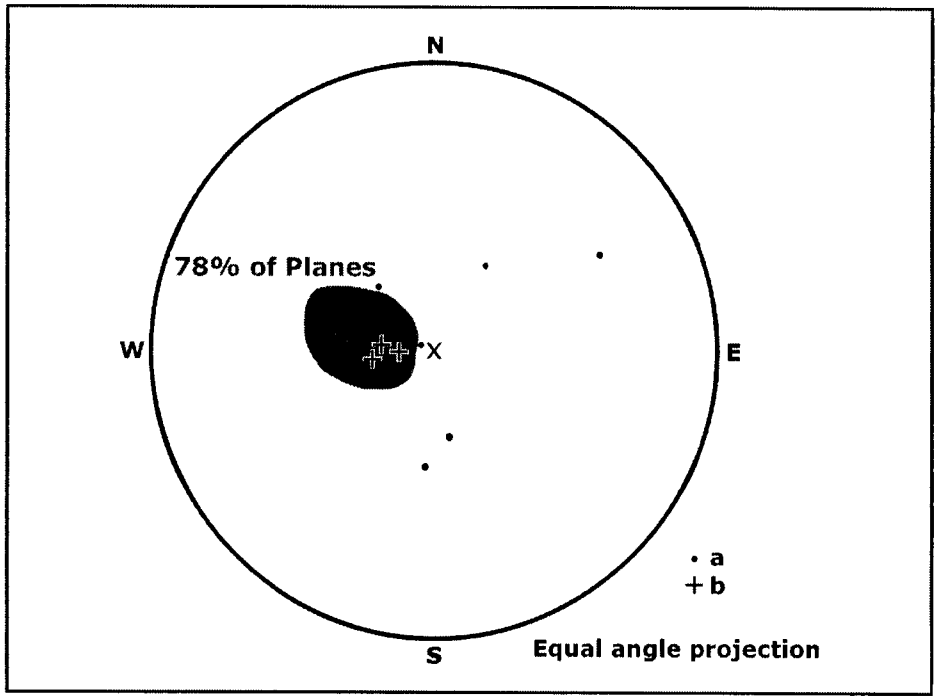

Figure 3-13: Poles to bedding measured in a) the Cerro de las Tórtolas Formation located between the Límite and Fabiana Faults (Veladero Section) and b) in the Fabiana prospect area. Average dip of the Veladero Section is 16°E whereas the Fabiana Section dips ~12°E. Steeper dips are associated with shallow domes and their flanking coarse-grained sandstone, conglomerate and volcanic breccias.

Bedding strikes northerly and dips an average of 16° to the east (Figure 3-13). The occurrence of very fine sandstone and siltstone layers of limited lateral continuity and non-erosive base to beds suggests a very low-energy deposition environment. Shallow intrusives have domed the rocks and steepen the bedding over 16° around younger intrusives at Cuatro Esquinas and on Cerro Pelado. In addition, steeper bedding is locally associated with the deposition of block-size material. For example, at the margins of the Cerro Pelado dome, the volcaniclastic rocks are subvertical, and the beds are contorted, and contain slump features. These textures and sedimentology of the volcaniclastic rocks suggest that deposition, deformation and dome intrusion likely occurred synchronously.

In the absence of large volumes of magmatic material to be sampled (pumice fragments or porphyritic matrix), geochronological studies have been carried on very fine grained, non-bedded, massive tuff horizons (Samples DC-374 and DC-375). The presence of an irregular basal contact (non-erosive) and of accretionary lapilli suggests that the sampled material is a primary ash-fall deposit. SHRIMP studies yield a 16.4 ± 1 Ma age (DC-375, Table 3-1, Figure 3-10c) that is statistically similar to a 15.8 ± 1.0 Ma age obtained by conventional U-Pb (DC-374, Table 3-2, Figure 3-11e).

Turbio River Section

Isolated outcrops of conglomerates and pyroclastic rocks located in the southern margin of the Turbio River valley represent the second section assigned to the Cerro de las Tórtolas Formation (Plate 1). The conglomerates are clast-supported, coarsely bedded, and polymictic. Advanced argillic alteration is superposed on the rocks from this unit. The clasts are subrounded and they are derived from dacitic rocks similar to the domes intruding the Veladero section, green andesites similar to the underlying Tilito Formation, and massive (sedimentary?) units. An assemblage of quartz and alunite, which obscures the original texture, largely replaces the yellowish matrix of the

conglomerates (Figure 3-14). Feldspar-rich sandstone lenses are the subordinate volcaniclastic rocks of this unit. Unlike the Veladero section, where volcanic processes dominate, sedimentary processes dominate the environment of deposition. Tuff occurs as very thin (<5 cm), massive beds that most likely represent fall deposits and evidence subordinate, contemporary volcanism, thus indicating that the sequence represents the transition from the volcanic complex to the volcaniclastic sedimentary apron.

Figure 3-14: Cerro de las Tórtolas Formation south of Turbio river. a) Coarsely bedded, polymict conglomerate with silicified and rounded clasts. b) Similar rock with advanced argillic alteration assemblages replacing the matrix.

Fabiana Section

Light yellow and grey tuffaceous sandstone, conglomerate and heterolitic breccia crop out at the Fabiana prospect (Plate 1). Based on texture and composition similarities, the less than 50-meter thick sequence is also included in the Cerro de las Tórtolas Formation and is referred to as the Fabiana section. The volcaniclastic rocks unconformably overlie the Tilito Formation. The sedimentary rocks consist of bedded volcaniclastic sandstones that grade into massive, moderately sorted, reworked tuffs (Figure 3-15). Discontinuous horizons of very well sorted, fine ash-size material with mud-cracks and evidence for bioturbation (?) are interbedded within the section; these

may represent deposition in ephemeral standing water in ponds or small lakes. The rocks gently dip east (<15°) or are almost horizontal. Clasts in the matrix-supported, heterolitic breccias do not exceed 20 cm long in dimension. The clasts are subangular to subrounded, and they consist of dacites and porphyritic andesites similar to those found south of the Turbio River and in the Veladero section. Textureless rocks are also present. The transition from coarsely bedded breccias to bedded conglomerates is gradual. The rocks from the Fabiana prospect are interpreted as the volcaniclastic, distal equivalent of the Veladero section.

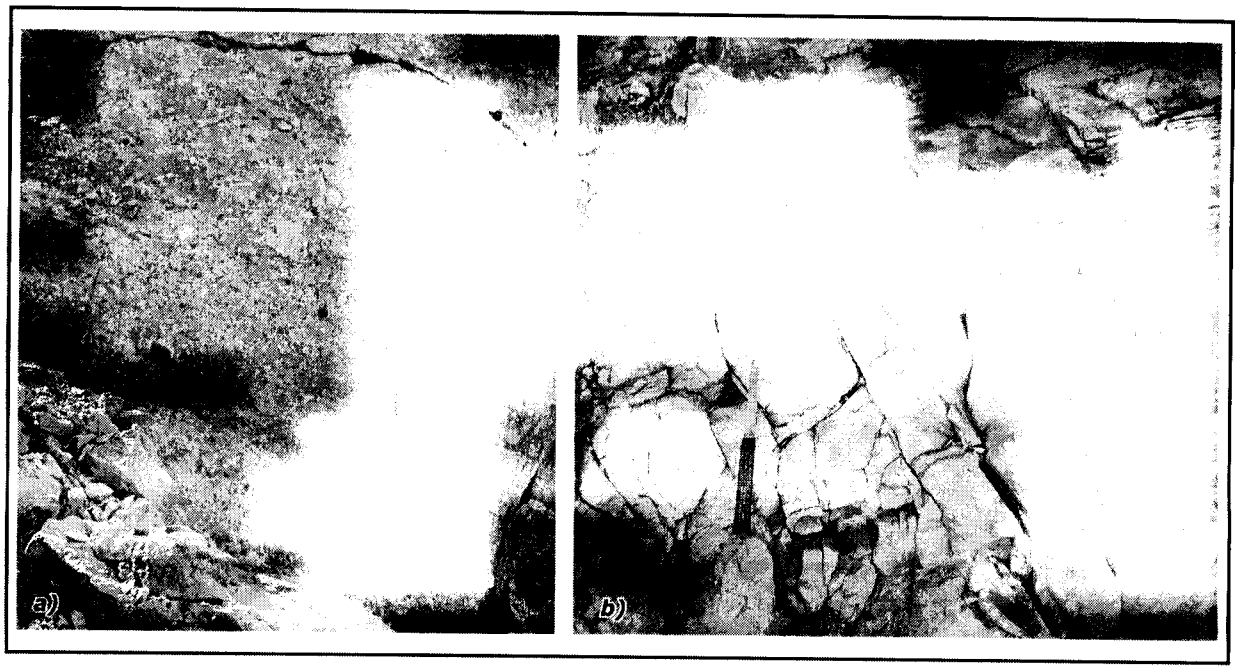

Figure 3-15: Cerro de las Tórtolas Formation in the Fabiana Prospect area. a) Coarsely bedded heterolitic breccias similar to the Veladero Section rocks. b) Reworked tuff and ash-size, laminated material very likely deposited in shallow water.

Infiernillo Intrusive Unit

Green weathering porphyritic intrusives of dacitic to andesitic composition and light grey to orange altered dacitic domes with associated pyroclastic vent products form the Infiernillo Unit. The intrusives are generally elongated in a north-south direction, and range from a few hundred of meters to as much as to 2 km in length. The widespread subvolcanic stocks are typically less than one kilometre in diameter. Some of the domes form prominent topographic features such as the Cerro Colorado, the Cerro Pelado, the

Cerro Libori and a small hill in the Canito Creek (Plate 1). In the Cerro Libori area, 350 m of vertical exposure shows the transition from crystalline intrusive rocks in the lower part to near-surface and probably sub-aerial flow-banded dacitic domes at the top (Figure 3-16a).

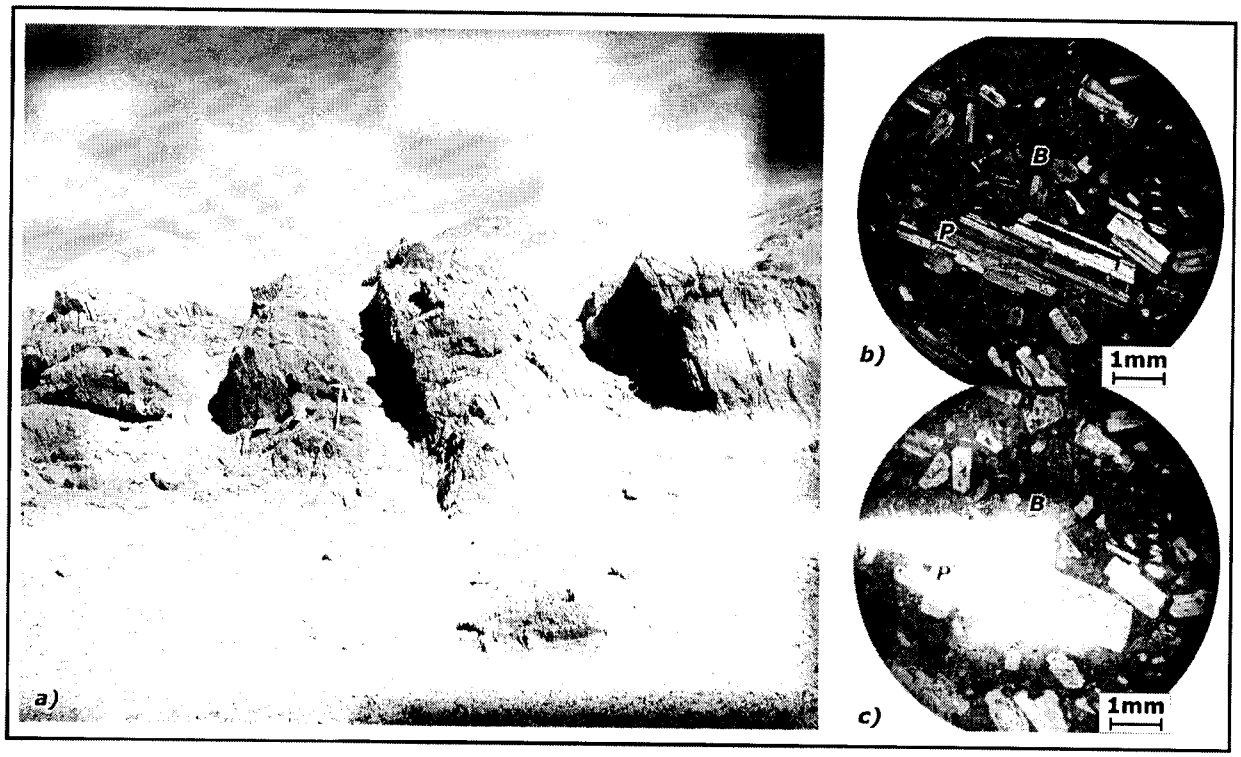

Figure 3-16: Infiernillo Intrusive Unit. a) Outcrops of flow-banded andesites in the upper part of the Cerro Libori. In the background to the left, altered rocks of similar composition form the summit of the Cerro Pupa. Andesitic porphyry in b) transmitted cross-polarized light and c) transmitted plane-polarized light: Crystals and fragments of plagioclase (P), altered biotite (B) in a fine-grained, slightly altered matrix.

Green porphyritic, plagioclase-, hornblende- and biotite-phyric intrusive andesite outcrops are concentrated on the east flank of Amable and the lower part of the Cerro Libori. Similar rocks intercepted in DDH042 beneath west Amable are also included in this unit. Plagioclase phenocrysts are 0.5 to 1 cm long and they compose up to 35% of the rock volume. Clinopyroxene is less common than in intrusive rocks of the Tilito Formation. The fine-grained matrix is generally altered to clays and composed of 15% to 25% opaque minerals (Figure 3-15b and c). Within the extrusive facies of the Cerro de las Tórtolas Formation, clasts lithologically similar to the porphyritic andesites very likely represent juvenile lithic fragments derived from the erupting magma.

Dacite, andesite and subordinate rhyolites with varying alteration assemblages form dome structures in the Veladero North area. The subvolcanic facies consist of quartz-poor porphyritic dacites with characteristic banding and flow textures. Monomict breccias are commonly associated with the subvolcanic rocks. Those breccias present a jigsaw-fit texture formed by closely packed blocky fragments of dacitic composition immersed in a microporphyritic matrix. Matrix-supported, monomict breccias with angular and sub-rounded clasts represent the transition towards the heterolithic breccias included in the Cerro de las Tórtolas Formation.

Conventional U-Pb geochronology from the Cerro Libori intrusive rocks yields an age of 16.6 ± 0.3 Ma (Sample DC-265, Table 3-2, Figure 3-11f and Appendix) that is slightly older than the minimum age (16.2 ± 0.2 Ma, ^{40}Ar-^{39}Ar data, Bissig *et al.*, 2001) of the Infiernillo Unit elsewhere in the El Indio Belt. Bissig (2001) reports an age of 15.3 ± 0.3 Ma (^{40}Ar-^{39}Ar data, plagioclase) from a dioritic intrusive related to the dome in the Canito Creek.

Preliminary U-Pb geochronology is not conclusive on the age of the intensely altered dacite from the Cerro Colorado dome. Available data show that these rocks were emplaced between 12 Ma and 16 Ma (Sample DC-304, Table 3-2 and Figure 3-11g). The maximum calculated alteration age of 10.7 ± 0.9 Ma for hydrothermal alunite (^{40}Ar-^{39}Ar data from Bissig *et al.*, 2001) places only a minimum age of the host rocks. Elsewhere in the El Indio-Pascua Belt, rocks that are age-equivalent to the minimum age (Vacas Heladas Formation) are lithologically and geochemically different from the Cerro Colorado rocks. Additionally, a 16 Ma whole-rock K-Ar date (Ramos *et al.*, 1998) from a sample collected near the intrusive (Plate 1) is interpreted as a complete resetting age. The lithological evidence as well as the interpretation of the geochronological data suggest that the age of the Cerro Colorado dome is closer to 16 Ma (see Appendix I).

Except for most of the Cerro Libori rocks, the Infiernillo Unit dome-related rocks are altered to advanced argillic or pervasive silicification alteration assemblages, and cut

by hydrothermal breccias. Heterolitic breccias from the Cerro de las Tórtolas Formation, particularly the Veladero section, are also intensely silicified. Hydrothermal breccias that crosscut the volcanic units are often difficult to distinguish from their host-rock. The precise timing of the hydrothermal alteration in the Veladero North area is not known.

Vacas Heladas Formation

Brown, biotite-phyric dacitic domes and flows and subordinate andesite form this unit. The rocks are distinctly fresh when compared to older units of the region. Flows partially cover the Cerro de las Tórtolas Formation at Fabiana, but in the southern part of the mapped area, they discordantly overlie or intrude volcanic rocks from the Tilito Formation (Plate 1). The Vacas Heladas Formation rocks are commonly porphyritic. Plagioclase (60%), hornblende (20%), biotite (15%) and reabsorbed quartz (5%) phenocrysts represent less than half of the rock volume. The matrix is fine-grained, partially recrystallized and contains small plagioclase laths. In the Fabiana prospect area, the rocks have a fragmental texture defined by lithic clasts that form less than 10% of the volume. Most of those clasts are preferentially oriented and have the same composition as the matrix; none is pumiceous. The rest (<3% volume) is formed by subrounded accessory lithic fragments of diverse composition (Figure 3-17).

The age of the Vacas Heladas Formation is well documented in the study area although the ages obtained by different methods do not overlap within their analytical uncertainties. Disagreement in biotite K-Ar data of 12.3 ± 0.3 Ma (Minera Río Frío, 2000) and ^{40}Ar-^{39}Ar data 11.0 ± 0.2 Ma (Bissig *et al.*, 2001) from samples collected in the Fabiana prospect area likely reflects the combination of post-crystallization isotopic remobilization and discrepancies between the two methods. The 12.7 ± 0.9 Ma to 11.0 ± 0.2 Ma emplacement interval proposed in Bissig *et al.* (2001) for the Vacas Heladas Formation has been determined regionally, and will be used in this study.

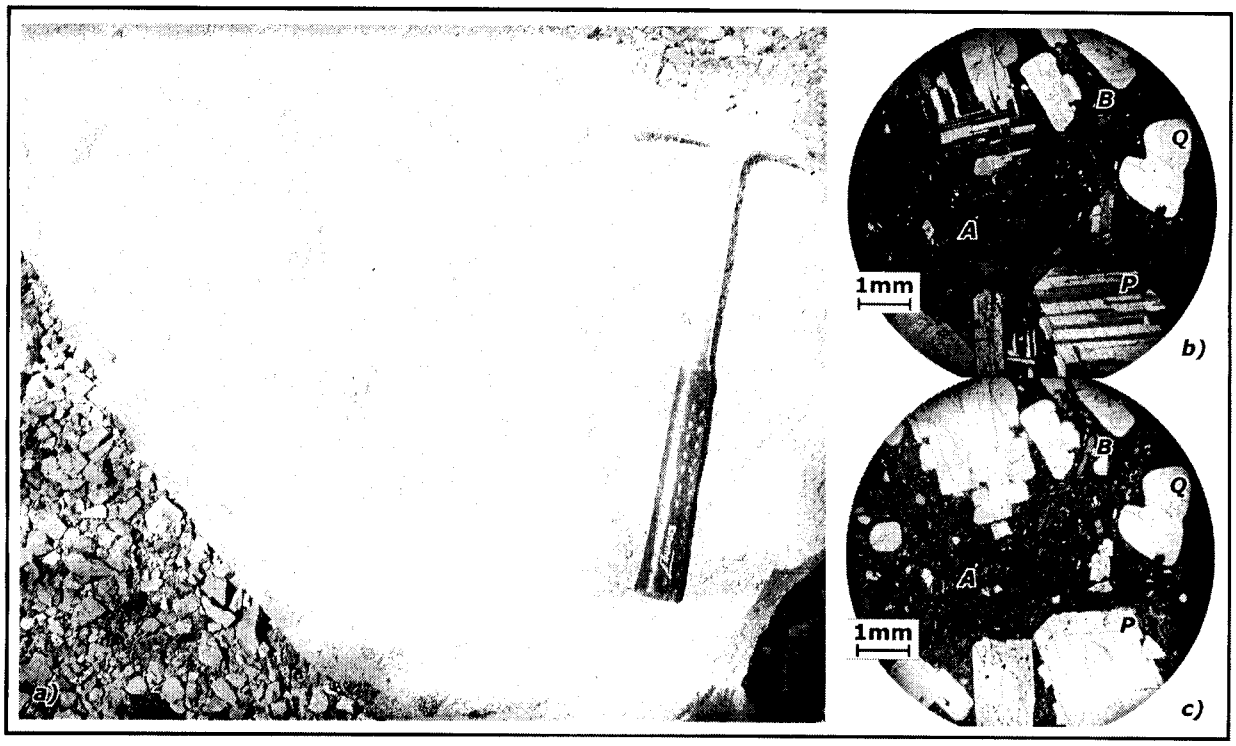

Figure 3-17: Vacas Heladas Formation. a) Fragmental dacite in the Fabiana Prospect area. Lithic fragments and matrix have the same composition, no accessory lithic fragments have been recognized. Dacitic matrix in b) transmitted cross-polarized light and c) transmitted plane-polarized light: Megacrysts of plagioclase (P), biotite (B), amphibole (A) and partially reabsorbed quartz (Q) in a fine-grained, devitrified matrix

Geochemistry

Trace and rare earth element concentrations and the isotopic compositions of igneous rocks have been related to the physico-chemical conditions prevailing at the origin of the magmas. Bissig *et al.* (2003) and Kay and Mpodozis (2002) review a series of petrotectonic models derived from geochemical data. In detail, these models are beyond the scope of this contribution. Only some general interpretations regarding the major difference between units will be discussed here.

Whole-rock geochemistry in the El Indio-Pascua Belt has been used to characterize volcanic formations of known age and as a preliminary correlation method when geochronological data are not available (Maksaev *et al.*, 1984; Martin *et al.*, 1995; Bissig *et al.*, 2001; Malizia *et al.*, 1997; Litvak *et al.*, 2002; Godeas *et al.*, 1993). In particular, the relative abundance of REEs and the signature displayed in normalized plots have proven to be an effective tool for discriminating between late Paleozoic to

Triassic and Tertiary units. Three parameters can be used to quantify this signature. First, the average slope of the curve in these plots reflects the overall REE fractionation (or the relative fractionation of light *versus* heavy REE) and can be approximated by the La_n/Lu_n ratio. Second, the HREE fractionation is calculated as the average of the normalized concentration of Er, Tm, Yb and Lu. Finally, the Eu anomaly (Eu* in Table 3-3) expressed as the normalized concentration of Eu. The characteristic REE pattern of late Paleozoic to Triassic volcanic rocks exhibits a prominent negative Eu anomaly and similar fractionation of light and heavy REE (e.g. Mpodozis and Kay, 1992). Tilito, Escabroso and Cerro de las Tórtolas Fromations as well as Bocatoma and Infiernillo Units present minor Eu anomalies and moderate HREE fractionation. In the Vacas Heladas, Pascua and Vallecito Formations the Eu concentration is normal and they show strong HREE fractionation (e.g. Bissig *et al.*, 2003). Figure 3-18 outlines the geochemical difference between late Paleozoic to Triassic and Tertiary rocks recognized in the El Indio-Pascua Belt as well as in the Veladero North area.

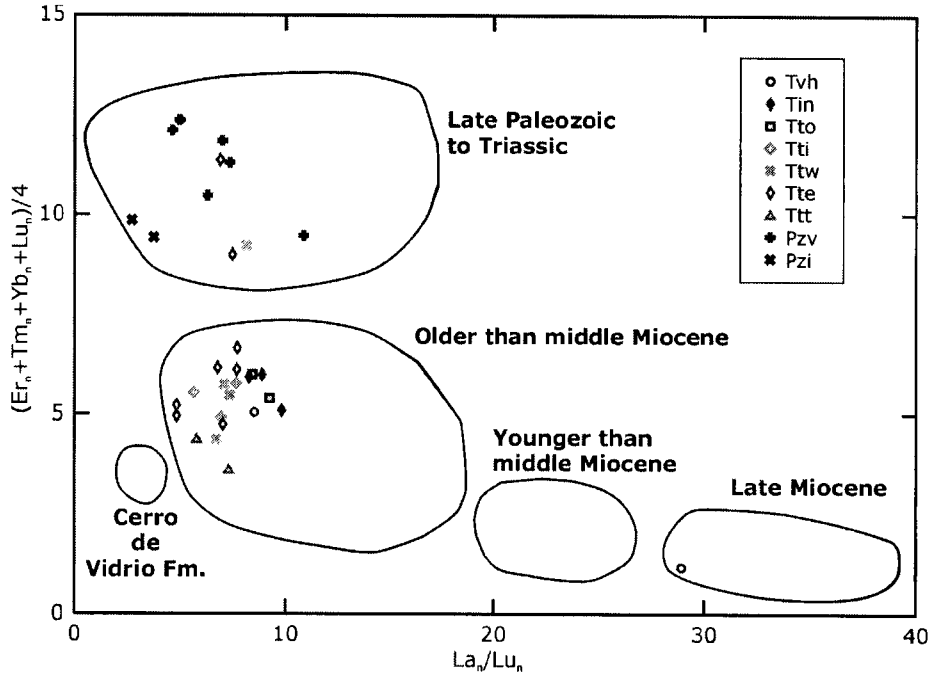

Figure 3-18: Whole-rock geochemistry of the Veladero North lithostratigraphic units. Ratio and average of normalized REE concentration. Normalization factors are those of the Primitive Mantle from Taylor and McLennan (1985). Late Paleozoic to Triassic field outlined using data from Bissig (2001) and from samples described in Chapter 2. Remaining fields outlined from Bissig et al. (2003) data and analyses in Table 3-3. Abbreviation:* Pzi, Pzv*: Permian volcanic, intrusive;* Ttt, Tte, Ttw, Tti*: Tilito Taguas, East, West, intrusive;* Tto*: Cerro de las Tórtolas;* Tin*: Infiernillo;* Tvh*: Vacas Heladas. See text for description.

Table 3-3: Geochemistry of Tertiary rocks from the Veladero North area.

		Bocatoma		Tilito Volcanic					C dl Tórtolas (V)		Vacas Heladas	
Sample		DC-108	DC-213	DC-129	DC-300	DC-133	DC-036	DC-298	DC-265	DC-117	DC-152	DC-311
SiO_2	wt%	64.94	57.60	56.80	56.80	72.03	65.52	60.62	63.14	63.07	62.41	63.68
TiO_2	wt%	0.50	0.76	0.76	0.90	0.35	0.58	0.88	0.72	0.69	0.71	0.55
Al_2O_3	wt%	17.45	19.07	19.35	18.73	15.21	16.56	17.40	16.72	16.53	20.43	17.42
Fe_2O_3	wt%	4.69	7.11	7.00	8.24	2.11	4.80	6.17	5.14	5.32	4.39	5.15
MnO	wt%	0.09	0.16	0.13	0.15	0.02	0.09	0.18	0.08	0.10	0.03	0.18
MgO	wt%	1.95	3.07	2.82	3.08	0.61	1.77	2.77	2.01	2.63	0.82	1.94
CaO	wt%	5.57	7.04	8.04	7.69	1.07	4.51	5.95	5.17	4.74	3.83	4.53
Na_2O	wt%	3.57	3.93	3.19	3.18	3.58	3.40	3.43	3.52	3.54	4.24	4.14
K_2O	wt%	1.06	1.03	1.60	0.86	4.96	2.60	2.37	3.29	3.18	2.92	2.08
P_2O_5	wt%	0.19	0.24	0.31	0.38	0.07	0.17	0.24	0.20	0.20	0.22	0.33
LOI	wt%	1.85	4.48	2.12	4.52	3.08	4.24	2.87	2.92	4.16	4.82	3.09
Total	wt%	*100*	*100*	*100*	*100*	*100*	*100*	*100*	*100*	*100*	*100*	*100*
Sr	ppm	371	456	556	791	136	324	401	339	339	561	413
Zr	ppm	106	125	155	163	265	134	179	209	145	136	166
Rb	ppm	53	43	34	25	180	88	96	186	149	84	54
Y	ppm	10	12	15	16	33	16	20	25	20	3	16
Nb	ppm	11	12	17	20	18	13	14	12	12	15	16
Ba	ppm	458	257	590	354	896	807	551	547	558	553	564
La	ppm	15.34	14.14	21.21	20.50	41.85	26.37	25.91	28.80	26.36	20.72	22.67
Ce	ppm	31.01	29.70	43.68	42.58	84.48	52.33	54.08	61.88	55.18	39.39	46.52
Pr	ppm	3.75	3.76	5.45	5.52	10.05	5.89	6.55	7.43	6.52	4.56	5.80
Nd	ppm	14.97	15.86	22.30	24.53	36.89	22.71	25.77	27.92	24.65	17.98	24.20
Sm	ppm	3.01	3.27	4.40	4.50	6.64	4.47	5.26	5.45	4.52	2.83	4.34
Eu	ppm	0.99	1.06	1.38	1.49	1.19	1.11	1.29	1.09	0.95	0.86	1.24
Gd	ppm	2.50	3.14	4.21	4.74	5.82	3.71	4.67	4.84	3.89	1.35	4.14
Tb	ppm	0.39	0.47	0.59	0.69	0.83	0.49	0.69	0.70	0.54	0.17	0.59
Dy	ppm	2.36	2.82	3.68	4.32	5.28	2.94	4.22	4.11	3.27	0.85	3.71
Ho	ppm	0.44	0.56	0.72	0.80	1.06	0.72	0.80	0.77	0.63	0.15	0.69
Er	ppm	1.27	1.60	2.07	2.26	3.20	2.04	2.33	2.30	1.87	0.42	1.95
Tm	ppm	0.20	0.23	0.30	0.32	0.51	0.30	0.34	0.33	0.28	0.06	0.27
Yb	ppm	1.31	1.62	2.07	2.10	3.57	1.99	2.19	2.14	1.98	0.45	1.91
Lu	ppm	0.22	0.25	0.30	0.30	0.53	0.30	0.32	0.34	0.28	0.07	0.28
Hf	ppm	3.49	3.42	4.64	4.24	8.42	4.76	5.84	6.55	6.02	4.21	4.47
Ta	ppm	0.42	0.25	0.61	0.38	1.79	0.94	0.69	0.96	0.95	0.75	0.53
Th	ppm	3.52	2.23	3.20	2.36	18.74	12.49	10.92	25.31	21.29	8.06	3.00

Major oxides concentration is recalculated to 100 wt% without accounting for Loss on Ignition (LOI)
Major oxides and Sr, Zr, Rb, Y, Nb and Ba from Bondar Clegg XRF
Other data from Memorial University of Newfoundland ICP-MS

Table 3-3: Geochemistry of Tertary rocks from the Veladero North area.

		Intrusives													
Sample		DC-304	DC-148	DC-124	DC-012	DC-056	DC-195	DC-100	DC-110	DC-079	DC-080	DC-163	DC-249	DC-095A	DC-243
SiO_2	wt%	78.24	55.75	54.35	55.50	58.52	72.06	66.11	76.43	50.82	52.18	80.85	75.65	61.92	63.60
TiO_2	wt%	1.03	0.90	0.96	1.00	0.89	0.50	0.62	0.26	1.24	1.21	0.27	0.31	0.92	0.78
Al_2O_3	wt%	17.98	19.93	18.72	19.65	17.75	13.62	16.52	14.84	20.33	19.07	13.97	13.95	16.64	16.94
Fe_2O_3	wt%	0.26	7.62	8.94	8.10	6.78	2.58	3.87	0.89	9.27	9.28	1.18	0.86	6.41	4.92
MnO	wt%	-0.01	0.12	0.17	0.18	0.11	0.15	0.03	0.02	0.25	0.15	0.02	0.04	0.14	0.10
MgO	wt%	0.36	1.72	3.63	3.11	3.52	0.88	1.42	0.46	3.90	4.63	0.64	0.36	2.52	2.61
CaO	wt%	0.22	8.80	8.53	7.90	6.31	3.10	4.10	0.23	9.26	10.53	0.06	0.72	3.45	6.23
Na_2O	wt%	0.03	3.61	2.96	3.51	3.59	4.20	3.77	3.44	4.35	2.55	-0.01	3.11	4.84	3.67
K_2O	wt%	1.66	1.19	1.37	0.67	2.29	2.78	3.37	3.38	0.31	0.15	2.95	4.93	2.94	0.97
P_2O_5	wt%	0.23	0.36	0.35	0.38	0.22	0.13	0.19	0.05	0.26	0.25	0.06	0.07	0.23	0.18
LOI	wt%	7.93	2.51	2.71	3.66	1.5	3.52	2.45	2.58	5.28	6.51	5.9	1.79	3.67	5.95
Total	wt%	*100*	*100*	*100*	*100*	*100*	*100*	*100*	*100*	*100*	*100*	*100*	*100*	*100*	*100*
Sr	ppm	105	539	471	503	459	112	384	100	563	521	35	124	296	722
Zr	ppm	142	134	135	135	178	375	139	153	131	119	146	236	227	280
Rb	ppm	82	24	33	27	109	107	156	113	15	7	114	179	95	30
Y	ppm	92	14	14	15	19	40	28	18	15	14	29	38	22	22
Nb	ppm	12	16	15	16	14	12	13	19	14	14	19	18	15	17
Ba	ppm	664	424	486	463	514	969	622	808	206	122	16	855	569	597
La	ppm	23.41	15.52	18.06	15.58	21.87	40.70	26.41	20.74	13.83	12.85	27.62	37.58	23.52	27.69
Ce	ppm	44.81	33.17	36.51	34.65	47.82	89.13	52.95	38.29	31.29	28.72	52.57	74.81	49.20	59.90
Pr	ppm	5.42	4.37	4.62	4.58	6.01	10.83	6.23	4.24	4.19	3.85	5.87	8.93	6.01	7.35
Nd	ppm	23.62	18.99	19.78	21.38	25.17	43.72	22.94	15.04	18.22	16.97	21.38	32.88	23.75	28.01
Sm	ppm	4.95	4.45	4.05	5.02	5.24	9.00	4.67	2.94	4.21	4.03	4.23	6.25	4.99	5.65
Eu	ppm	1.86	1.43	1.36	1.72	1.31	2.39	1.09	0.56	1.32	1.27	0.82	1.01	1.21	1.02
Gd	ppm	10.36	3.96	3.98	4.77	4.52	8.50	4.13	2.41	3.81	3.58	4.11	5.30	4.15	4.92
Tb	ppm	2.39	0.58	0.55	0.59	0.58	1.29	0.67	0.40	0.61	0.58	0.65	0.82	0.66	0.76
Dy	ppm	17.12	3.42	3.39	3.51	3.47	7.91	4.19	2.63	3.73	3.62	3.90	5.23	4.10	4.56
Ho	ppm	3.01	0.63	0.66	0.83	0.82	1.53	0.78	0.50	0.71	0.68	0.75	1.06	0.77	0.85
Er	ppm	7.44	1.74	1.89	2.24	2.29	4.42	2.29	1.56	1.96	1.93	2.15	3.19	2.27	2.47
Tm	ppm	0.93	0.24	0.27	0.32	0.33	0.63	0.33	0.25	0.29	0.27	0.32	0.49	0.33	0.38
Yb	ppm	5.12	1.54	1.84	1.94	2.07	4.21	2.21	1.81	1.85	1.77	2.22	3.42	2.25	2.42
Lu	ppm	0.63	0.24	0.27	0.29	0.30	0.61	0.36	0.31	0.30	0.28	0.35	0.52	0.36	0.37
Hf	ppm	4.52	3.91	3.92	4.00	5.73	11.36	4.96	4.49	3.72	3.49	4.11	6.63	6.54	7.65
Ta	ppm	0.31	0.41	0.43	0.50	0.76	0.28	1.07	1.54	0.31	0.27	1.41	1.49	0.85	0.80
Th	ppm	12.35	1.40	2.16	1.10	13.02	9.46	20.77	9.06	1.92	1.67	10.24	16.77	7.81	19.16

Major oxides concentration is recalculated to 100 wt% without accounting for Loss on Ignition (LOI)
Major oxides and Sr, Zr, Rb, Y, Nb and Ba from Bondar Clegg XRF
Other data from Memorial University of Newfoundland ICP-MS

Structural framework of the Veladero North area

An homoclinal sequence that unconformably covers a fold and thrust belt defines the overall structural geometry of the Veladero North area. Late Paleozoic Guanaco Sonso Formation and late Oligocene-early Miocene Tilito Formation are superposed in a northerly striking fold and thrust belt. From east to west, Fabiana, MAGSA and Límite faults, three north-striking faults, bound the major structural packages within the fold and thrust belt in the study area (Figure 3-5). Within these packages, similar structures are also present, but the rocks are very different. The middle Miocene Cerro de las Tórtolas Formation unconformably overlies the fold and thrust system and dips homoclinally eastward.

Faults within the fold and thrust belt do not usually outcrop and their location is inferred from older-over-younger stratigraphic relationships, abrupts changes in bedding dips and the presence of tight to open folds. Exploration trenches or roads locally uncover the fault zones for closer examination.

The Fabiana fault, in the eastern part of the mapped area, strikes northerly and places Permian over late Oligocene-early Miocene rocks. In an exploration trench, the fault zone locally dips ~75° to the west. Asymmetric fractures bounded between thrust parallel microfaults imply a reverse displacement of the fault, which is consistent with the older over younger structural relation along the fault. On the eastern flank of the Río Taguas valley, andesitic porphyries from the Infiernillo Unit (?) intrude and have steepened the Fabiana fault plane. Folding associated with the fault is preserved in the upper plate where Permian rocks form an anticline that plunges to the north (Figure 3-19).

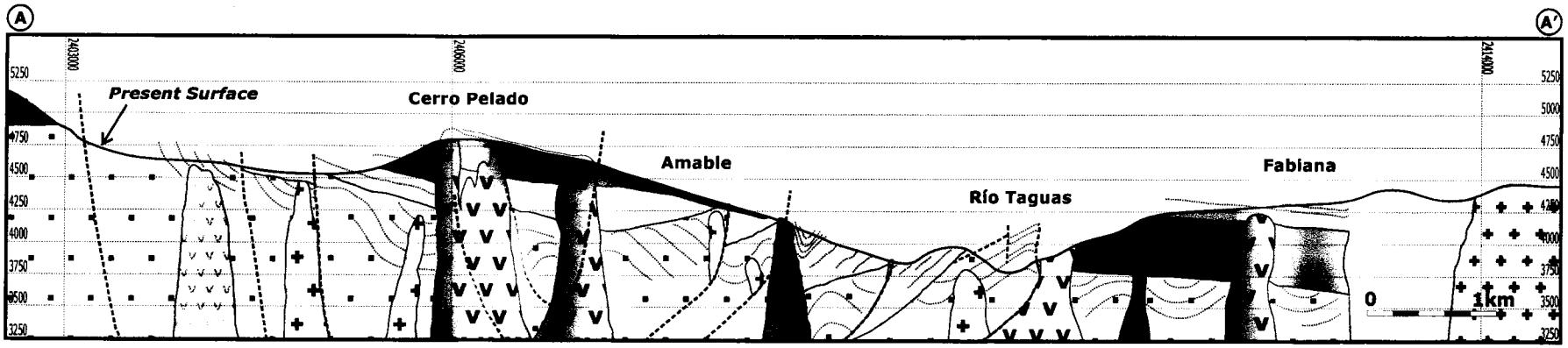

Figure 3-19: East-West cross-section across the northern portion of the study area. Bedding and subsurface information is projected from surface data and from section B-B'. No vertical exaggeration, section location in Figure 3-5.

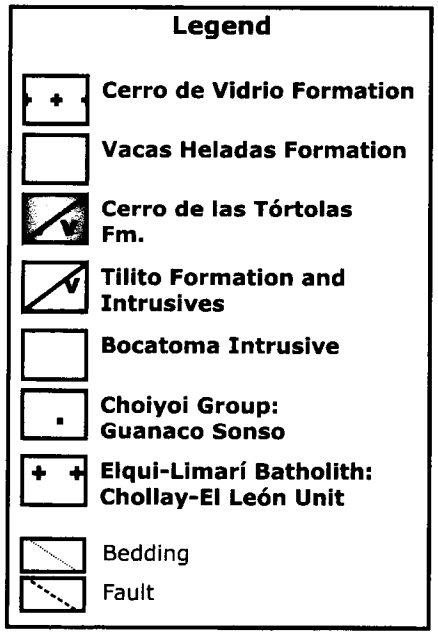

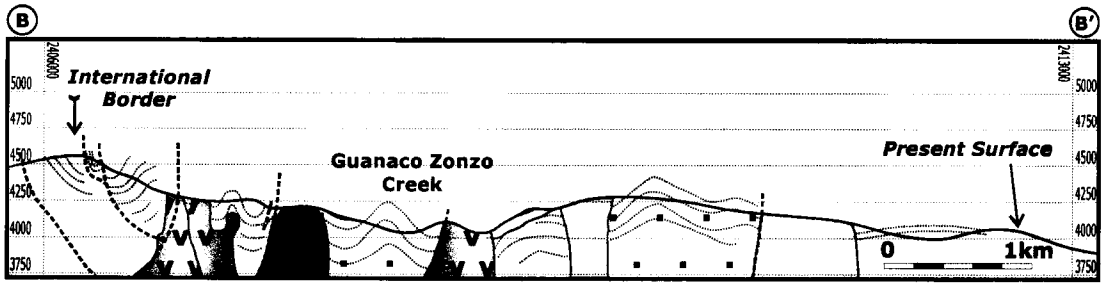

Figure 3-20: East-West cross-section across the southern portion of the study area. The fold and thrust belt that underlies the International borders in the Guanaco Zonzo Creek area is intruded by andesitic and dacitic domes from the Infiernillo Unit. No vertical exaggeration, elevation is represented in metres above sea level. Section location in Figure 3-5.

In the central part of the study area, the north-striking MAGSA fault superposes Permian over late Oligocene-early Miocene rocks. It is covered by ~16 Ma breccias of the Cerro de las Tórtolas Formation. Middle Miocene dacitic and andesitic intrusives emplaced along the fault obscure the sense of displacement. Bedding of Permian rocks that occur near the fault is consistent with a fault that dips to the west (Figure 3-20).

In the northwestern part of the study area, the Límite fault and the Muñeco fault represent two branches that form a subvertical, north-striking structure. Field evidence records reverse and normal displacement along the structure that separates two blocks with contrasting characteristics. The western block is formed by late Paleozoic units whereas the eastern block includes a late Oligocene-early Miocene volcanic sequence. Middle Miocene rocks that dip to the east unconformably overlie older units on both sides of the Límite fault. The projection of the discordance plane from both sides of the fault as well as geomorphological features interpreted as scarps record a normal sense of displacement along the fault plane. However, it is very likely that, following the same structural style as the MAGSA and Fabiana faults, the Límite fault had initial reverse displacement, which superposed late Paleozoic rocks in the west over younger rocks in the east.

The area between the MAGSA fault in the east and the Límite fault in the west represents the most intensely deformed portion of the fold-and-thrust belt. Thrusts that dip steeply (>70°) to the west and back-thrusts that dip steeply (>70°) to the east involve the Tilito (late Oligocene-early Miocene) and the Guanaco Sonso (Permian) Formations. Within each thrust panel, a specific rock sequence is exposed and is not repeated in other panels. The faults strike generally in a north-south to NNE direction. The traces of the axial planes of the folds are parallel to the faults, however, the fold and thrust vergence is unclear from the field exposures.

Lithologic association of the epithermal deposit

The Veladero North epithermal deposit is hosted in intensely altered subaerial heterolitic breccias, volcaniclastic rocks and subordinate fall tuffs of the (16 Ma to 15 Ma) Cerro de las Tórtolas Formation and underlying dacitic flow tuff and sandstone of the (25 Ma to 23 Ma) Tilito Formation and dacitic flows and tuffs of the (270 Ma to 250 Ma) Guanaco Sonso Formation. The latter two formations are structurally superposed in a fold-and-thrust system that unconformably underlies the Cerro de las Tórtolas Formation. Only a small portion of the Au ore body is apparently hosted in these rocks. Mineralized, hydrothermal breccias of presumed Miocene age cut the Cerro de las Tórtolas Formation as well as older units.

Geologic mapping demonstrates that volcanic and volcaniclastic rocks from the Cerro de las Tórtolas Formation are spatially linked to a series of dacitic to andesitic domes assigned to the Infiernillo Unit. Monolithologic, clast-supported breccias represent proximal facies near the intrusives. The proximal breccias grade outwards to heterolithic, bedded volcanic breccias and volcaniclastic rocks. Well-bedded volcaniclastic rocks, sandstones and siltstones characterize the distal facies of the system. The low proportion of ash pyroclasts and vesiculated fragments suggest that non-explosive conditions prevailed at the time of emplacement of the sequence. Although sub-surface data are needed to corroborate the hypothesis, available information suggests that the Cerro de las Tórtolas Formation in the Veladero North area represents a dome field that was active *ca.* 16 Ma. Explosive vent-clearing eruptions were the source of fragmental juvenile material as well as the common, thin ash beds.

Elsewhere in the El Indio-Pascua Belt, high-sulfidation style alteration has been thought to have formed contemporary with the (16 Ma to 15 Ma) Infiernillo Unit and the Cerro de las Tórtolas Formation (Nasi *et al.*, 1990; Maksaev *et al.*, 1984; Clavero *et al.*, 1997; Martínez *et al.*, 1993; Bissig *et al.*, 2001). However, Bissig *et al.* (2001, 2002) demonstrated that the bulk of the currently known economic Au in the El Indio-Pascua

Belt was deposited between 9.5 Ma and 6 Ma and represents the youngest hydrothermal event in the belt. They further suggest that the Miocene high-sulfidation style epithermal alteration may have been accompanied by some gold. However, erosion has stripped the upper parts of those systems, and the gold, if deposited, has been removed. At Veladero North area (Filo Federico), limited chronologic data suggest that the advanced argillic alteration presumably associated with gold deposition occurred in the 11.0 Ma to 10.5 Ma interval (Bissig *et al.*, 2001). This data imply that the Au is somewhat older than gold at Pascua-Lama and El Indio. Conversely, it confirms that the volcaniclastic rocks from the Cerro de las Tórtolas Formation and the intrusions from the Infiernillo Unit are considerably older than the mineralization. Thus, at the moment, there is no concrete evidence to support a direct relationship between the genesis of the host-rock package and the epithermal gold.

Timing of deformation

Late Paleozoic to Mesozoic structures in the high Andes are difficult to identify since they have been reactivated by younger deformation events, eroded or covered by younger rocks. Northwest trending lineaments such as the Pascua-Veladero lineament (Figure 3-2) are very likely the expression of Triassic extensional faults (Ramos and Kay, 1991) that were inverted during Tertiary tectonism (Jones *et al.*, 1999). Furthermore, west of the Baños del Toro Fault (Figure 3-2), high-angle reverse faults and associated folds appear to be pre- to syntectonic with (~40 Ma to 31 Ma) Bocatoma Unit intrusions (Martin *et al.*, 1997, 1995). Many of these faults may be reactivated margin parallel faults formed in the Paleozoic, coincident with the formation of the Carboniferous and Permian arcs (Mpodozis and Kay, 1992).

Because of the relative youthfulness, the timing and complexity of Miocene deformation is more apparent. Multiple episodes of deformation occurred in the El Indio-Pascua Belt throughout the Neogene (e.g. Martin *et al.*, 1995) in sharp contrast with

observations made farther south in the Cordillera Frontal (e.g. Heredia *et al.*, 2002). Specifically, the regional relations in the El Indio and Pascua-Lama Veladero areas indicate two Miocene deformation events older than 16 Ma. The angular unconformity and the regolith horizon that separate the Tilito Formation from the overlying (22 Ma to 17 Ma) Escabroso Formation rocks set the minimum age of the first early Miocene regional shortening event to between 23 Ma and 22 Ma (Martin *et al.*, 1995; Bissig *et al.*, 2001). The Escabroso Formation rocks are not found in the Veladero North area. The second phase of reverse faulting and folding involves rocks as young as the early Miocene (22 Ma to 17 Ma) Escabroso Formation. These structures likely represent the main phase of deformation, and is constrained to have occurred between 18 Ma and 16 Ma (Martin *et al.* 1995, 1997).

In the Veladero North area, the fold and thrust belt is constrained between the emplacement of the (~24 Ma) early Miocene rocks from the Tilito Formation and the deposition of the (~16 Ma) middle Miocene flows that constitute the Cerro de las Tórtolas Formation and intrusion of the (~16 Ma) domes that form the Infiernillo Unit. In the absence of the Escabroso Formation andesites deposited during the 24 Ma to 16 Ma period, the deformation event that shaped the fold and thrust belt in the study area cannot be more precisely dated. It may have formed largely during one or the other, or is a combination of both Miocene episodes of shortening.

The three regional erosional surfaces recognized in the El Indio-Pascua Belt, also found in the Veladero North area Figure 3-21), provide additional constraints on deformation episodes that are younger than 16 Ma. In the study area, ~16 Ma volcaniclastic rocks from the Cerro de las Tórtolas Formation discomformably overlie a regional low-relief unconformity, which is equivalent to the Frontera-Deidad surface. Based on relationships throughout the El Indio-Pascua Belt, the surface formed between 17 Ma and 15 Ma (Bissig *et al.*, 2001). At Veladero North, the Cerro de las Tórtolas Formation rocks and subjacent Frontera-Deidad erosional surface dip shallowly (<20°) to

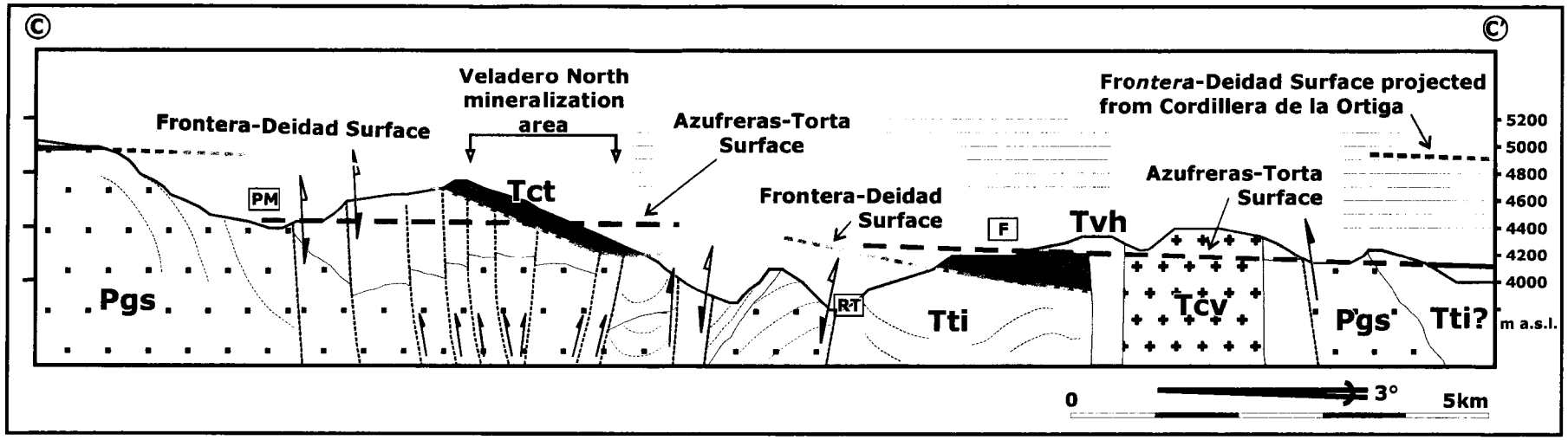

Figure 3-21: East-west cross section of the Veladero North area. Vertical exaggeration (1.5 times) enhances the position of the regional erosion surfaces defined by Bissig et al. (2001). Thickness of Cerro de las Tórtolas Formation (Tct) is assumed consistent and approximately 150 m. Fold and thrust belt geometry beneath Tct is inferred from data south of Veladero North (see Plate 1). Small intrusives are not shown. Abbreviations: PM= Portezuelo Matías, RT= Río Taguas, F= Fabiana and as in Figure 3-3. Section location in Figure 3-5.

the east at an elevation close to 4200 m a.s.l. At Fabiana the surface lies at slightly lower elevations. To the west along the Argentina-Chile frontier and east on the Cordillera de la Ortiga, the Frontera-Deidad surface lies at approximately 5000 m elevation (Figure 3-21). Deformation therefore must have postdated the Cerro de las Tórtolas Formation and either folded or faulted the erosional surface after 16 Ma.

A younger regional low-relief pediment cut the ~16 Ma tilted rocks, the fold and thrust belt and is locally covered by ~11 Ma volcanic rocks. The pediment is comparable to the Azufreras-Torta surface, a region-scale erosional feature incised between 14 Ma and 12.5 Ma (Bissig *et al.*, 2002). In the Portezuelo Matías area, the Azufreras-Torta surface which is at 4400 m a.s.l. lies below the Frontera-Deidad surface. Conversely, in the Fabiana area the Azufreras-Torta surface is above the Frontera-Deidad surface at approximately 4200 m a.s.l. (Figure 3-21) and it is covered by 11 ± 0.2 Ma dacitic tuff (Bissig *et al.*, 2001). The relative position of the surfaces is inconsistent with regional relations throughout the El Indio-Pascua Belt where the Frontera-Deidad surface is 300 to 450 m topographically higher than the Azufreras-Torta surface (Bissig *et al.*, 2002). Interestingly, the top of the ore zone in Veladero North defines a flat horizon that lies at 4200 m a.s.l., approximately 200 vertical metres below the Azufreras-Torta surface. A similar spatial relation between the mineralization and the Azufreras-Torta surface was noted also at Pascua-Lama and El Indio. Gold deposition in those areas occurred between 9.5 Ma and 6 Ma, and was influenced by the incision of a younger (10 Ma to 6 Ma) planar landform (Bissig *et al.*, 2002). A similar timing could be inferred at Veladero North.

In the study area, tilting of the Frontera-Deidad surface and the superjacent rocks post-dates the 17 Ma to 15 Ma erosive surface but occurred prior to the Azufreras-Torta surface incision and burial beneath Vacas Heladas Formation at ~11 Ma. The resulting geometry could be explained by large amplitude folds (Charchaflie *et al.*, 2002) as shown by the broad antiformal shape of the Frontera-Deidad surface west from

Veladero North (Figure 3-21).

The relative position of the Azufreras-Torta surface, expressed by approximately 150 m of vertical separation on each side of the Río Taguas valley, impies that post-11 Ma deformation disrupted the Miocene fold and thrust belt and regional erosional surfaces (Figure 3-21). Available data fail to determine the nature of the tectonic event. However, as many of the older, northerly-striking thrust faults are reactivated as normal slip faults, it seems likely that the deformation was largely extensional. Alternatively, the deformation could reflect a renewed shortening and thrusts reactivation that uplifted the structural blocks located to the west of the faults.

Conclusions

In the Veladero North area, Permian dacites and rhyolites from the Guanaco Sonso Formation and late Oligocene to early Miocene andesites and dacites from the Tilito Formation form a north-south striking fold and thrust belt. Shortening necessarily predates deposition of rocks older than the overlying middle Miocene Cerro de las Tórtolas Formation. Unfortunately, evidence in the Veladero North area is not conclusive as to the precise age of the fold and thrust system; it may have been formed either during an (23 Ma to 21 Ma) early Miocene or a (18 Ma to 16 Ma) middle Miocene deformation event, or be a composite of both events.

Tilted volcanic and volcaniclastic rocks from the (16 Ma to 14 Ma) middle Miocene Cerro de las Tórtolas Formation cover the Frontera-Deidad pediplain, an erosional surface that truncates the fold and thrust system. Syn-volcanic domes of the Infiernillo Intrusive Unit appear to be the source of the pyroclastic and volcaniclastic rocks. Near the domes, the volcaniclastic rocks dip steeply but, in general, the sequence dips gently (<20°) to the east. Tilting of the Cerro de las Tórtolas Formation rocks corresponds to a deformation event that, in the study area, is constrained between 16 Ma and 11 Ma. Region-scale relations suggest that the deformation occurred between 15 Ma and 13 Ma

(Martin *et al.*, 1995; Bissig *et al.*, 2001).

Sub-horizontal volcanic rocks and intrusives that represent the (12 Ma to 11 Ma) Vacas Heladas Formation unconformably overlie and intrude units of every age in the Veladero North area. The volcanic rocks overlie the (14 Ma to 12.5 Ma) Azufreras-Torta surface in the eastern part of the study area. The same erosion surface is recognized in the west, approximately 150 m higher, supporting a post-Vacas Heladas deformation.

References

Allmendinger, R.W., Figueroa, D., Snyder, D., Beer, J., Mpodozis, C., and Isacks, B.L., 1990, Foreland shortening and crustal balancing in the Andes at 30 degrees S latitude: Tectonics, v. 9, p. 789-809.

Barazangi, M., and Isacks, B.L., 1976, Spatial distribution of earthquakes and subduction of the Nazca Plate beneath South America: Geology (Boulder), v. 4, p. 686-692.

Bissig, T., 2001, Metallogenesis of the Miocene El Indio-Pascua gold-silver-copper Belt, Chile/Argentina: geodynamic, geomorphological and petrochemical controls on epithermal mineralization [Ph.D. thesis]: Kingston, Queen's University.

Bissig, T., Lee, J., W, Clark, A., H, and Heather, K., B, 2001, The Cenozoic history of volcanism and hydrothermal alteration in the Central Andean Flat-Slab Region: New 40Ar-39Ar constraints from the El Indio-Pascua Au (-Ag, Cu) Belt, 29°20'-30°30' S: International Geology Review, v. 43, p. 312-340.

Bissig, T., Clark, A.H., and Lee, J.K.W., 2002, Cerro de Vidrio rhyolitic dome: evidence for Late Pliocene volcanism in the central Andean flat-slab region, Lama-Veladero district, 29°20'S, San Juan Province, Argentina: Journal of South American Earth Sciences, v. 15, p. 571-576.

Bissig, T., Clark, A., H, Lee, J., W, and Hodgson Jay, C., 2002, Miocene Landscape Evolution and Geomorphologic Controls on Epithermal Processes in the El Indio-Pascua Au-Ag-Cu Belt, Chile and Argentina: Economic Geology, v. 97, p. 971-996.

Bissig, T., Clark, A., H, Lee, J., K, W, and Von Quadt, A., 2003, Petrogenetic and Metallogenic Responses to Miocene Slab Flattening: New Constraints from the El Indio-Pascua Au-Ag-Cu Belt, Chile/Argentina: Mineralium Deposita, (submitted).

Cahill, T.A., and Isacks, B.L., 1992, Seismicity and shape of the subducted Nazca Plate: Journal of Geophysical Research, B, Solid Earth and Planets, v. 97, p. 17,503-17,529.

Charchaflie, D., Tosdal, R.M., Mortensen, J.K., and Bissig, T., 2002, Polyphase Miocene Deformation in the Argentine Andes: Evidence from the Veladero North Area, GSA Annual Meeting, Volume 34: Denver, CO, Geological Society of America, p. 437.

Clavero R., J., Martin, M.W., Mpodozis, C., and Cuitiño, L., 1997, Eventos de Alteración-Mineralización en la Franja El Indio (29-30° S): Nuevos Antecedentes Geológicos y Geocronológicos, Actas del Octavo Congreso Geológico Chileno, Volume 2: Actas del Congreso Geológico Chileno, p. 896-900.

Corbett, G., 1999, Further Comments on the Geology and Gold Mineralization at Veladero, Argentina, Corbett Geological Services, 12 p.

Cristallini, E.O., and Ramos, V.A., 2000, Thick-skinned and thin-skinned thrusting in the La Ramada fold and thrust belt; crustal evolution of the High Andes of San Juan, Argentina (32 degrees SL): Tectonophysics, v. 317, p. 205-235.

Deyell, C.L., 2001, Alunite and high sulfidation gold-silver-copper mineralization in the El Indio-Pascua belt, Chile-Argentina [Ph. D. thesis]: Vancouver, Mineral Deposit Research Unit. University of British Columbia. Canada.

Dilles, J.H., and Camus, F., 2001, A special issue devoted to porphyry copper deposits of northern Chile (Preface): Economic Geology and the Bulletin of the Society of Economic Geologists, v. 96, p. 233-430.

Godeas, M., Pezzutti, N., Nullo, F., and Otamendi, J., 1993, Caracterización Petrográfica y Geoquímica del Volcanismo Terciario en el Area del Río Taguas (Formaciones Doña Ana y Cerro de las Tórtolas). San Juan, in Anonymous, *ed.*, Actas del Décimo Segundo Congreso Geológico Argentino y Segundo Congreso de Exploración de Hidrocarburos, Volume 4: Actas del Congreso Geológico Argentino. 12, Vol, Asociación Geológica Argentina, p. 216-224.

Groeber, P., 1946, Observaciones geologicas a lo largo del meridiano 70; 1, Hoja Chos Malal: Revista de la Sociedad Geológica Argentina, v. 1, p. 177-208.

Groeber, P., 1951, La alta cordillera entre las latitudes 34 degrees y 29 degrees 30': Inst. Nac. Inves. Cienc. Nat., Buenos Aires, Rev., Cienc. Geol., v. 1, p. 233-352.

Heredia, N., Rodríguez Fernández, L., R, Gallastegui, G., Busquets, P., and Colombo, F., 2002, Geological setting of the argentine Frontal Cordillera in the flat-slab segment (30°00'- 31°30' S latitude): Journal of South American Earth Sciences, v. 15, p. 79-99.

Hervé, F., Godoy, E., Parada, M.A., Ramos, V., Rapela, C.W., Mpodozis, C., and Davidson, J., 1987, A general view on the Chilean-Argentine Andes, with emphasis on their early history, in Monger, J.W.H., and Francheteau, J., *eds.*, Circum-Pacific orogenic belts and evolution of the Pacific Ocean basin., Volume 18: Geodynamics Series: Washington, DC, United States, American Geophysical Union, p. 97-113.

Isacks, B.L., 1988, Uplift of the Central Andean Plateau and bending of the Bolivian Orocline: Journal of Geophysical Research, B, Solid Earth and Planets, v. 93, p. 3211-3231.

Jannas, R.R., Bowers, T.S., Petersen, U., and Beane, R.E., 1999, High-sulfidation deposit types in the El Indio District, Chile, in Skinner, B.J., *ed.*, Geology and ore deposits of the Central Andes., Volume 7: Special Publication - Society of Economic Geologists: Littleton, CO, United States, Society of Economic Geologists, p. 219-266.

Jones, P.J., Martínez, R.D., Vitaller, A.O., Chavez, I., Carrizo, M.M., La Motte, M.G., and Riveros, S.E., 1999, El Depósito Epitermal Aurífero Veladero, San Juan, in Zappettini, E.O., *ed.*, Recusos Minerales de la República Argentina, Anales 35: Buenos Aires, Instituto de Geología y Recursos Minerales SEGEMAR, p. 1673-1648.

Jordan, T.E., Isacks, B.L., Allmendinger, R.W., Brewer, J.A., Ramos, V.A., and Ando, C.J., 1983, Andean tectonics related to geometry of subducted Nazca Plate: Geological Society of America Bulletin, v. 94, p. 341-361.

Jordan, T.E., Isacks, B.L., Ramos, V.A., and Allmendinger, R.W., 1983, Mountain building in the central Andes: Episodes, v. 1983, p. 20-26.

Kay, S.M., Maksaev, V., Moscoso, R., Mpodozis, C., and Nasi, C., 1987, Probing the

evolving Andean lithosphere; mid-late Tertiary magmatism in Chile (29 degrees - 30 degrees 30') over the modern zone of subhorizontal subduction: Journal of Geophysical Research, B, Solid Earth and Planets, v. 92, p. 6173-6189.

Kay, S.M., Mpodozis, C., Ramos, V.A., and Munizaga, F., 1991, Magma source variations for mid-late Tertiary magmatic rocks associated with a shallowing subduction zone and a thickening crust in the Central Andes (28 to 33 degrees S), in Harmon, R.S., and Rapela, C.W., *eds.*, Andean magmatism and its tectonic setting., Volume 265: Special Paper - Geological Society of America: Boulder, CO, United States, Geological Society of America (GSA), p. 113-137.

Kay, S.M., and Abbruzzi, J.M., 1996, Magmatic evidence for Neogene lithospheric evolution of the central Andean "flat-slab" between 30 degrees S and 32 degrees S, in Dewey, J.F., and Lamb, S.H., *eds.*, Geodynamics of the Andes., Volume 259: Tectonophysics: Amsterdam, Netherlands, Elsevier, p. 15-28.

Kay, S.M., Mpodozis, C., and Coira, B., 1999, Neogene magmatism, tectonism, and mineral deposits of the Central Andes (22 degrees to 33 degrees S latitude), in Skinner, B.J., *ed.*, Geology and ore deposits of the Central Andes, Volume 7: Special Publication - Society of Economic Geologists: Littleton, CO, United States, Society of Economic Geologists, p. 27-59.

Kay, S.M., and Mpodozis, C., 2001, Central Andean ore deposits linked to evolving shallow subduction systems and thickening crust: GSA Today, v. 11, p. 4-9.

Kay, S.M., and Mpodozis, C., 2002, Magmatism as a probe to the Neogene shallowing of the Nazca Plate beneath the modern Chilean flat-slab: Journal of South American Earth Sciences, v. 15, p. 39-57.

Litvak, V.D., Page, S., and Kay, S.M., 2002, La Cordillera del Zancarrón en el Valle del Cura, Provincia de San Juan: un centro eruptivo Mioceno?, Actas del XV Congreso Geológico Argentino, Asociación Geológica Argentina.

Maksaev, J.V., Moscoso, D.R., Mpodozis, M.C., and Nasi, P.C., 1984, Las unidades volcánicas y plutónicas del Cenozoico superior en la Alta Cordillera del Norte Chico (29°-31°S); geología, alteración hidrotermal y mineralización: Revista Geológica de Chile, v. 21, p. 11-51.

Malizia, D., Limarino, C.O., Sosa Gomez, J., Kokot, R., Nullo, F.E., and Gutierrez, P.R., 1997, Hoja geológica Cordillera del Zancarrón (Provincia de San Juan) N° 3169-26 y 25: Buenos Aires, Servicio de Geología y Mineria de Argentina (SEGEMAR), 197 p.

Marín, G., and Nullo, F.E., 1988, Geología y estructura al oeste de la Cordillera de la Ortiga, San Juan: Revista de la Asociación Geológica Argentina, v. 43, p. 153-162.

Martin, M.W., Clavero, J., Mpodozis, C., and Cuitiño, L., 1995, Estudio geológico regional de la franja El Indio Cordillera de Coquimbo, Servicio Nacional de Geología y Minería, Compañía Minera San José, 238 p.

Martin, M.W., Clavero R., J., and Mpodozis, C., 1997, Eocene to Late Miocene Magmatic Development of El Indio Belt, ~30° S, North- Central Chile, Actas del Octavo Congreso Geológico Chileno, Volume 1: Actas del Congreso Geológico Chileno, p. 149-153.

Martin, M.W., Clavero R., J., and Mpodozis, C., 1997, Eocene to Late Miocene Structural Development of Chile's El Indio Gold Belt, ~30° S, Actas del Octavo Congreso Geológico Chileno, Volume 1: Actas del Congreso Geológico Chileno, p. 144-148.

Martin, M.W., Clavero, R.J., and Mpodozis, C., 1999, Late Paleozoic to Early Jurassic tectonic development of the high andean Principal Cordillera, El Indio region, Chile (29-30°S): Journal of South American Earth Sciences, v. 12, p. 33-49.

Martínez, R.D., Grassi, J.I., and Hernández, M.B., 1993, Consideraciones Estructurales sobre las Alteraciones Epitermales de la Región del Valle del Cura, San Juan: Sus Implicancias en Prospección Metalífera, in Anonymous, *ed.*, Actas del Décimo Segundo Congreso Geológico Argentino y Segundo Congreso de Exploración de Hidrocarburos, Volume 4: 12, Asociación Geológica Argentina, p. 202-210.

Minera Río Frío, S.A., 2000, Edades K-Ar (Biotita) de Intrusivos Terciarios: San Juan, p. 3.

Moscoso, R., and Mpodozis, C., 1988, Estilos estructurales en el Norte Chico de Chile (28-31° S), regiones de Atacama y Coquimbo: Revista Geológica de Chile, v. 15, p. 151-166.

Mpodozis, C., and Cornejo, P., 1988, Hoja Pisco Elqui, IV Región de Coquimbo: Santiago, Servicio Nacional de Geología y Minería, 164 p.

Mpodozis, C., and Kay, S.M., 1992, Late Paleozoic to Triassic evolution of the Gondwana margin; evidence from Chilean Frontal Cordilleran batholiths (28° S to 31° S); with Suppl. Data 92-22: Geological Society of America Bulletin, v. 104, p. 999-1014.

Mpodozis, C., and Ramos, V.A., 1990, The Andes of Chile and Argentina, in Ericksen, G.E., Pinochet, M.T.C., and Reinemund, J.A., *eds.*, Geology of the Andes and its relation to hydrocarbon and mineral resources.: Circum-Pacific Council for Energy and Mineral Resources, Earth Science Series: Houston, TX, United States, Circum-Pacific Council for Energy and Mineral Resources, p. 59-90.

Nasi, C.P., Moscoso, R.D., and Maksaev, V.J., 1990, Hoja Guanta, IV Región de Coquimbo: Santiago, Servicio Nacional de Geología y Minería, 140 p.

Nullo, F., 1988, Geología y Estructura del area de Guanaco Zonzo y Veladero, Oeste de Cordillera del Sancarrón, San Juan, in Anonymous, *ed.*, Actas del Tercer Congreso Nacional de Geología Económica, Volume 2: Olavarría, Pcia. de Buenos Aires, p. 503-515.

Nullo, F.E., and Marín, G., 1990, Geologia y estructura de las quebradas de La Sal y de La Ortiga, San Juan: Revista de la Asociación Geológica Argentina, v. 45, p. 323-335.

Pardo, C.F., and Molnar, P., 1987, Relative motion of the Nazca (Farallón) and South American plates since Late Cretaceous time: Tectonics, v. 6, p. 233-248.

Pilger, R.H., Jr., 1981, Plate reconstructions, aseismic ridges, and low-angle subduction beneath the Andes: Geological Society of America Bulletin, v. 92, p. I 448-I 456.

Pilger, R.H., 1984, Cenozoic plate kinematics, subduction and magmatism; South American Andes: Journal of the Geological Society of London, v. 141, p. 793-802.

Ramos, V.A., 1998, Análisis Geocronológico de la región de Veladero Norte (Valle del Cura), p. 21.

Ramos, V.A., Kay, S.M., Page, R.N., and Munizaga, F., 1989, La ignimbrita Vacas Heladas y el cese del volcanismo en el Valle del Cura, Provincia de San Juan: Revista de la Asociacion Geológica Argentina, v. 44, p. 336-352.

Ramos, V.A., Cegarra, M., and Cristallini, E., 1996, Cenozoic tectonics of the high Andes of west-central Argentina (30-36 degrees S latitude), in Dewey, J.F., and Lamb, S.H., *eds.*, Geodynamics of the Andes., Volume 259: Tectonophysics: Amsterdam, Netherlands, Elsevier, p. 185-200.

Ramos, V.A., and Kay, S.M., 1991, Triassic rifting and associated basalts in the Cuyo Basin, central Argentina, in Harmon, R.S., and Rapela, C.W., *eds.*, Andean magmatism and its tectonic setting., Volume 265: Special Paper - Geological Society of America: Boulder, CO, United States, Geological Society of America (GSA), p. 79-91.

Ramos, V.A., Page, R.N., Kay, S., Lapido, O., and Delpino, D.H., 1987, Geología de la región del Volcán Tórtolas, Valle del Cura, Provincia de San Juan, in Acenolaza, F.G., *ed.*, Actas del Décimo Congreso Geológico Argentino., Volume 4: Buenos Aires, Argentina, Asociación Geológica Argentina, p. 260-263.

Somoza, R., 1998, Updated Nazca (Farallón)-South America relative motions during the last 40 My; implications for mountain building in the Central Andean region: Journal of South American Earth Sciences, v. 11, p. 211-215.

Taylor, S.R., and McLennan, S.M., 1985, The continental crust: its composition and evolution: Oxford, Blackwell, 312 p.

Thiele, C.R., 1964, Reconocimiento geológico de la alta cordillera de Elqui: Santiago, Universidad de Chile, Departamento de Geología, 73 p.

Uliana, M.A., Biddle, K.T., and Cerdan, J., 1989, Mesozoic extension and the formation of Argentine sedimentary basins, in Tankard, A.J., and Balkwill, H.R., *eds.*, Extensional tectonics and stratigraphy of the North Atlantic margins., Volume 46: AAPG Memoir: Tulsa, OK, United States, American Association of Petroleum Geologists, p. 599-614.

Winchester, J.A., and Floyd, P.A., 1977, Geochemical discrimination of different magma series and their differentiation products using immobile elements: Chemical Geology, v. 20, p. 325-343.

Yañez, G.A., Ranero, C.R., von Huene, R., and Díaz, J., 2001, Magnetic anomaly interpretation across the southern Central Andes (32° -34° S); the role of the Juan Fernández Ridge in the late Tertiary evolution of the margin: Journal of Geophysical Research, B, Solid Earth and Planets, v. 106, p. 6325-6345.

Chapter 4

Conclusions and recommendations for future research

Conclusions

Based on field mapping, geochronology and geochemistry, this study defines the geologic framework of the Veladero North epithermal deposit within the El Indio-Pascua Belt in the Cordillera Frontal of Argentina and Chile. The 1:20,000-scale map in Plate 1 summarizes the geology of the study area and represents the first attempt to correlate locally defined, lithological units with time-constrained, regional stratigraphic units. Prior to this investigation, available geochronological data were scarce and often inconclusive on the stratigraphic position of the sampled unit. From a region-scale viewpoint, the revision of published and new information in this portion of the Andean cordillera contributes to the comprehensive model of the Cordillera Frontal and represents the foundation upon which to define the geology of the eastern flank of the Andes.

Geology

Six lithostratigraphic units, equivalent to regional units defined in the El Indio-Pascua Belt (Bissig *et al.*, 2001), are recognized in the Veladero North area. From oldest to youngest these units are: 1) the Guanaco Sonso Formation, consisting predominantly of rhyolitic to dacitic flows and shallow level intrusives emplaced between 259 Ma and 254 Ma; 2) the Bocatoma Unit, formed by dioritic stocks intruded between 36 Ma and 30 Ma; 3) the Tilito Formation, comprising volcanic rocks that range in composition from andesite to dacite as well as volcaniclastic rocks formed between 24.5 Ma and 22.8 Ma; 4) the Cerro de las Tórtolas Formation, including volcanic and sedimentary rocks intimately associated to the dacitic to andesitic domes from the Infiernillo Unit emplaced

around 16 Ma; 5) the Vacas Heladas Formation, consisting of 12.7 Ma to 11 Ma biotite-rich dacites; and 6) the 2.1 Ma Cerro de Vidrio Formation represented in the type-locality by a rhyolitic dome that is the youngest volcanic feature of the El Indio-Pascua Belt.

Late Paleozoic volcanic-plutonic arc

Late Paleozoic to middle Mesozoic volcanic and plutonic units are widespread in the Cordillera Frontal where they are referred as granite-rhyolite province. Plutonic episodes are represented by the (320 Ma to 280 Ma) Guanta and Cochiguás units, the (270 Ma to 325 Ma) Chollay-El León Unit and the (220 Ma to 190 Ma) Los Colorados and Carricitos units. Volcanism is characterized by the extensive Choiyoi Group, tentatively subdivided into the (275 Ma to 250 Ma) Guanaco Sonso Formation and the (225 Ma to 210 Ma) Los Tilos Formation. The Permian rocks in the Veladero North area are equivalent in age and lithology to the (275 Ma to 250 Ma) Guanaco Sonso Formation, the oldest member of the Choiyoi Group.

Revision of available geochronologic information suggests that, between late Paleozoic and Triassic, episodes of magmatic activity alternate with 15 m.y.- to 25 m.y.-long quiescence periods in a similar way as the Tertiary arc. In addition, the reassessment of the geochronological data implies that rocks with contrasting geochemical characteristics were emplaced simultaneously and also, that chemical signatures are not unique features of any magmatic episode. Petrotectonic interpretations, largely derived from geochemical data, indicate a complex scenario that will require future studies to fully elucidate.

Miocene volcanism and deformation

A north-trending fold and thrust belt characterized by steeply dipping faults and tight to open folds underlies the Veladero North area. Permian Guanaco Sonso rhyolitic to dacitic volcanic and volcaniclastic rocks intruded by Oligocene Bocatoma Unit dioritic

porphyries are superposed over Miocene Tilito Formation andesitic to dacitic lavas, pyroclastic and sedimentary rocks. Unique portions of the stratigraphic column, not repeated in other sheets, form each structural panel precluding a shortening estimation. Shortening predates the emplacement of middle Miocene (*ca.*16 Ma) pyroclastic rocks and porphyries of the Cerro de las Tórtolas and Infiernillo Unit that unconformably overlie and intrude the fold and thrust belt. Available data, however, is inconclusive as to the precise age of the fold and thrust system that might have formed during one or both of regionally defined shortening episodes between 23 Ma and 21 Ma or 18 Ma and 16 Ma.

Rocks from the Cerro de las Tórtolas Formation overlie the (17 Ma to 15 Ma) Frontera-Deidad pediplain, a regional erosional surface that truncates the fold and thrust belt. The Frontera-Deidad surface and the superjacent rocks dip gently (<20°) to the east. Tilting necessarily predates the incision of the (14 Ma to 12.5 Ma) Azufreras-Torta surface and the emplacement of the *ca.* 11 Ma volcanic rocks from the Vacas Heladas Formation that horizontally overlie the Cerro de las Tórtolas Formation. The deformation is compatible with a shortening event that, in El Indio-Pascua Belt, has been constrained between 15 Ma and 13 Ma (Martin *et al.*, 1995; Bissig *et al.*, 2001).

Sub-horizontal volcanic rocks and intrusives that represent the (12 Ma to 11 Ma) Vacas Heladas Formation were emplaced over the Azufreras-Torta surface. The erosional surface is cut on volcanic and intrusive rocks of dissimilar age in the Veladero North area. The relative position of the Azufreras-Torta surface and overlying rocks suggests that post-11 Ma deformation disrupted the Miocene fold and thrust belt as well as the regional erosion surfaces.

Lithologic association of the epithermal deposit

Strongly altered, subaerial heterolithic breccias in coarsely to well-bedded packets and interbedded volcaniclastic sandstones and subordinate fall tuffs form the

Veladero section of the middle Miocene Cerro de las Tórtolas Formation in the study area. These rocks host the greater part of the epithermal mineralization. Only a small portion of the Au ore body is apparently hosted in Permian and Miocene rocks in the subjacent fold and thrust belt. These lesser host rocks are formed by dacitic flow tuff and sandstone of the Oligocene Tilito Formation and dacitic flows and tuffs of the Permian Guanaco Sonso Formation.

Volcanic and volcaniclastic rocks from the Veladero Section are spatially and genetically linked to a series of dacitic to andesitic domes assigned to the coeval Infiernillo Intrusive Unit. Field observations indicate that scattered, vent clearing eruptions occurred during the emplacement of the sequence but that non-explosive conditions prevailed at that time. Limited chronologic data further suggest that the advanced argillic alteration presumably associated with the gold mineralization occurred in the 11.0 Ma to 10.5 Ma interval (Bissig *et al.*, 2001). This data confirm that the volcanic and volcaniclastic rocks from the Veladero Section and the intrusions from the Infiernillo Unit are at least 4 m.y. older than the epithermal mineralization, thus precluding a direct relationship between the genesis of the host-rock package and the gold.

Recommendations

The geologic framework established in this study represents the first step towards a comprehensive model of the Veladero North epithermal deposit. The lithologic association and the structural geometry, as defined here, are consistent with regional scale units and the overall tectonic style of the El Indio-Pascua Belt. Moreover, this research proves that the epithermal mineralization and the host-rock are genetically unrelated. In contrast to the Pascua-Lama deposit where the Miocene Pascua Formation is of the same age as the advanced argillic alteration and the gold (Bissig *et al.*, 2001, 2002), this study fails to identify a magmatic unit that is coeval to the epithermal

mineralization in the Veladero North area. High-sulfidation epithermal deposits are, however, closely related to degassing magmas (e.g. White and Hedenquist, 1990; Sillitoe, 1993; Arribas, 1995; Hedenquist and Arribas, 1999; Cooke and Simons, 2000). Thus, it seems likely that the coeval igneous rocks must be present, but they are yet unidentified.

Future geochronologic studies should constrain the precise timing of the mineralization, for example, by dating, hydrothermal alunite associated with gold within the ore body. Furthermore, determining the age of sub-economic epithermal mineralization, as found in the alteration haloes around late Paleozoic porphyries, may test hypotheses such as: 1) favourable periods for mineralization, 2) magmatic association of epithermal systems or 3) lithologic and textural control on the mineralization.

Geochronology may also help to elucidate the age of the dacitic flows that underly the Veladero section in an attempt to clarify the contact between the Tilito and Cerro de las Tórtolas Formations within the mineralized body.

In terms of regional geology and paleotectonic reconstructions, the Argentinean flank of the Cordillera Frontal in the Central Andes remains largely undocumented. It is, however, the place where future research may find new evidence regarding the evolution from the Gondwana margin to the Cenozoic arc.

References

Arribas, A.J., 1995, Characteristics of high sulfidation epithermal deposits, and their relation to magmatic fluids, *in* Thompson, J.F.H., *ed.*, Magmas, Fluids and Ore Deposits, Volume 23, Mineralogical Association of Canada Short Course Notes, p. 419-454.

Cooke, D.R., and Simmons, S.F., 2000, Characteristics and genesis of epithermal gold deposits, *in* Hagemann, S.G., and Brown, P.E., *eds.*, Reviews in Economic Geology, Volume 13, p. 221-244.

Bissig, T., Lee, J., W, Clark, A., H, and Heather, K., B, 2001, The Cenozoic history of volcanism and hydrothermal alteration in the Central Andean Flat-Slab Region: New 40Ar-39Ar constraints from the El Indio-Pascua Au (-Ag, Cu) Belt, 29°20'-30°30' S: International Geology Review, v. 43, p. 312-340.

Bissig, T., Clark, A., H, Lee, J., W, and Hodgson Jay, C., 2002, Miocene Landscape Evolution and Geomorphologic Controls on Epithermal Processes in the El Indio-Pascua Au-Ag-Cu Belt, Chile and Argentina: Economic Geology, v. 97, p. 971-996.

Hedenquist, J.W., and Arribas, A.J., 1999, Epithermal gold deposits: I. Hydrothermal processes in intrusion-related systems, and II. Characteristics, examples, and origin of epithermal gold deposits, *in* Molnar, F., Lexa, J., and Hedenquist, J.W., *eds.*, Epithermal Mineralization of the Western Carpathians, Volume 31, Society of Economic Geologists, Guidebook Series, p. 13-63.

Sillitoe, R.H., 1993, Epithermal models: Genetic types, geometric controls, and shallow features, *in* Kirkham, R.V., Sinclair, W.D., Thorpe, R.I., and Duke, J.M., *eds.*, Mineral Deposit Modelling, Geological Association of Canada Special Paper 40, p. 403-417.

White, N.C., and Hedenquist, J.W., 1990, Epithermal environments and styles of mineralization: variations and their causes, and guidelines for exploration: Journal of Geochemical Exploration, v. 36, p. 445-474.

Appendix I Geochronology

Thirteen samples from surface exposures were prepared for U-Pb geochronological studies. Sample preparation and mass spectrometry were performed at the Geochronology Laboratory of the University of British Columbia. Zircons from samples DC-128, DC-163 and DC-375 were analyzed at the Stanford-U.S. Geological Survey SHRIMP-RG because the amount of material was insufficient for conventional dating techniques or to corroborate the possible effects of inheritance.

Zircon was separated from 15-20 kilogram samples by crushing, grinding and heavy-mineral concentration using a conventional Wilfley table followed by heavy liquid and magnetic separation. Zircon crystals and fragments were grouped into fractions according to their magnetic susceptibility, grain size and morphology.

Conventional U-Pb

Most fractions were abraded before dissolution to minimize post-crystallization lead loss following the technique of Krogh (1982). Fine zircon needles were not abraded. Fractions were dissolved in a mixture of concentrated hydrofluoric acid, nitric acid and $^{233\text{-}235}U$ - ^{205}Pb tracer. U and Pb were separated using an ion exchange column techniques (Parrish *et al.*, 1987), eluted separately and loaded together on a Re filament with a phosphoric acid silica-gel emitter. Isotopic ratios were measured with a single collector VG-54R thermal ionization mass spectrometer equipped with a Daly photomultiplier. Uranium fractionation was determined on every run using the $^{233\text{-}235}U$ tracer. Daly runs of Pb isotopic ratios were corrected for a fractionation of 0.43%/amu determined by replicate analyses of the NBS-981 Pb standard and values recommended by Thirlwall (2000). Analytical results with their corresponding uncertainties propagated through the age calculations following the numerical technique of Roddick (1987) are summarized at the 2σ level in Tables 2-3 and 3-2.

Guanaco Sonso Formation

Zircon crystals and fragments were recovered using gravity and magnetic separation, then grouped into fractions (A, B, etc.) that include morphologically similar individuals. Published common-Pb isotopic compositions are preferred for data reduction (see Table 2-3), assuming that samples from the Veladero North area have an isotopic composition similar to units defined regionally.

DC-119: Rhyolitic ash-flow tuff from the Río Taguas late Paleozoic structural package

This sample is from an advanced argillic altered, matrix supported quartz-rich lapilli-tuff with small fiamme located at the top of the Río Taguas structural package (Figure 2-5). The sample was selected from the tuff horizon because it lacked accessory lithic fragments, which are common in all other ignimbrites. Zircon grains are pale pink prisms with simple tips, abundant fractures and no visible cores or elongate (length-width ratios > 7) "needles". Their sizes range from larger than 104 µm to 74 µm. The $^{206}Pb/^{238}U$ age of the concordant fraction B is interpreted as the igneous crystallization age of the rock at 263.7 ± 0.7 Ma. The other fractions contain zircon that are interpreted to have lost Pb from their rims during younger hydrothermal alteration or weathering.

DC-239: Dacitic ash-flow tuff from the Guanaco Zonzo area late Paleozoic structural package

Advanced argillic altered, poorly sorted, matrix-supported, (volcanic) lithic-poor dacite with fiamme-like and feldspar vugs was sampled in the Guanaco Zonzo area (Figure 2-5). Accessory volcanic lithic fragments form less than 5% of the rock volume and were removed during the sampling stage. Abundant colourless to pale pink zircon grains and fragments were recovered. Fractions B, E, F and G combine crystals or fragments that range from smaller than 74 µm to coarser than 104 µm. Fraction A

groups fine, elongate zircon "needles" smaller than 104 μm. The crystallization age of the rock is calculated from the $^{206}Pb/^{238}U$ age of fractions E and F, of which the former is concordant. Zircon in fractions B, G and particularly A, very likely lost Pb after crystallizing. Rhyolitic flows in the Guanaco Zonzo area are interpreted to have a crystallization age of 262.6 ± 0.7 Ma.

DC-142: Rhyolitic-dacitic dome intruding the Río Taguas late Paleozoic structural package

The sampled rock is a clay and silica (?) altered, porphyritic, intensely recrystallized dacite with spherulites. The sample is representative of the Guanaco Zonzo creek intrusive dome. Colourless to pale pink elongate prismatic zircon fragments and grains with simple faceted tips and no visible cores were recovered. Pale pink prismatic crystals with length-width ratio of 3 constitute fraction A. Fractions D, E and F include small fragments and grains that are concordant or slightly discordant. Elongate zircon coarser than 104 μm with fractures form fraction C. Fraction C is discordant in the Concordia diagram of Figure 2-9, most likely because of some inherited zircon. The crystallization age of the rock is indicated by the overlap of fractions D, E and F at 259.0 ± 0.7 Ma ($^{206}Pb/^{238}U$ age and uncertainty take into account the maximum and minimum possible ages at a 2 sigma level).

DC-181: Rhyolitic-dacitic dome intruding the Late Paleozoic rocks of Potrerillos and Canito areas

Coarse grained, matrix-supported, porphyritic rhyolite-dacite with clay altered feldspars and rounded quartz crystals form the intrusive dome that crop out in the northern part of the study area (Figure 2-5). The sampled rock has a moderate advanced argillic superposed alteration that is more intense outside the intrusion. Abundant colourless to pale pink zircon grains were recovered. Based on size and morphological characteristics, nine fractions were picked, of which only fractions C and I

("needles") were not abraded. The discordant character of fraction D is probably related to a small amount of inherited zircon. Lead loss accounts for the discordant character of the rest of the fractions in a Concordia plot (Figure 2-9). Fractions A, B, C, H and I have been used to calculate the age of the sample. The upper intercept of the regression line forced through the origin and fractions A, B, C, H and I with Concordia at 254.5 ± 4.2 Ma is interpreted as the crystallization age.

DC-162: Rhyolitic dacitic dome intruding the Guanaco Zonzo area late Paleozoic structural package

Advanced argillic altered, quartz-phyric porphyritic dacite with relict flow-banding texture characterize the intrusive rocks sampled as DC-162 (Figure 2-5). Abundant pale pink, elongate zircon grains with rods, bubbles and no visible cores were recovered and grouped into eight fractions of which only four yielded reliable isotopic data (Table 2-3). The age of the intrusion is preliminarily reported as the $^{206}Pb/^{238}U$ age of fractions A and G. Other fractions very likely lost Pb after crystallization.

Tertiary rocks

Zircon crystals and fragments were recovered from volcanic and intrusive rocks using gravity and magnetic separation techniques and then grouped into fractions (A, B, etc.) that include morphologically similar individuals. The common Pb isotopic composition from Bissig *et al.* (2003) is preferred for data reduction in conventional analyses, assuming that, samples from the Veladero North area have a similar isotopic composition as the same units defined elsewhere in the region.

Tilito Formation

DC-120, Andesitic flow tuff, 24.5 ± 0.2 Ma

The reported age of the sample considers the ^{206}Pb-^{238}U age of four concordant

fractions (A, C, E and F) and their respective uncertainties. Four discordant fractions (D, G, H and I) indicate the likelihood of inheritance. Although fraction B has ^{206}Pb-^{238}U and ^{207}Pb-^{235}U apparent ages consistent with the rock age, it is not considered in the age estimation as it reversely discordant.

DC-111, Andesitic flow tuff, 22.8 ± 1.7 Ma

Four concordant fractions (A, B, F and G) and a slightly discordant fraction (D) define the age of the sample. The associated uncertainty is relatively large as it considers the whole range of ^{206}Pb-^{238}U ages from fractions A, B, F and G. Inheritance and lead-loss processes affected the zircon population.

DC-163, Dacitic flow tuff, 23.5 ± 0.9 Ma

The reported age of the sample represents the ^{206}Pb-^{238}U age of two concordant fractions (C and F) and agrees, within uncertainty, with the age obtained from SHRIMP analyses from the same rock. Fraction G yields a relatively younger age that results from post-crystallization lead-loss. Inherited zircon is very common in this sample, as shown by the isotopic composition of fractions A, B, D and E.

DC-249, Dacitic flow tuff, 23.9 ± 0.2 Ma (preliminary)

Zircon is not abundant in this sample and the recovered grains are of poor quality. The age of the sample is calculated from a single concordant fraction (A) formed by multifaceted, prismatic and elongated grains, a morphology that most likely represents magmatic zircons. Fractions B, E and C yield discordant ages, and represent the inherited population. Isotopic data from three fractions are expected to resolve the age of sample DC-249.

Cerro de las Tórtolas Formation and Infiernillo Intrusive Unit

DC-265, Andesitic porphyry, 16.6 ± 0.3 Ma

The age of the sample is constrained by the ^{206}Pb-^{238}U age of three concordant fractions (A, B and E). Fraction D is discordant and it is not considered in the age calculation but yields a similar ^{206}Pb-^{238}U age than the rock. Only zircon with morphological characteristics as fraction C is likely to be inherited.

DC-374, Dacitic fall tuff, 15.8 ± 1 Ma

Three concordant fractions (B, C and F) overlap to define the age of the sample. The reported age is a conservative estimate that takes into account the extreme ^{206}Pb-^{238}U ages from fractions B and C. The age is indistinguishable from the SHRIMP age yield by sample DC-375 collected less than 5 metres away from DC-374. Both conventional and SHRIMP analyses reveal zircon inheritance.

DC-304, Dacitic intrusive, 16.4 ± 0.3 Ma (preliminary)

Very abundant zircon grains were recovered from this sample. However, isotopic data are not conclusive as to the age of the sample. Four concordant fractions range in age between 16 and 12 Ma. Alteration age from Bissig *et al.* (2001) is younger than the youngest possible U-Pb age. In agreement with a 16 Ma whole-rock K-Ar date (Ramos *et al.*, 1998) interpreted as complete resetting, the age of the sample is preliminarily reported as the ^{206}Pb-^{238}U age of fraction G. Additional fractions are expected to resolve the age of sample DC-304.

SHRIMP

Three samples were analyzed using the Stanford-U.S. Geological Survey SHRIMP-RG (Sensitive High-mass-Resolution Ion MicroProbe-Reverse Geometry) by Richard Tosdal (written communication, 2002). Reviews of the ion microprobe technique and

data interpretation are given in Ireland (1994) and Compston (1999). Operation conditions for the Stanford-U.S. Geological Survey SHRIMP-RG have also been recently summarized (Bacon *et al.*, 2000; Ayuso *et al.*, in press) and a short description is provided below. The SHRIMP-RG differs from the earlier SHRIMP instruments built at the Australian National University because of its reverse geometry design. The design uses an electrostatic mass analyzer downstream of the magnet and permits the SHRIMP-RG to be capable of third order focusing resulting in improved mass resolution compared to conventional SHRIMP designs (Williams, 1998; Bacon *et al.*, 2000). Common Pb used for age corrections is from the model by Cumming and Richards (1975). The zircon and Pb isotope data were reduced using the programs PRAWN and LEAD (Ireland, 1994) and ISOPLOT/EX (Ludwig, 1999). Table 3-1 shows the analytical results of the geochronology study.

Tilito Formation

DC-128b, Andesite, 25 ± 1.4 Ma

The reported age is a weighted mean of eight ^{206}Pb-^{238}U ages determined from elongate, prismatic zircon crystals, which are most likely to be magmatic. Age, uncertainty, mean standard weighted deviation (mswd in Figure 3-10a) and probability values do not vary significantly if zircon grain 1.1 is excluded from the analysis.

Cerro de las Tórtolas Formation and Infiernillo Intrusive Unit

DC-163, Dacitic flow tuff, 23 ± 1.1 Ma

The reported age is a weighted mean of eight ^{206}Pb-^{238}U ages determined in elongate, prismatic zircon crystals, which are most likely to be magmatic. Age, uncertainty, mean standard weighted deviation (mswd in Figure 3-10b) and probability values do not vary significantly if zircon grain 1.3 is excluded.

DC-375, Dacitic fall tuff (?), 16.4 ± 1.0 Ma

The reported age is a weighted mean of six ^{206}Pb-^{238}U ages determined near the rim of clear, elongate and prismatic zircon crystals, which are assumed to be magmatic. The age of Permian, inherited zircons (sampling points 1.5 and 1.8) is not considered in the statistical analysis. Age, uncertainty, mean standard weighted deviation (mswd in Figure 3-10c) and probability values do not vary significantly if zircon grain 1.4 is excluded.

References

Bacon, C.R., Persing, H.M., Wooden, J.L., and Ireland, T.R., 2000, Late Pleistocene granodiorite beneath Crater Lake caldera, Oregon, dated by ion microprobe: Geology (Boulder), v. 28, p. 467-470.

Bissig, T., Clark, A., H, Lee, J., K, W, and Von Quadt, A., 2003, Petrogenetic and Metallogenic Responses to Miocene Slab Flattening: New Constraints from the El Indio-Pascua Au-Ag-Cu Belt, Chile/Argentina: Mineralium Deposita, (submitted).

Compston, W., 1999, Geological age by instrumental analysis; the 29th Hallimond Lecture: Mineralogical Magazine, v. 63, p. 297-311.

Cumming, G.L., and Richards, J.R., 1975, Ore lead isotope ratios in a continuously changing Earth: Earth and Planetary Science Letters, v. 28, p. 155-171.

Ireland T, R., 1994, Ion Microprobe mass spectrometry: Techniques and applications, in Hyman, M. and .R., M., *eds.*, Cosmochemistry, geochemistry and geochronology: Advances in analytical Geohemistry, JAI Press, p. 1-118.

Krogh, T.E., 1982, Improved accuracy of U-Pb zircon ages by the creation of more concordant systems using an air abrasion technique: Geochimica et Cosmochimica Acta, v. 46, p. 637-649.

Ludwig, K., R, 1999, ISOPLOT: A plotting and regression program for radiogenic-isotope data: U.S. Geological Survey Open File, v. 91-445, 41p.

Parrish, R.R., Roddick, J.C., Loveridge, W.D., and Sullivan, R.W., 1987, Uranium-lead analytical techniques at the Geochronology Laboratory, Geological Survey of Canada, Radiogenic age and isotopic studies; Report 1., Volume 87-2: Geological Survey of Canada: Ottawa, ON, Canada, Geological Survey of Canada, p. 3-7.

Roddick, J.C., 1987, Generalized numerical error analysis with applications to geochronology and thermodynamics: Geochimica et Cosmochimica Acta, v. 51, p. 2129-2135.

Thirlwall, M.F., 2000, Inter-laboratory and other errors in Pb isotope analyses investigated using a ^{207}Pb- ^{204}Pb double spike: Chemical Geology, v. 163, p. 299-322.

Williams, I.S., 1998, U-Th-Pb geochronology by ion microprobe, in McKibben, M.A., Shanks, W.C., III, and Ridley, W.I., *eds.*, Applications of microanalytical techniques to understanding mineralizing processes., Volume 7: Reviews in Economic Geology: Socorro, NM, United States, Society of Economic Geologists, p. 1-35.

Appendix II Sample description and location

The following table is a compilation of field observations recorded during two campaigns to the Veladero North area.

Abbreviations used in table

C=Coherent, V=Volcaniclastic

Alteration type
p-propylitic
a-argyllic
aa-advanced argillyc
s-silica
sh-steam-heated

Texture: phenocrysts, groundmass
p-porphyritic
a-aphanitic
g-glassy
v-vesicular
s-spherulitic
f-fine <1 mm
m-medium
c-coarse >5 mm
fm-ferromagnesian
op-opaque
c-cryptocrystalline
f-very fine grained
m-microcrystalline
g-glassy
r-rcrystallized
d-devitrified

Lithofacies
w-welded
ff-flow foliated
fb-flow banded
ps-poorly sorted
fs-fairly sorted
ws-well sorted
ma-massive
xg-non graded
ng-normal graded
rg-reverse graded
cs-clast supported
ms-matrix supported

Components
x-crystal fragments
l-lithic fragments
lv-volcanic lithic
li-intrusive lithic
ls-sedimentary lithic
j-juvenile
p-pumice fragments
s-shards
f-fiamme

Grain Size
b->64 mm
a-<2 mm
fl-fine lapilli 2-34 mm
cl- 34-64 mm

Composition
and-andesite
dac-dacite
dio-diorite

Sample	Location (GK 2)		Color	Alteration		C	Texture		Lithofacies	Components	Grain Size	Comp.
DC-	2.4M+	6.7M+		intensity	type	V	phenocrysts	groundmass				
002	8642	50848	grey	3	p	v			w, cs,	x plag 60, x b	l-fl	and, no q
006	8768	50993	green	3	p	v			ms, ma	x plag 30, x b	l-fl	and, no q
008	8882	51684	dark green	2	p	c	pm, plag 80, f	60, f	ma			
009	8970	51696	light grey	5	aa	v			cs, ma	lv = aphanitic	l-cl	and?
012	9508	51619	dark grey	1	p	c	pf to a, plag 6	70, f	ma			and, no q
014	8666	52139	orange	5	aa	x	ma			alunite, jarosite		
015	8667	52066	orange-black	5	aa-s	x	hydrotermal breccia			very angular l	l-b	dac?
020	9266	52148	green	3	p	v			ms, ma	x plag, fm, lv	l-fl	and, no q
024	9815	52610	dark grey	2	p	v			ms, ma	x plag, fm, lv	l-fl	and, no q
025	9140	52911	light grey	2	a	c	pc, plag 80, fr	60, c	fm poorly define	ff, volcanic xenolith		and
026	9147	53276	light tan	5	aa-s	x	hydrotermal breccia			alunite, jarosi	frag <20 mm	
027	9040	53346	light grey	5	aa-s	v			ma,	lv = plag vugh	lv-cl, 80% ash	
028	9068	53407	light tan	5	aa-s	v?			ma	lithic molds, x	l-cl, x molds-ash	
032	10088	52823	yellow	5	aa	x	altered matrix of volcaniclastic breccia			alunite,silica		
033	10012	52750	light purple	3	a	v			ms, ma	x plag 40, x fr	l-cl, aphanitic	and, 2% q
034	10013	52749	grey	3	p	c	pf, plag 80, fn	30, f				basaltic andes
035	9395	52204	dark green	4	s? py	v			w, ms, xg	x plag, fm, lv,	l-cl	and
036	8866	50927	green	3	p	v			w, ms, xg	x plag 60, x b	l-fl	and
037	8964	51156	green	4	p, py	v			ma	x plag, fm, lv,	l-cl	and
042	10276	50220	pale pink	4	aa	v			w, ms	matrix microc	lv-fl, matrix a:	and-dac
043			white	3	a	v			sph <10 mm,	sph 40, matri:	very fine-grai	dac?
044			pale grey	3	a	v			w, ms, xg	r matrix 60, x	p-f-fl	dac
046			pale grey	3	a	v			ma, ms, xg	matrix 70, q 5	p-fl	dac
048			green	3	s	vc			cs, ng	lv 50, x (plag)	lv-fl	coarse sandst
048			dark green	3	s	vc			fg, la	x? lithics	a	
049			light grey	4	s	v			ms, ma, ps	matrix 50, lv :	lv-cl	dac
050	10611	50333	light grey	4	s	v			ms, ma	matrix 70, q 1	lv-fl	dac
056	8423	47685	dark grey	2	p	c	pm, plag 50, (	50, f	ma			and
060	10208	48615	light tan	4	aa	v			ms, r	x plag 80, lv?		and
062	10225	48863	white	5	aa	x	barite breccia		barite matrix,	barite crystals	lv-cl	
066	11115	49244	dark green	2	p	v?	pf, 2 generati	60, f	ma			and
066b	11115	49244	dark green	2	p	v?	pm, cs	10, f	ff	plag, no q		and
069	6393	47445	light brrown	5	s	v			ms, ps, xg	lv: dacite, ma	lv-fl-b	dac?
074	6293	47773	dark green	2	p	c	pf, plag 70, bi	30, f	ma			and
075	5909	47073	dark green	3	p	c	pm, plag 70, (	20, f	ma			and
079	6672	47173	dark green	3	p	c	pf, plag 80, fn	10, f, r	ma			and
080	6882	47336	dark green	2	p	c	pf, plag 90, fn	20, f	ff			and
090	4816	50298	dark green	3	p	c	pf, plag 90, o	10, f	ma			and
091	4670	50239	grey	4	aa-s	v			ff, ms, ps	lv 40 silicified	lv-cl	dac
092	4490	50230	light grey	1	p	c	pc-f, plag 70,	5, coarse	ma			and-dio
095a	5879	48178	green	2	p	c	pf, plag 70, bi	30, f	fb			and
095b	11115	48178	dark green	1	p	c	pf, plag 70, bi	40, g	ff			and
099	3547	50755	light grey	4	aa	v			ms, fs, r	lv? Completel	lv-fl, matrix a:	and
100	3169	50493	grey	1	a	c	pm-c, plag 70	40, f, r	ma			and

Sample	Location (GK 2)		Color	Alteration		C	Texture		Lithofacies	Components	Grain Size	Comp.
DC-	2.4M+	6.7M+		intensity	type	V	phenocrysts	groundmass				
105	3776	50417	purple	5	aa-s	v			ms, fb, r	lithics, x plag,	l-fl-cl	and
106	3996	50458	tan	3	a	c	pm, plag q and	fm	ma			dio
107	4078	50453	grey	2	a	c	pc, plag 90, fr	20, m	ma			dio
108	4190	50426	grey	1	a	c	pc, plag and fl	20, m	ma			dio
110	8701	50280	white	4	aa	c			ms, ps, xg	x reabsorbed	l-p-fl-cl	dac
114	8854	50301	green	4	p	c	pm, plag 80 o	30, f	ma			and
114b	8854	50301	green	4	p	c	pm, plag 80 o	30, f	ma			and
115	8852	50924	green	5	p	vc			ms, ps, fb	x plag 30, x h	l-fl-cl	and
117	8628	50778	green	2	p	c	pc, plag 80, 2	40, f	ma			and
118	10089	49849	green	2	p	c	pf, only plag a	60, m	ma			and
119	10277	50214	pale pink	2	a	v			ms, ps	x reabsorbed	lv-fl-cl	dac
120	9953	49475	brown	3	a	v			w, ff, ms, xg	x plag 20, x q	lv-p-fl	and
122	10242	48058	dark green	2	p	c	pf-a, plag 80,	50, f	ma			and
123	10242	48058	pale pink	3	a	v			w, ms, ps, xg	p-welded 15,	lv and p-fl-cl	dac
124	9649	49152	dark green	1	p	c	pf, plag 60, o	40, m	ma			and
126	10435	52333	green	3	a	c	pf, plag 70, a	50, f	ma			and
129	11191	52667	light green	3	p	c	pm, plag 80,	40, g, d	ma			and
130	11461	45950	green	3	p	v			ms, ps	lv 40, x	lv-b-cl	and
131			green	3	p	c	pm, plag 80, a	30, f	ma			and
132			green	3	p	c	pm, plag 80, a	30, f	ma			and
133	11605	45897	red	2	a	v			w, ms, ps, xg	x 30 (plag an	lv-fl-b	and-dac
137	11010	49591	green	2	p	v-c?	plag and carb	15, f	ma	lv same comp	cl-b	and
141	10902	47709	white-grey	4	aa	v			fb, prismatic j	small lithophyseae, x 5		dac
142	10694	47651	white	4	aa	c	spherulitic coa	20, m	ma			dac
144	12056	49013	dark green	3	p	c	pf-m, plag an	30, f	ma			and
145	12108	49395	light green	3	p	v			ps, ms, xg	lv 50, x plag a	lv-b	and
146	12182	49662	dark green	2	p	c	pf, plag 70, cl	60, f	ma			and
148	10879	51882	dark green	2	p	c	pf, plag 70, cl	60, f				and
152	12760	51947	light red	1	p	c	pm, plag 80, l	60, g	ma			dac-and
159	9183	47746	pale tan	4	aa-s	c	pm, q, plag, b	40, m	fb, xenoliths			dac
160	8798	47260	dark green	3	a	c	pf, plag 70 alt	50, r	ma			and
162	8271	49743	grey	4	aa	c	pm, q only cry	60, r to q	fb			dac
163	5339	51366	grey	3	aa	v			ms, fs, xg	x embayed q	lv cl	dac
167	4820	51360	pink	4	aa	c	fb, visible q a	70, f	fb			dac
168	4711	51509	white	3	aa	v			ms, xg, fs	x q 20, other	lv-fl	dac
169	4564	51510	dark green	3	p	c	pm, plag 70,	30, f	ma			and
172	5392	51523	grey	5	aa-s	v			cs, ps	lv: silicified ar	lv b-cl	dac
181	5997	52256	light grey	4	aa	c	pc, plag alt 2(	65, f, r	fb			dac
183	5446	52293	grey	4	aa	c	fb silicified, q	and fk? M				dac
184	4808	52346	red	3	p	v			w, ms, ps, xg	lv 20, x plag a	lv-fl	and
188	4955	48190	grey	3	aa	v			ms, weak wel	x q 15, plag 1	lv-cl	dac
193	5757	48536	pale tan	3	aa-py	v			w, fs, ms	s 20, q veinlet	lv-cl	and-dac
195	7381	48674	grey-gree	3	p	v			w, ms, xg	lv altered in v	lv-fl-b	and
204	5689	47184	green	3	p	c	pm, plag 15, f	75, c	ma to fb			and

Sample	Location (GK 2)		Color	Alteration		C	Texture		Lithofacies	Components Grain Size	Comp.
DC-	2.4M+	6.7M+		intensity	type	V	phenocrysts	groundmass			
213	4626	49013	green	3	p	c	a, plag 75, ch	20, f	ma		and
218	5981	46450	dark green	2	p	c	pm, plag 60, (	50, m	ma		and
226	6599	45106	light brown	3	a	v			w, ms, fs, xg	x plag alteres, q lenses	dac
237	8592	46736	pale pink	3	a	v			w, ms, ps	x embayed ro p-cl	dac
239	8454	45971	white	4	a	v			w, bedded, ps	x embayed rounded q 20, pl	dac
243	6633	46518	green	2	p	c	pm, plag 70, (	60, c	ma		and
249	6582	45928	grey	3	a	v			w, ms	x plag and q l	few l-fl and-dac
261	9644	46384	green	4	a	v			cs,	x plag? Intens	l-cl-fl and
265	8695	45430	dark grey	3	p	c	pm, plag 70, l	50, c, altered	fb		and
267	9651	45682	light grey	4	aa	v			ms, ps	lithics v?, pun	l-cl-b and
270a	11360	45674	grey	1	p	c	pm, plag 60, (	60, f	ma		and
270b	11360	45674	grey	1	p	c	pm, plag 60, (	60, f	ma		and
283	8154	46313	pale pink	3	a	v			w, ms, xg	x q 20, plag 2	p-fl dac
284	7917	46525	grey	2	a	v			w, ms, fs	p 30, lv 20, pl	p-fl, lv-fl and
286	6679	43506	dark grey	3	a	c	pm, plag 70, (	60, m, 90% p	ma		and
288	8286	44705	grey brown	2	p	c	pm, plag 80, (	60, c, r	fb		and
290	9724	45070	dark green	2	p	c	a, plag 90, fm	40, c, with op	ma		and
293	10123	45259	lihgt tan	5	aa	v			ms, xg	x q 5, plag vughs 15, groun	dac?
298a	9616	44435	dark green	4	p-a	c	pm, plag 70, f	40, f	ma to banded		and
298b	9616	44435	green-purple	2	p	c	pm, plag 70, f	60, f	fb to ma		and
298c	9616	44435	green-grey	2	p	c	pm, plag 70, (	60, f	fb to ma		and
300	12364	45963	green	2	p	c	pm, plag 80, (	50, f to c	ma		and
302	5909	51039	white	4	aa	v			ms, ng, fb	small lithics o	l-a-fl dac?
304	8801	47921	white	4	aa	v			ms, xg	x plag 20, x q x< 2 mm	dac
306	12841	50246	white	3	a	vc					sandstone
310	13743	49925	purple	4	a?	v			ms, ff, ng	l-v? very alter	l-cl dac?
311	13967	49718	grey	2	p	c	pm, plag 80, l	60, m, c	ma		and-dac
315	12584	49346	green	2	p	c	pm-c, plag 70	60, m	ma		and-dac
317	13155	49394	light grey	4	a	v			fb, ms	x plag very alt	none and

Appendix III XRF and ICP-MS Geochemistry

Whole-rock geochemistry

Eighteen samples from the late Paleozoic sequence and 25 Tertiary samples were processed and analysed for major and six trace elements (Sr, Zr, Rb, Y, Nb and Ba) using X-ray fluorescence (XRF) at Bondar-Clegg, North Vancouver BC, Canada. From that group, nine samples were selected for further REE and trace elements analysis based on petrography and previous geochemistry. The new measurements were done by Inductively Coupled Plasma Mass Spectroscopy (ICP-MS) at Memorial University, St. Johns NF, Canada. Major oxides were extracted by borate fusion and their concentration was measured by XRF. Trace element abundance measured by Bondar-Clegg was done by XRF on pressed pellets. The same elements were measured at Memorial University by XRF and ICP-MS after sodium peroxide sinter decomposition. The replicate data agree for key elements such as Y, Ba and Ce. This suggests no dissolution problems that may be associated to samples containing refractory minerals such as zircons.

Detection limits

The following table summarizes the detection limits reported by the laboratories where the Veladero North area samples were analyzed.

Element	XRF	ICP-MS
SiO_2	0.01 %	-
TiO_2	0.01 %	-
Al_2O_3	0.01 %	-
Fe_2O_3	0.01 %	-
MnO	0.01 %	-
MgO	0.01 %	-
CaO	0.01 %	-
Na_2O	0.01 %	-
K_2O	0.01 %	-
P_2O_5	0.01 %	-
LOI	2 %	-
Sr	2 ppm	-
Zr	2 ppm	-
Rb	2 ppm	-
Y	1 ppm	-
Nb	2 ppm	-
Ba	1 ppm	0.138 ppm
La	-	0.022 ppm
Ce	-	0.024 ppm
Pr	-	0.002 ppm
Nd	-	0.011 ppm
Sm	-	0.005 ppm
Eu	-	0.004 ppm
Gd	-	0.005 ppm
Tb	-	0.001 ppm
Dy	-	0.002 ppm
Ho	-	0.001 ppm
Er	-	0.003 ppm
Tm	-	0.001 ppm
Yb	-	0.003 ppm
Lu	-	0.002 ppm
Hf	-	0.012 ppm
Ta	-	0.003 ppm
Th	-	0.011 ppm

Appendix IV Alteration

Present-day concentration of major oxides is largely influenced by superposed post-crystallization alteration. Geochemically, the alteration can be characterized by silica addition and alkali leaching as shown by a general displacement of the Veladero North samples towards the bottom-right corner in Figure 2-10 a. Nb, Y and Zr are generally considered immobile elements under weak alteration conditions. However, in the study area, Nb, Y and Zr were partially remobilized. Although for most of the collected samples the original concentration of those elements is very close to the present-day concentration, only the samples that plot within the non-altered field will be considered (Figure 2-10 B). REE mobility in a rock unit is principally controlled by the stability of the mineral phases that concentrate them, the distribution coefficients between hydrothermal fluids and rock and the stability of secondary minerals that may fractionate them (Humphris, 1984). REE patterns of the Tertiary volcanic rocks in contact with late Paleozoic rocks are identical to the patterns of unaltered samples documented in the region (see chapter 3 for Tertiary rocks geochemistry). Since the samples collected from Tertiary and late Paleozoic volcanic rocks are similarly altered, it is very likely that the measured REE abundance reflects the original concentration in both groups. In that sense, the effect of advanced argyllic alteration is negligible as long as the feldspars or the secondary clays are not removed by weathering or by hydrothermal alteration. Conversely, most of the late Paleozoic intrusive rocks are pervasively altered and feldspar molds are common suggesting that the original magmatic REE concentration has been modified.